



SAPIENZA  
UNIVERSITÀ DI ROMA

Department of Computer Science

TOWARDS SELF-POWERED WIRELESS SENSOR NETWORKS

A Dissertation in  
Computer Science by  
**Dora Spenza**

Submitted in partial fulfillment of the requirements for  
the Degree of DOCTOR OF PHILOSOPHY  
in COMPUTER SCIENCE

November 2013

© Dora Spenza



## **Thesis Committee**

Prof. Chiara Petrioli (advisor)  
Department of Computer Science  
Sapienza University of Rome  
Rome, Italy

Prof. Thomas F. La Porta (second member)  
Department of Computer Science and Engineering  
The Pennsylvania State University  
State College, Pennsylvania

Prof. Roberto Navigli (third member)  
Department of Computer Science  
Sapienza University of Rome  
Rome, Italy

## **External Reviewers**

Prof. Wendi Heinzelman  
Department of Electrical and Computer Engineering  
University of Rochester  
Rochester, New York

Prof. John Stankovic  
Department of Computer Science  
University of Virginia  
Charlottesville, Virginia



# Abstract

Ubiquitous computing aims at creating smart environments in which computational and communication capabilities permeate the world at all scales, improving the human experience and quality of life in a totally unobtrusive yet completely reliable manner. According to this vision, an huge variety of *smart* devices and products (e.g., wireless sensor nodes, mobile phones, cameras, sensors, home appliances and industrial machines) are interconnected to realize a network of distributed agents that continuously collect, process, share and transport information. The impact of such technologies in our everyday life is expected to be massive, as it will enable innovative applications that will profoundly change the world around us. Remotely monitoring the conditions of patients and elderly people inside hospitals and at home, preventing catastrophic failures of buildings and critical structures, realizing smart cities with sustainable management of traffic and automatic monitoring of pollution levels, early detecting earthquake and forest fires, monitoring water quality and detecting water leakages, preventing landslides and avalanches are just some examples of life-enhancing applications made possible by smart ubiquitous computing systems.

To turn this vision into a reality, however, new raising challenges have to be addressed, overcoming the limits that currently prevent the pervasive deployment of smart devices that are long lasting, trusted, and fully autonomous. In particular, the most critical factor currently limiting the realization of ubiquitous computing is energy provisioning. In fact, embedded devices are typically powered by short-lived batteries that severely affect their lifespan and reliability, often requiring expensive and invasive maintenance.

In this PhD thesis, we investigate the use of *energy harvesting* techniques to overcome the energy bottleneck problem suffered by embedded devices, particularly focusing on Wireless Sensor Networks (WSNs), which are one of the key enablers of pervasive computing systems. Energy harvesting allows to use energy readily available from the environment (e.g., from solar light, wind, body movements, etc.) to significantly extend the typical lifetime of low-power devices, enabling ubiquitous computing systems that can last virtually forever. However, the design challenges posed both at the hardware and at the software levels by the design of energy-autonomous devices are many. This thesis addresses some of the most challenging problems of this emerging research area, such as devising mechanisms for energy prediction and management, improving the efficiency of the energy scavenging process, developing protocols for harvesting-aware resource allocation, and providing solutions that enable robust and reliable security support.



*A mio padre*





## Acknowledgments

First and foremost, I would like to express my sincere appreciation and gratitude to my advisor, Professor Chiara Petrioli, for her help and guidance during the past years. She has undoubtedly been the most important person shaping my academic evolution: Her in-depth knowledge, breadth of vision, dedication, enthusiasm and unfailing energy are a constant source of inspiration for me. She did a terrific job at introducing me to the academic world, and I am greatly indebted to her for providing me with many opportunities. Thanks to her, my Ph.D. has been a very stimulating and rewarding experience.

I would like to thank the members of my thesis committee, Professor Thomas La Porta and Professor Roberto Navigli, as well as the external reviewers of my Ph.D. thesis, Professor Wendi Heinzelman and Professor John Stankovic, for their valuable advice and comments. I truly appreciate they took time out of their busy schedules to review my dissertation and to provide me with in-depth feedbacks.

During my Ph.D., I was very fortunate to collaborate with many people from outside Sapienza, whom have influenced me greatly. I wish to thank all my coauthors, and especially Prof. Stefano Basagni, Prof. Thomas La Porta, Prof. Cynthia Phillips, Prof. Giuseppe Bianchi, Prof. Luca Benini, and Prof. Davide Brunelli, for giving me the opportunity of working with them.

The research presented in this thesis was made possible by the financial assistance of many parties, which I gratefully acknowledge. Since 2010, my Ph.D. was supported by the Google Europe Fellowship in Wireless Networking. The research presented in this thesis was also sponsored in part by the FP7 project GENESI, by the CHIRON ARTEMIS project, by the TENACE PRIN Project, and by the US National Science Foundation.

I want to thank all the people at the C.S. Department, and especially my Ph.D. colleagues and the members of the Senses Lab, which have contributed to making these past years a great experience.

Finally, a very special thank-you to Marco, to my wonderful family, and to all my awesome friends, for always giving me unconditional love and support. I am really blessed to have you.



# CONTENTS

---

<b>Introduction</b>	<b>1</b>
List of publications . . . . .	5
<b>1 Review of wireless sensor networks with energy harvesting</b>	<b>7</b>
1.1 Energy harvesting architectures . . . . .	8
1.2 Techniques of energy harvesting . . . . .	11
1.3 Energy prediction models . . . . .	15
1.4 Power management and task scheduling in EHWSNs . . . . .	16
<b>2 Pro-Energy: an energy prediction model for energy-harvesting WSNs</b>	<b>19</b>
2.1 Pro-Energy . . . . .	20
2.1.1 Short-term energy predictions . . . . .	21
2.1.2 Medium-term energy predictions . . . . .	22
2.1.3 Stored profiles updates . . . . .	23
2.2 Improving prediction accuracy by combining multiple profiles . . . . .	24
2.3 Performance evaluation . . . . .	25
2.3.1 Accuracy of short and medium term energy predictions . . . . .	25
2.3.2 Prediction algorithms evaluation . . . . .	25
2.3.3 Accuracy of energy predictions for varying parameter settings . . . . .	28
2.3.4 Pro-Energy Overhead . . . . .	29
2.4 Conclusions . . . . .	29
<b>3 Adaptive rectifier driven by power predictions for wind EHWSNs</b>	<b>31</b>
3.1 Related Works . . . . .	32
3.2 Architecture of the energy harvester . . . . .	35
3.2.1 Wind Generator . . . . .	35
3.2.2 Hybrid Full-Wave Rectifier . . . . .	36
3.2.3 MPPT Circuit and Output Stage . . . . .	36
3.3 Real-life air-flow data collection . . . . .	37
3.3.1 Collected Air-flow Data . . . . .	37
3.3.2 Trains Passage Detection . . . . .	38
3.3.3 Energy Intake Calculation . . . . .	39
3.4 Power management algorithm . . . . .	40
3.4.1 Adaptive and adaptive-f strategies . . . . .	40
3.4.2 Smart strategy . . . . .	41
3.5 Experimental comparison of power management policies . . . . .	42
3.6 Conclusions . . . . .	43

<b>4</b>	<b>Sensor-mission assignment in rechargeable WSNs</b>	<b>45</b>
4.1	Related work . . . . .	47
4.2	Problem formulation . . . . .	48
4.2.1	Node architecture . . . . .	48
4.2.2	Application scenarios . . . . .	49
4.2.3	Analytical model . . . . .	49
4.2.4	Sensor-mission assignment problem: MIP formulation . . . . .	51
4.2.5	Sensor-mission assignment problem in energy harvesting WSNs . . . . .	59
4.3	EN-MASSE . . . . .	60
4.3.1	Communication protocol . . . . .	61
4.3.2	Bidding scheme . . . . .	61
4.3.3	Task allocation to sensors . . . . .	64
4.3.4	Energy prediction models and solar energy datasets . . . . .	65
4.4	Performance evaluation . . . . .	67
4.4.1	Simulation setup . . . . .	67
4.4.2	Benchmark assignment schemes . . . . .	68
4.4.3	Simulation results . . . . .	69
4.4.4	Comparison with the MIP solution . . . . .	75
4.5	Experimental testbed: implementation and validation . . . . .	78
4.5.1	EN-MASSE assignment scheme and energy models validation . . . . .	79
4.6	Conclusions . . . . .	81
<b>5</b>	<b>Exploiting energy harvesting to support access control in WSNs</b>	<b>83</b>
5.1	Related works . . . . .	85
5.2	CP-ABE overview . . . . .	86
5.2.1	Preliminaries . . . . .	86
5.2.2	Setup and decentralized attribute issuing . . . . .	87
5.2.3	Message encryption . . . . .	87
5.2.4	Message decryption . . . . .	87
5.3	AGREE . . . . .	88
5.3.1	WSN specific optimizations . . . . .	88
5.3.2	Access policies updates . . . . .	89
5.3.3	Pre-computation of policies . . . . .	90
5.3.4	Caching strategy . . . . .	91
5.4	Performance evaluation . . . . .	93
5.4.1	Experimental results: energy cost of CP-ABE encryption . . . . .	93
5.4.2	Energy model and real-life energy harvesting traces . . . . .	94
5.4.3	AGREE simulation results . . . . .	95
5.5	Conclusions . . . . .	97
	<b>Concluding remarks</b>	<b>99</b>
	<b>Bibliography</b>	<b>101</b>

## INTRODUCTION

---

Over the past decade, progress in computing and communication capabilities of embedded devices has played a major role in the advent of the *Internet of Things* (IoT), a technology that enables *smart* devices (e.g., mobile phones, cameras, sensors, home appliances and industrial machines) to communicate and share data over the Internet [8]. The concept of IoT is motivated by the fact that the Internet will no longer be just a network of computers, but it will potentially involve trillions of smart devices with embedded systems, thus greatly increasing its size and scope. Industry experts predict 50 billion Internet-connected devices by 2020 [9], and, according to the U.S. National Intelligence Council, “*by 2025 Internet nodes may reside in everyday things – food packages, furniture, paper documents, and more*” [10]. The impact of IoT on everyday-life is thus expected to be massive, enabling applications such as assisted living, e-health, domotic, home automation, smart cities and buildings, and smart agriculture and animal farming.

One of the key enablers to realize the vision of the Internet of Things is Wireless Sensor Networks (WSNs) [11, 12]. Due to their low cost and pervasive capability, WSNs have gained increasing popularity in the last decade, as they allow for accurate real-time information in a multitude of application scenarios that conventional cabled or wireless networks are unable to handle. Acting as a bridge to the physical world, wireless sensor networks will eventually make possible the automatic monitoring of vital signs and health conditions in assisted living and e-health applications, of environmental parameters such as air quality and pollution, and of energy and water use in civil and industrial buildings, among others.

To turn such a vision into a reality, new raising challenges have to be addressed, overcoming the limits that currently prevent the pervasive deployment of smart devices that are long lasting, trusted, and fully autonomous. Energy provisioning is presently one of the most critical factors limiting the realization of ubiquitous computing, as the lifespan of embedded systems is severely reduced by their scarce energy resources. We experience the problem of energy consumption on a small scale in our everyday life, when dealing with the short-lived batteries that power our smartphones and tablets, which often have to be recharged daily. Although annoying, however, recharging such batteries does not pose particular problems, as they can be easily accessed. This is not the case for many other application scenarios. In smart-buildings and structural health monitoring applications, for instance, battery-powered wireless sensor nodes are often embedded in the structure or located in inaccessible or hazardous areas. Battery replacement and recharging is thus highly impractical and very expensive at best, if not altogether impossible. In assisted living and e-health applications, the impact of energy issues is even more serious. In fact, batteries are one of the weakest points in medical implants, requiring invasive and expensive maintenance. As reported in [13], battery-powered

implantable medical devices require additional surgery every three to five years just to change the battery. Even secondary cells are an impractical solution, as they need to be recharged through cumbersome external devices. For these reasons, overcoming the energy bottleneck suffered by embedded nodes is clearly a necessary step towards the realization of the future Internet of Things.

In wireless sensor networks, a well understood and widely studied solution to extend the lifetime of wireless nodes is to minimize the energy consumption by duty-cycling their radio transceivers [14]. This approach allows to extend the typical duration of a node's battery to up to a few years, usually at the cost of increased data latency and reduced performance. Though acceptable in some application scenarios, however, a lifetime horizon of 2-3 years is still far away from the goal of pervasive, autonomous networks that are able to operate maintenance-free for decades or more. Employing bigger batteries does not allow to meet such a requirement, as self-discharge and aging deplete electrochemical cells within a few years even if they are seldom used [15, 16]. Moreover, the current trend is for electronic embedded systems to continue to shrink in both size and weight, thus further reducing the amount of energy that is possible to store on board.

The most promising technology towards the goal of very long-lasting WSNs is *energy harvesting*, which allows to use energy readily available from the environment (e.g., from solar light, wind, body movements, etc.) to power embedded devices [2]. By scavenging energy from the surroundings, wireless sensor nodes can significantly increase their typical lifetime: If the harvested energy is efficiently utilized, low-power devices can last virtually forever. To reach this ambitious goal, however, energy harvesting *hardware* alone is not usually sufficient. In fact, although potentially unlimited, the energy provided by ambient power sources is not constant nor always available. For this reason, environmental-powered nodes experience an alternation between periods in which energy must be sparingly used, and situations in which there may even be an excess of energy available, which would be wasted unless used in the short term. In addition, energy harvesters are typically able to scavenge energy only in the range of milliwatts, so the energy capturing and storing processes must be performed with very high efficiency. At a software level, dedicated harvesting-aware solutions are needed, which adapt the workload scheduling of the nodes to the stochastic nature of the environmental source. In Chapter 1 we give a general introduction to the background, opportunities and challenges of energy-harvesting WSNs, including a survey on state-of-the-art solutions on power management and task scheduling and on energy prediction models.

In the case of predictable energy sources, such as solar light, energy prediction models are a precious tool to devise smart energy allocation strategies. In fact, by forecasting the source availability and estimating the expected energy intake in the near future, such models allow the system to make critical decisions about the utilization of the available energy, enabling the development of a wide range of proactive power management strategies and sophisticated system optimizations. In Chapter 2, we contribute to this topic by developing a general framework for multi-source (i.e., solar and wind) energy-harvesting systems, which is able to accurately predict the energy intake within a forecasting horizon that is dynamically chosen based on the application needs. The key component of our solution is *Pro-Energy* (PROfile Energy prediction model), a novel energy prediction model that leverages past energy observations to provide estimations of future energy availability [4]. To this end, Pro-Energy stores and uses a pool of *harvested profiles* observed in the past, which represent the energy intake recorded during different types of "typical" days. For instance, days may be classified into sunny, cloudy or rainy, and a characteristic profile may be associated to each of these categories. When delivering energy predictions, Pro-Energy looks at the stored profile that is the most similar to the current day. Prediction for the next timeslots are then computed based on a combination of the energy reported in the stored profile and of the energy observed

during the current day. We assess the performance of our proposed solution by using real-life solar and wind traces that we collected by interfacing TelosB nodes with solar cells and wind micro-turbines, as well as publicly available traces of solar and wind obtained from weather monitoring stations in the US. A comparative performance evaluation between Pro-Energy and other energy predictors previously proposed in the literature confirms that our solution significantly outperforms existing algorithms, improving the prediction accuracy up to 60%.

A practical application of energy prediction techniques is presented in Chapter 3, in which we address the problem of improving the efficiency of scavenging energy from airflows. In networks of embedded devices, energy is typically harvested from airflows by using small-scale spinning turbines that generate energy when wind flows across their blades. Efficient design of such harvesters is still the subject of ongoing research. In fact, even though large-scale wind harvesting systems are well-understood and highly efficient, the performance of small-scale airflows harvesters is limited by factors such as the unpredictability of flow sources and very low flow rates. In addition, the energy generated by the wind micro turbine is delivered through alternating currents that can not be used directly to power the node. Such currents are thus converted, further reducing the harvester efficiency, into more suitable DC signals by a *rectifier* circuit. In ultra-low power applications, rectification is typically realized through a diode full wave bridge (passive rectifier) or by using MOSFETs (active rectifier). In terms of efficiency, active rectifiers usually outperform passive ones when the input power is greater than a given threshold, but their performance may significantly degrade when the incoming power is low. To improve the efficiency of such a rectifier stage, we present a hardware and software solution, i.e., an *adaptive hybrid rectifier* which exploits both passive and active topologies combined with power prediction algorithms [6]. According to our approach, data about the incoming wind power are periodically collected and elaborated by a microcontroller, which delivers estimations about the future energy availability, and determines which topology of rectifier is the most efficient under the expected air-flow speed conditions. To assess the performance of this approach in a real-life scenario, we collected air-flow data by deploying WSN nodes interfaced with a wind micro-turbine in an underground tunnel of the Metro B1 line in Rome [3]. We shown that, by using the adaptive AC-DC converter combined with power prediction algorithms, nodes deployed in the tunnel can harvest up to 22% more energy with respect to previous methods. However, periodically sampling air-flow data and elaborating predictions introduces additional overhead. We address this aspect by devising a power management technique specifically tailored to the underground tunnel scenario. Without impairing the energy harvesting process, this technique reduces the overall overhead of the system up to 93% in terms of the average number of sampling performed per day by a node with respect to the strategy that constantly monitors the power generated by the turbine.

In addition to enabling novel power management strategies at a node level, energy harvesting techniques also impact network-wide solutions and protocols. Routing, MAC, clustering and data collections are just a few examples of topics in which energy-harvesting capabilities may fundamentally change traditional solutions [17]. For example, smart harvesting-aware protocols may achieve network-wide optimizations by allocating collaborative tasks to suitably chosen nodes, so to exploit their current and future energy recharging opportunities, and to minimize energy waste. Sensor mission assignment, which concerns matching the sensing resources of a wireless sensor network to appropriate tasks that comes to the network dynamically, is an example of a problem that can benefit from this kind of approach. In sensor mission assignment, each task (mission) arriving in the network can be performed by a subset of sensor nodes, and multiple, simultaneous missions may be active in the network at the same time. Missions may vary in importance and amount of resources they require. They may also appear in the network at any time and may have different durations. Moreover, assignment of nodes to missions must consider the fact that each node may offer support to

different missions with different levels of accuracy and fit. In this context, assigning sensor resources to missions in an optimal way poses a significant challenge. Different versions of this problem have been addressed for traditional battery-powered WSNs by prior works, including [18, 19, 20]. Some previous solutions are energy aware [21], in the sense that they take into account the node residual energy to decide mission assignments. In doing so, however, they make the specific assumption that energy is monotonically decreasing, as is typical with a battery, and therefore residual energy is the only criterion for assigning missions. We argue that for energy-harvesting networks new paradigms for mission assignments are needed, which take into account that nodes currently having little or no energy left might have enough in the future to carry out new missions. These solutions should also consider that energy availability is time-dependent and that energy storage is limited in size and time. Our contribution to this topic is presented in Chapter 4, in which we propose an analytical model and a distributed solution, called *EN-MASSE*, for sensor-mission assignment in WSNs with energy harvesting. Our problem formulation captures advanced real-life details of the behavior of a typical energy harvesting subsystem, and it provides upper bounds on the optimal solution for real-life sized instances, consisting of hundreds of nodes and with target lifetimes of several months. Despite the theoretical difficulty of the general sensor-mission assignment problem, our distributed scheme, *EN-MASSE*, is shown to perform very close to the optimum provided by the analytical formulation. Moreover, *EN-MASSE* significantly outperforms other harvesting-unaware assignment schemes. By comparing mission assignment schemes in several different scenarios, we demonstrate that traditional assignment algorithms cannot harness the full potential provided by the harvesting technology, which is instead taken into account efficiently by our proposed scheme. Finally, we experimentally validate *EN-MASSE* and the accuracy of the energy models we used in simulations in a testbed of Telos B motes powered by energy harvesting. The work discussed in Chapter 4 has been presented in [7]. An earlier version of this work also appears in [5].

Application scenarios of WSNs with energy harvesting capabilities are ever increasing, and in many of them ensuring reliable security support is a critical requirement. In health care and assisted living applications, in particular, providing reliable mechanisms to duly control access to the collected (sensitive) data is of paramount importance. In Chapter 5 we study how to exploit the opportunities provided by energy harvesting to support extremely powerful, but complex, fine-grained data-centric access control mechanisms. In particular, we focus on multi-authority Ciphertext Policy Attribute Based Encryption (CP-ABE) schemes, which are particularly well-suited for WSN scenarios, since they do not require any server-based access control infrastructure. Unfortunately, as we concretely show by a proof-of-concept implementation carried out on TelosB and MicaZ motes, the energy toll of state-of-the-art multi-authority CP-ABE schemes is still critical for traditional battery-powered WSNs, due to the severe energy limitation of the wireless motes. Energy harvesting, however, opens up new opportunities: to mitigate the relatively large energy consumption of the CP-ABE cryptographic operations we propose *AGREE* (Access control for GREEN wireless sensor networks). *AGREE* is a framework that exploits energy harvesting to pre-compute and cache suitably chosen CP-ABE-encrypted keys, so as to minimize the need to perform CP-ABE encryptions when no energy from harvesting is available. We assess the performance of *AGREE* by means of simulation and actual implementation, and by validating its operation with real-world energy-harvesting traces collected indoor by Telos B motes equipped with photovoltaic cells, as well as publicly available traces of radiant light energy. Our results, also presented in [1], show that complex security mechanisms may become significantly less demanding when implemented so as to take advantage of energy harvesting opportunities.



## LIST OF PUBLICATIONS

The following list summarizes the accepted and submitted publications that constitute the basis of this thesis. For each work, the pertinent chapter is reported in brackets.

- S. Basagni, M. Y. Naderi, C. Petrioli, and D. Spenza, “Wireless sensor networks with energy harvesting”. In *Mobile Ad Hoc Networking: The Cutting Edge Directions* (Chapter 20), IEEE Series on Digital and Mobile Communication. Hoboken, NJ: John Wiley and Sons, Inc., 2013.  
(Chapter 1)
- A. Cammarano, C. Petrioli, and D. Spenza, “Pro-Energy: a novel energy prediction model for solar and wind energy harvesting WSNs”. In *Proceedings of the 9th IEEE International Conference on Mobile Ad hoc and Sensor Systems, IEEE MASS 2012*, Las Vegas, Nevada, October 8-11 2012.  
(Chapter 2)
- A. Cammarano, D. Spenza, and C. Petrioli, “Energy-harvesting WSNs for structural health monitoring of underground train tunnels”. In *The 32nd IEEE International Conference on Computer Communications, IEEE INFOCOM 2013, Student Session*, Torino, Italy, 14-19 April 2013, **Best Student Poster**. Accepted for publication in the Workshop proceedings.  
(Chapter 3)
- D. Porcarelli, D. Spenza, D. Brunelli, A. Cammarano, C. Petrioli, and L. Benini, “Adaptive rectifier driven by power intake predictors for energy harvesting sensor networks,” *IEEE Journal of Emerging and Selected Topics in Power Electronics*, 2014, To appear.  
(Chapter 3)
- T. La Porta, C. Petrioli, and D. Spenza, “Sensor-mission assignment in wireless sensor networks with energy harvesting”. In *Proceedings of the 8th Annual IEEE Communications Society Conference on Sensor, Mesh and Ad Hoc Communications and Networks, IEEE SECON 2011*, Salt Lake City, UT, June 27-30, 2011, pp. 413–421.  
(Chapter 4)
- T. La Porta, C. Petrioli, C. Phillips, and D. Spenza, “Sensor-mission assignment in rechargeable wireless sensor networks,” *ACM Transactions on Sensor Networks*, 2014, To appear.  
(Chapter 4)
- G. Bianchi, A. T. Caposelle, C. Petrioli, and D. Spenza, “AGREE: exploiting energy harvesting to support data-centric access control in WSNs”. Accepted for publication in *Elsevier Ad Hoc Networks, Special Issue on Security, Privacy and Trust Management in the Internet of Things Era (SePriT)*, 2013.  
(Chapter 5)



---

## REVIEW OF WIRELESS SENSOR NETWORKS WITH ENERGY HARVESTING

Wireless sensor networks have played a major role in the research field of multi-hop wireless networks as enablers of applications ranging from environmental and structural monitoring to border security and human health control. Research within this field has covered a wide spectrum of topics, leading to advances in node hardware, protocol stack design, localization and tracking techniques and energy management [22].

Research on WSNs has been driven (and somewhat limited) by a common focus: Energy efficiency. Nodes of a WSN are typically powered by batteries. Once their energy is depleted, the node is “dead.” Only in very particular applications batteries can be replaced or recharged. However, even when this is possible, the replacement/recharging operation is slow and expensive, and decreases network performance. Different techniques have therefore been proposed to slow down the depletion of battery energy, which include power control and the use of *duty cycle*-based operation. The latter technique exploits the low power modes of wireless transceivers, whose components can be switched off for energy saving. When the node is in a low power (or “sleep”) mode its consumption is significantly lower than when the transceiver is on [23, 24]. However, when asleep the node cannot transmit or receive packets. The duty cycle expresses the ratio between the time when the node is on and the sum of the times when the node is on and asleep. Adopting protocols that operate at very low duty cycles is the leading type of solution for enabling long lasting WSNs [25]. However, this approach suffers from two main drawbacks. 1) There is an inherent tradeoff between energy efficiency (i.e., low duty cycling) and data latency, and 2) battery operated WSNs fail to provide the needed answer to the requirements of many emerging applications that demand network lifetimes of decades or more. For these reasons recent research on long-lasting WSNs is taking a different approach, proposing energy harvesters combined with the use of rechargeable batteries and super capacitors (for energy storage) as the key enabler to “perpetual” WSN operations. By endowing WSN nodes with the capability of extracting energy from the surrounding environment, *energy-harvesting wireless sensors networks* (EHWSNs) can be realized.

This chapter explores the background, opportunities and challenges of EHWSNs. The general architecture of the energy subsystem of a EHWSNs is described in Section 1.1, including models for the harvesting hardware and for batteries. The various forms of energy that are available and ways for harvesting them are presented in Section 1.2. Models for predicting availability of wind and solar energy are described in Section 1.3. Finally, section 1.4 surveys some of power management and task scheduling solutions for energy harvesting networks that have been recently proposed in the literature.

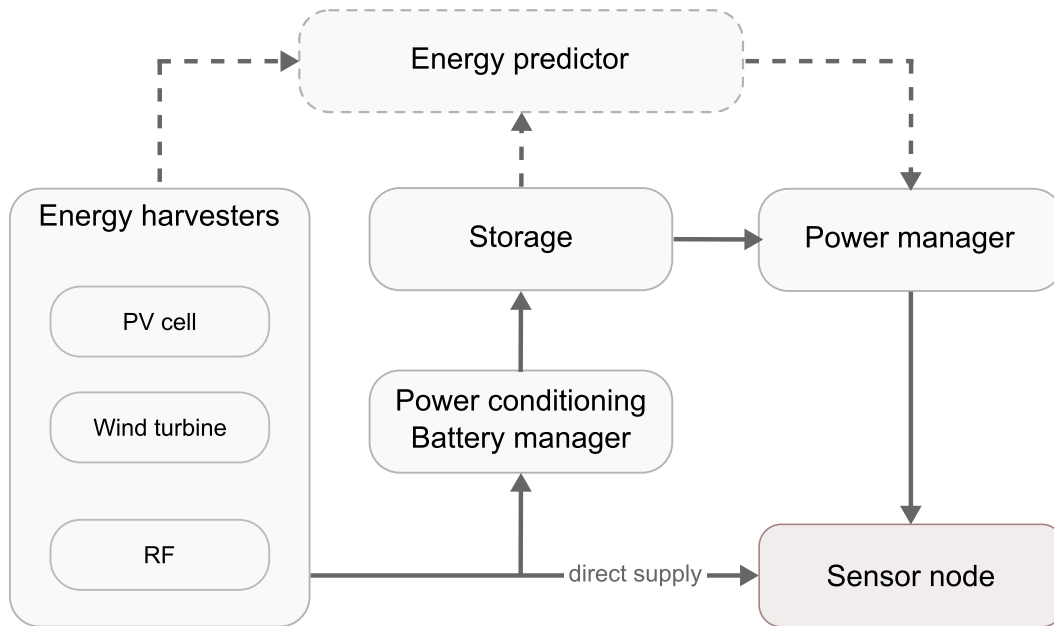


Figure 1.1: General architecture of the energy subsystem of a wireless sensor node with energy harvesting capabilities.

### 1.1 ENERGY HARVESTING ARCHITECTURES

The general architecture of the energy subsystem of a wireless sensor node with energy harvesting capabilities is shown in Figure 1.1.

The energy subsystem includes one or multiple harvesters that convert energy available from the environment to electrical energy. The energy obtained by the harvester may be used to directly supply energy to the node, or it may be stored for later use. Although in some applications it is possible to directly power the sensor node using the harvested energy, with no energy storage (*harvest-use* architecture [17]), in general this is not a viable solution. In fact, the energy source needs to be available when the device is operational, which can be an unrealistic assumption. Additionally, every fluctuation in the power level emitted by the source will immediately affect the operation of the node. In particular, if the amount of energy harvested is close to the minimum operational point of the node, every variation might cause the sensor node to oscillate between active and inactive states. Moreover, harvested energy will be wasted either when it is greater than zero, but not enough to power the sensor node, or when it is greater than the energy required by the node. Finally, in many application scenarios, the power emitted by the environmental source is typically too low to directly power a sensor node. A more reasonable architecture enables the node to directly use the harvested energy, but also includes a storage component that acts as an energy buffer for the system, with the main purpose of accumulating and preserving the harvested energy. When the harvesting rate is greater than the current usage, the buffer component can store excess energy for later use (e.g., when harvesting opportunities do not exist), thus supporting variations in the power level emitted by the environmental source.

The two alternatives commonly used for energy storage are *secondary rechargeable batteries* and *supercapacitors* (also known as ultracapacitors). Supercapacitors are similar to regular capacitors, but they offer very high capacitance in a small size. They have several advantages with respect to rechargeable batteries [26]. First of all, supercapacitors can be recharged and discharged virtually an unlimited number of times, while typical lifetimes of an electrochemical battery is less than 1000 cycles [15]. Second, they can be charged quickly using simple

charging circuits, thus reducing system complexity, and do not need full-charge or deep-discharge protection circuits. They also have higher charging and discharging efficiency than electrochemical batteries [26]. Another additional benefit is the reduction of environmental issues related to battery disposal. Thanks to these characteristics, many platforms with harvesting capabilities use supercapacitors as energy storage, either by themselves [27, 28] or in combination with batteries [29, 30, 31]. Other systems, instead, focus on platforms using only rechargeable batteries [32, 33, 34].

Both types of storage devices deviate from ideal energy buffers in a number of ways: They have a finite size  $B^{Max}$  and can hold a finite amount of energy; they have a charging efficiency  $\eta_c < 1$  and a discharging efficiency  $\eta_d < 1$ , i.e., some energy is lost while charging and discharging the buffer, and they suffer from leakage and self-discharge, i.e., some stored energy is lost even if the buffer is not in use. Leakage and self-discharge are phenomena that affect both batteries and supercapacitors. All batteries suffer from self-discharge: A cell that simply sits on the shelf, without any connection between the electrodes, experiences a reduction in its stored charge due to internal chemical reactions, at a rate depending on the cell chemistry and the temperature. A similar phenomenon affects electrochemical super-capacitors in the charged state. They suffer gradual loss of energy and reduction of the inter-plate voltage. In order to reduce the energy lost through buffer inefficiencies, many platforms allow the node to directly use the energy harvested. In particular, if the current energy consumption is greater than or equal to the energy currently harvested, then the node can use the harvested energy for its operations. This is the most efficient way of using the environmental energy, because it is used directly and there is no energy loss. Otherwise, if the amount of energy harvested is greater than the current energy consumption, some energy is directly used to sustain the node operations, while excess energy is stored in the buffer for later use.

**Supercapacitor leakage models** Considering leakage current is important while dealing with energy harvesting systems, especially if the application scenario requires the harvested energy to be stored for long periods of time. In general, if the energy source is sporadic or if it is only able to provide a small amount of energy, the portion of the harvested energy lost due to leakage may be significant. The leakage is of particular relevance for supercapacitors, because their energy density is about one orders of magnitude lower than that of an electrochemical battery, but they suffer from considerably higher self-discharge. A supercapacitor leakage is strongly variable and depends on several factors, including the capacitance value of the supercapacitor, the amount of energy stored, the operating temperature, the charge duration, etc. For this reason, the leakage pattern of a particular supercapacitor must often be determined experimentally [30, 35, 26]. Additionally, the leakage current varies with time: It is considerably higher immediately after the supercapacitor has been charged, then it decreases to a plateau.

Several models for the leakage from a charged supercapacitor have been proposed in the literature, modeling the leakage as a constant current [36], or as an exponential function of the current supercapacitor voltage [37], or by using a polynomial approximation of its empirical leakage pattern [35], or, finally, by using a piecewise linear approximation of its empirical leakage pattern [26]. These models have been proposed after experimental observations of actual supercapacitor leakage, such as those shown in Figure 1.2 showing the self-discharge experienced by a charged 25F supercapacitor over a two-weeks period.

Another aspect to consider in the supercapacitors vs. battery comparison is that in many application scenarios it is not possible to use the full energy stored in the supercapacitor. The voltage of a supercapacitor drops from full voltage to zero linearly, without the flat curve that is typical of most electrochemical batteries. The fraction of the charge available to the sensor node depends on the voltage requirements of the platform. For example, a Telos B

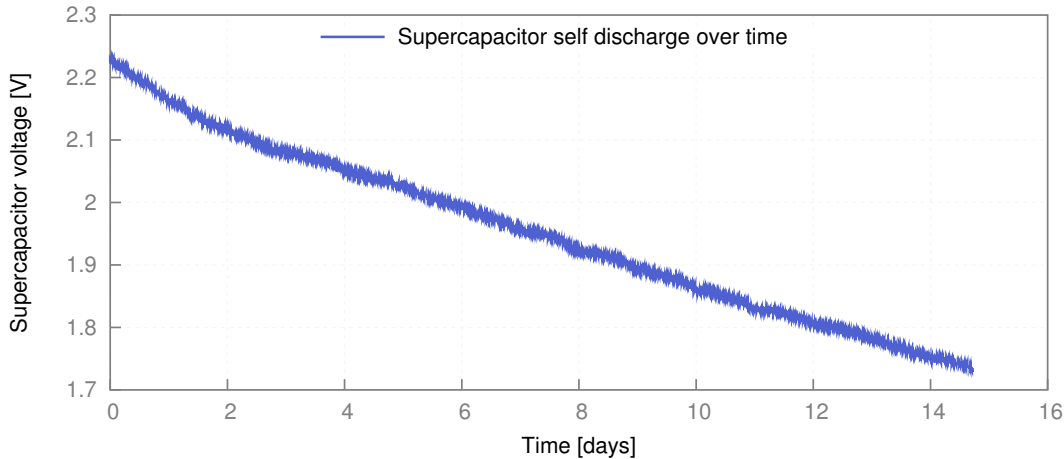


Figure 1.2: Self discharge of a supercapacitor over time.

note requires a minimal voltage ranging from 1.8 V to 2.1 V. When the supercapacitor voltage drops below this threshold, its residual energy can no longer be used to power the node. This aspect may be partially mitigated by using a DC-DC converter to increase the voltage range, at the cost of introducing inefficiencies and an additional source of power consumption.

**Battery models** Batteries are usually seen as ideal energy storage devices, containing a given amount of energy units. Executing a node operation, e.g., sending or receiving a packet, uses a certain amount of energy units, depending on the energy cost of the operation. Battery charge is assumed to be decreased of the amount of energy required by an operation only when the operation is performed. Real batteries, however, operate differently. As mentioned earlier, all batteries suffer from self-discharge. Even a cell that is not being used experiences a charge reduction caused by internal chemical activity. Batteries also have charge and discharge efficiency strictly  $< 1$ , i.e., some energy is lost when charging and discharging the battery. Additionally, batteries have some non-linear properties [15, 38]. These are: *Rate-dependent capacity*, i.e., the delivered capacity of a battery decreases, in a non-linear way, as the discharge rate increases; *temperature effect*, in that the operating temperature affects the battery discharge behavior and directly impacts the rate of self-discharge; *recovery effect*, for which the lifetime and the delivered capacity of a battery increases if discharge and idle periods alternate (pulse discharge). Furthermore, rechargeable batteries experience a reduction of their capacity at each recharge cycle, and their voltage depends on the charging level of the battery and varies during discharge. These characteristics should be taken into account when dimensioning and simulating energy harvesting systems, because they can easily lead to wrong estimations of the battery lifetime. For example, if the harvesting subsystem uses a rechargeable battery to store the energy harvested from the environment, it is important to consider that the reduction in capacity experienced by the battery at each recharge cycle is likely to reduce both its delivered capacity and its lifetime.

Many types of battery models have been proposed recently in the literature [39]. These include: *Physical models* that simulate the physical processes that take place into an electrochemical battery. These models are usually very accurate, but have high computational complexity and require high configuration effort [40, 41]. *Empirical models* that approximate the discharge behavior of a battery with simple equations. They are generally the least accurate. However, they require low computational resources and configuration effort [42, 43]. *Abstract models* that emulate battery behavior by using simplified equivalent representation, such as stochastic system [44], electrical-circuit models [45, 46], and discrete-time VHDL specification [47], and *mixed models* that use both a high-level representation of a battery

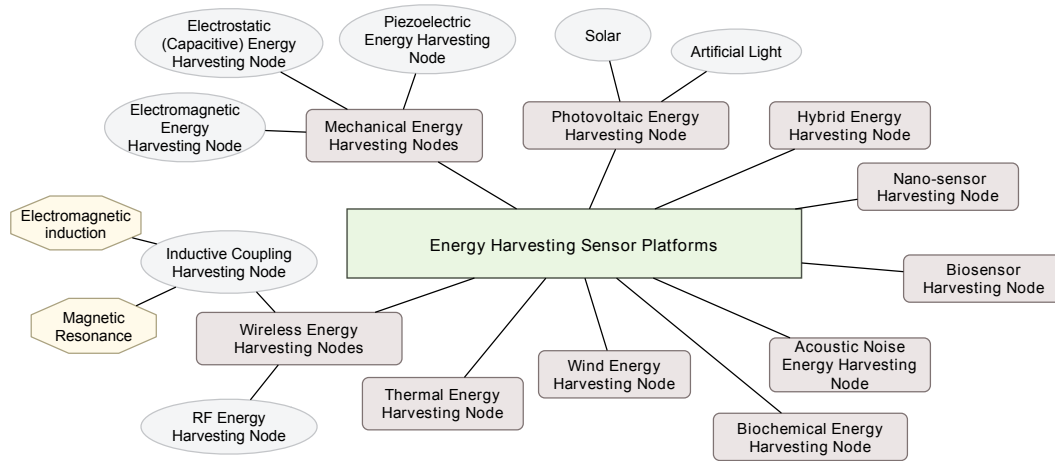


Figure 1.3: Different energy types (rectangles) and sources (ovals).

(simpler than a real battery) and analytical expressions based on low-level analysis and physical laws [48].

## 1.2 TECHNIQUES OF ENERGY HARVESTING

Figure 1.3 shows the variety of energy types that can be harvested. In this section we provide their brief description and relevant references.

**Mechanical energy harvesting** indicates the process of converting mechanical energy into electricity by using vibrations, mechanical stress and pressure, strain from the surface of the sensor, high-pressure motors, waste rotational movements, fluid, and force. The principle behind mechanical energy harvesting is to convert the energy of the displacements and oscillations of a spring-mounted mass component inside the harvester into electrical energy [49, 50]. Mechanical energy harvesting can be: *Piezoelectric*, *electrostatic* and *electromagnetic*.

*Piezoelectric energy harvesting* is based on the piezoelectric effect for which mechanical energy from pressure, force or vibrations is transformed into electrical power by straining a piezoelectric material. The technology of a piezoelectric harvester is usually based on a cantilever structure with a seismic mass attached into a piezoelectric beam that has contacts on both sides of the piezoelectric material [50]. In particular, strains in the piezoelectric material produce charge separation across the harvester, creating an electric field, and hence voltage, proportional to the stress generated [51, 52]. Voltage varies depending on the strain and time, and an irregular AC signal is produced. Piezoelectric energy conversion has the advantage that it generates the desired voltage directly, without need for a separate voltage source. However, piezoelectric materials are breakable and can suffer from charge leakage [53, 50]. Examples of piezoelectric energy harvesters can be found in [54, 55, 56, 57, 58] and references therein.

The principle of *electrostatic energy harvesting* is based on changing the capacitance of a vibration dependent variable capacitor [59, 60]. In order to harvest the mechanical energy a variable capacitor is created by opposing two plates, one fixed and one moving, and is initially charged. When vibrations separate the plates, mechanical energy is transformed into electrical energy from the capacitance change. This kind of harvesters can be incorporated into microelectronic-devices due to their integrated circuit-compatible nature [61]. However, an additional voltage source is required to initially charge the capacitor [53]. Recent efforts to prototype sensor-size electrostatic energy harvesters can be found in [62, 63].

*Electromagnetic energy harvesting* is based on Faraday's law of electromagnetic induction. An electromagnetic harvester uses an inductive spring mass system for converting mechanical energy to electrical. It induces voltage by moving a mass of magnetic material through a magnetic field created by a stationary magnet. Specifically, vibration of the magnet attached to the spring inside a coil changes the flux and produces an induced voltage [59, 50, 51]. The advantages of this method include the absence of mechanical contact between parts and of a separate voltage source, which improves the reliability and reduce the mechanical damping in this type of harvesters [64, 60]. However, it is difficult to integrate them in sensor nodes because of the large size of electromagnetic materials [64]. Some examples of electromagnetic energy harvesting systems are presented in [65, 66].

**Photovoltaic energy harvesting** is the process of converting incoming photons from sources such as solar or artificial light into electricity. Photovoltaic energy can be harnessed by using photovoltaic (PV) cells. These consist of two different types of semiconducting materials: *n-type* and *p-type*. An electrical field is formed in the area of contact between these two materials, called the P-N junction. Upon exposure to light a photovoltaic cell releases electrons. Photovoltaic energy conversion is a traditional, mature, and commercially established energy-harvesting technology. It provides higher power output levels compared to other energy harvesting techniques and is suitable for larger-scale energy harvesting systems. However, its generated power and the system efficiency strongly depend on the availability of light and on environmental conditions. Other factors, including the materials used for the photovoltaic cell, affect the efficiency and level of power produced by photovoltaic energy harvesters [34]. Some recent prototypes of photovoltaic harvesters are described in [67, 68, 69]. Known implementations of solar energy harvesting sensor nodes include Fleck [70], Enviro-mote [71], Trio [29], Everlast [28], and Solar Biscuit [72]. Another relevant example is Solar Dust [73], a hybrid multi-channel energy-harvesting and sensing device that monitors the incident light over time by means of solar cells, which are also used to scavenge energy to power the mote.

**Thermal energy harvesting** is implemented by *thermoelectric energy harvesting* and *pyroelectric energy harvesting*.

*Thermoelectric energy harvesting* is the process of creating electric energy from temperature difference (thermal gradients) using thermoelectric power generators (TEGs). The core element of a TEG is a thermopile formed by arrays of two dissimilar conductors, i.e., a p-type and n-type semiconductor (thermocouple), placed between a hot and a cold plate and connected in series. A thermoelectric harvester scavenges the energy based on the Seebeck effect, which states that electrical voltage is produced when two dissimilar metals joined at two junctions are kept at different temperatures [74]. This is because the metals respond differently to the temperature difference, creating heat flow through the thermoelectric generator. This produces a voltage difference that is proportional to the temperature difference between the hot and cold plates. The thermal energy is converted into electrical power when a thermal gradient is created. Energy is harvested as long as the temperature difference is maintained.

*Pyroelectric energy harvesting* is the process of generating voltage by heating or cooling pyroelectric materials. These materials do not need a temperature gradient similar to a thermocouple. Instead, they need time-varying temperature changes. Changes in temperature modify the locations of the atoms in the crystal structure of the pyroelectric material, which produces voltage. To keep generating power, the whole crystal should be continuously subject to temperature change. Otherwise, the produced pyroelectric voltage gradually disappears due to leakage current [75].

Pyroelectric energy harvesting achieves greater efficiency compared to thermoelectric harvesting. It supports harvesting from high temperature sources, and is much easier to get to work



using limited surface heat exchange. On the other hand, thermoelectric energy harvesting provides higher harvested energy levels. The maximum efficiency of thermal energy harvesting is limited by the Carnot cycle [59]. Because of the various sizes of thermal harvesters, they can be placed on the human body, on structures and equipment. Some example of this kind of harvesters for WSN nodes are described in [76, 77].

**Wireless energy harvesting** techniques can be categorized into two main categories: *RF energy harvesting* and *resonant energy harvesting*.

*RF energy harvesting* is the process of converting electromagnetic waves into electricity by a rectifying antenna, or *rectenna*. Energy can be harvested from either ambient RF power from sources such as radio and television broadcasting, cellphones, WiFi communications and microwaves, or from EM signals generated at a specific wavelength. Although there is a large number of potential ambient RF power, the energy of existing EM waves are extremely low because energy rapidly decreases as the signal spreads farther from the source. Therefore, in order to scavenge RF energy efficiently from existing ambient waves, the harvester must remain close to the RF source. Another possible solution is to use a dedicated RF transmitter to generate more powerful EM signals merely for the purpose of powering sensor nodes. Such RF energy harvesting is able to efficiently delivers powers from micro-watts to few milliwatts, depending on the distance between the RF transmitter and the harvester.

A notable application of RF energy harvesting is the realization of passive wake-up radios that can wake up sensor nodes in deep sleep state upon request. For example, the passive radio-triggered circuit proposed by Lin and Stankovic in [78] uses the power scavenged from wireless messages to wake up a node by triggering an interrupt. In [79], Chen et al. describes an energy harvester circuit combined with an ultra-low-power pulse generator that can trigger the wake-up of a mote.

*Resonant energy harvesting*, also called resonant inductive coupling, is the process of transferring and harvesting electrical energy between two coils, which are highly resonant at the same frequency. Specifically, an external inductive transformer device, coupled to a primary coil, can send power through the air to a device equipped with a secondary coil. The primary coil produces a time-varying magnetic flux that crosses the secondary coil, inducing a voltage. In general, there are two possible implementations of resonant inductive coupling: Weak inductive coupling and strong inductive coupling. In the first case, the distance between the coils must be very small (few centimeters). However, if the receiving coil is properly tuned to match the external powered coil, a “strong coupling” between electromagnetic resonant devices can be established and powering is possible over longer distances. Note that since the primary and secondary coil are not physically connected, resonant inductive coupling is considered a wireless energy harvesting technique.

Some recent implementations of wireless energy harvesting techniques for WSNs can be found in [80, 81, 82].

**Wind energy harvesting** is the process of converting energy from air-flows (e.g., wind) into electrical energy. A properly sized wind turbine is used to exploit linear motion coming from wind for generating electrical energy. Efficient design of small-scale wind energy harvesters is still an ongoing research, challenged by very low flow rates, fluctuations in wind strength and unpredictability of flow sources. In fact, even though the performance of large-scale wind turbines is highly efficient, small-scale wind turbines show inferior efficiency due to the relatively high viscous drag on the blades at low Reynolds numbers [83, 49]. Recent examples of wind energy harvesting systems designed for WSNs include [84, 85, 86].

Table 1.1: Power density and efficiency of energy harvesting techniques.

Harvesting technique	Power density	Efficiency
Photovoltaic	Outdoors (direct sun): $15 \text{ mW/cm}^2$	Highest: $32 \pm 1.5\%$
	Outdoors (cloudy day): $0.15 \text{ mW/cm}^2$	Typical: $25 \pm 1.5\%$ [97]
	Indoors: $<10 \text{ } \mu\text{W/cm}^2$ [98, 64, 53, 99]	
Thermoelectric	Human: $30 \text{ } \mu\text{W/cm}^2$	$\pm 0.1\%$
	Industrial: 1 to $10 \text{ mW/cm}^2$ [100, 99]	$\pm 3\%$ [99]
Pyroelectric	$8.64 \text{ } \mu\text{W/cm}^2$ at the temperature rate of $8.5^\circ \text{ C/s}$ [101]	$3.5\%$ [102]
Piezoelectric	$250 \text{ } \mu\text{W/cm}^3$	<sup>a</sup>
	$330 \text{ } \mu\text{W/cm}^3$ (shoe inserts) [64, 53]	
Electromagnetic	Human motion: 1 to $4 \text{ } \mu\text{W/cm}^3$ [103, 86]	<sup>a</sup>
	Industrial: $306 \text{ } \mu\text{W/cm}^3$ [104], $800 \text{ } \mu\text{W/cm}^3$ [86]	
Electrostatic	50 to $100 \text{ } \mu\text{W/cm}^3$ [51]	<sup>a</sup>
RF	GSM 900/1800 MHz: $0.1 \text{ } \mu\text{W/cm}^2$	$50\%$ <sup>b</sup> [105]
	WiFi 2.4 GHz: $0.01 \text{ } \mu\text{W/cm}^2$ [98]	
Wind	$380 \text{ } \mu\text{W/cm}^3$ at the speed of 5 m/s [56, 106]	$5\%$ [56]
Acoustic noise	$0.96 \text{ } \mu\text{W/cm}^3$ at 100 dB	<sup>c</sup>
	$0.003 \text{ } \mu\text{W/cm}^3$ at 75 dB [107, 34]	

<sup>a</sup> Maximum power and efficiency are source dependent.

<sup>b</sup> Excluding transmission efficiency.

<sup>c</sup> Noise power densities are theoretical values.

**Biochemical energy harvesting** is the process of converting oxygen and endogenous substances into electricity via electrochemical reactions [87, 88]. In particular, biofuel cells acting as active enzymes and catalysts can be used to harvest the biochemical energy in biofluid into electrical energy. Human body fluids include many kinds of substances that have harvesting potential [89]. Among these, glucose is the most common used fuel source. It theoretically releases 24 free electrons per molecule when oxidized into carbon dioxide and water. Even though biochemical energy harvesting can be superior to other energy harvesting techniques in terms of continuous power output and biocompatibility [87], its performance depends on the type and availability of fuel cells. Advantages and disadvantages of using enzymatic fuel cells for energy production are described in [90]. Research efforts such as [91, 87, 88] are examples of recent proposed prototypes that use biochemical energy harvesting to power microelectronic devices.

**Acoustic energy harvesting** is the process of converting high and continuous acoustic waves from the environment into electrical energy by using an acoustic transducer or resonator. The harvestable acoustic emissions can be in the form of longitudinal, transverse, bending, and hydrostatic waves ranging from very low to high frequencies [92]. Typically, acoustic energy harvesting is used where local long term power is not available, as in the case of remote or isolated locations, or where cabling and electrical commutations are difficult to use such as inside sealed or rotating systems [93, 92]. However, the efficiency of harvested acoustic power is low and such energy can only be harvested in very noisy environments. Harvestable energy from acoustic waves theoretically yields  $0.96 \mu\text{W/cm}^3$  [94], which is much lower than what is achievable by other energy harvesting techniques. As such, limited research has been performed to investigate this type of harvesters. Examples of acoustic energy harvesting systems can be found in [95, 96].

All previously described harvesting techniques can be combined and concurrently used on a single platform (**hybrid energy harvesting**).

A bird's eye view of the amount of energy harvestable from different sources is given in Table 1.1. For each energy harvesting technique we show its *power density* and *conversion efficiency*. The power density expresses the harvested energy per unit volume, area, or mass. Common unit measures of power density include watts per square centimeter and watts per

cubic centimeter. Conversion efficiency is defined as the ratio of the harvested electrical power to the harvestable input power. The energy conversion efficiency is a dimensionless number between 0 and 100%.

### 1.3 ENERGY PREDICTION MODELS

Practical use of energy harvesting technologies needs to deal with the variable behavior of the energy sources, which impose the amount and the rate of the harvested energy over time. In case of predictable, non controllable power sources, such as the solar one, energy prediction methods can be used to forecast the source availability and estimate the expected energy intake [36]. Such a predictor can alleviate the problem of the harvested power being neither constant nor continuous, allowing the system to take critical decisions about the utilization of the available energy. In this section, we give an overview of the different energy predictors proposed in the literature for two popular forms of energy harvesters, namely, solar and wind harvesters.

The Exponentially Weighted Moving-Average (EWMA) algorithm is a widely used solar energy prediction scheme proposed by Kansal et al. in [36], which is based on an exponentially weighted moving-average filter [108]. EWMA relies on the assumption that the energy available at a given time of the day is similar to the energy generation observed at the same time on the previous days. The amount of energy available during the past days is maintained as a weighted average, in which the contribution of older data is exponentially decaying. This approach is able to both exploit the diurnal cycle in solar energy and to adapt to seasonal variations, but leads to significant prediction errors in case of frequently changing weather conditions, i.e. when sunny and cloudy days are mixed.

In order to address this problem, a new estimation method, the Weather-Conditioned Moving Average (WCMA), has been proposed by Piorno et al. in [109]. The high prediction errors shown by EWMA when sunny and cloudy days alternate is due to the high impact that the weather conditions of the previous day have when estimating the energy generation for the current day. The WCMA prediction algorithm avoids this effect by taking into account, when computing the prediction for a given timeslot, the average energy availability experienced in that slot in the previous days. Such average value is then scaled according to a weighting factor indicating how the weather conditions of the current day changed with respect to the previous days. In case of frequently changing weather conditions, WCMA is shown to obtain average prediction errors almost 20% smaller than EWMA.

Another estimation method based on a weighted sum of historical data is presented by Moser et al. in [110], to provide information to a predictive controller able to adapt parameters of an application. Their prediction algorithm assumes the solar power to be periodic on a daily basis. To estimate the energy which will be harvested in the next time interval it combines the value of the energy harvested during the current time interval with the energy harvested in the past (whose age is a multiple of days). As for EWMA, the contribution of older data is exponentially decaying. In [111], this predictor is shown to often result in underestimation of the forecast values, thus in high prediction errors.

The solution proposed by Noh et al. in [112] is similar to previous approaches. They use the EWMA model to keep track of the solar energy profile observed in the past. In order to account for short-term varying weather conditions, they also introduce a scaling factor to adjust future energy expectations. At the end of each slot, scaling is performed by computing the ratio between the actual energy harvested during the current timeslot and the energy predicted for the same timeslot, appropriately scaled for future timeslots that are far away in time.

Lu et al. addressed the problem of energy-harvesting prediction for real-time embedded systems (RTES) in [113]. They argue that accurate prediction of the energy intake in the near future is crucial for RTES, as the performance of optimization techniques depends on harvesting predictions. Thus, they investigate three common techniques in real time series prediction (regression analysis, moving average and exponential smoothing), showing that regression analysis has the best accuracy for energy predictions within a time horizon of 1 second. Their approach, however, works well for real-time energy predictions, but it is not designed for medium-term prediction horizons.

A completely different approach is proposed by Sharma et al. in [114]. The authors explore a system for solar and wind powered sensor node that is able to derive energy harvesting predictions based on weather forecast. More in detail, they observe that, when predicting energy availability at timescales between 3 hour to 3 days, using forecasting data provides higher accuracy than calculating energy predictions based on past observation. The reason they give for the scarce performance of traditional predictors is the fact that weather patterns are not consistent in many regions of the United States. They thus formulate a model for solar panel and wind turbine that is able to convert weather forecast data into energy harvesting predictions. However, they compare the performance of their solution with simple energy predictors based on past observations; a comparison with state-of-the-art solutions is not presented. Beyond being applicable only in some application scenarios, periodic forecast transmissions introduce an overhead that impacts on network lifetime.

#### 1.4 POWER MANAGEMENT AND TASK SCHEDULING IN EHWSNS

Environmentally-powered systems have the potential for unlimited lifetime, but the great variability of environmental energy sources and their unpredictable nature poses new challenges in terms of energy management. New harvesting-aware power management and task scheduling techniques are thus required for network performance, lifetime enhancement and full exploitation of energy recharging opportunities.

Power management policies that allow rechargeable nodes to achieve near perpetual lifetime have been proposed in [36, 115, 116]. The main idea of such works is to dynamically adapt the duty cycle of the nodes according to the environmental power conditions, in order to achieve the so called *energy-neutral* (ENO) mode, in which nodes consume only as much energy as harvested. Although effective in many application, such duty-cycle-based approach, however, is not sufficient for complex system in which more sophisticated task scheduling techniques are required. The problem of how to schedule local tasks of nodes while dealing with uncertainty in energy availability is thus an active area of research.

One of the earliest works in task scheduling for energy-harvesting WSNs is the *Lazy Scheduling algorithm* (LSA) [117]. LSA dynamically schedules tasks depending on the future energy availability, the capacity of the energy storage, the residual energy, and the maximum power consumption of the sensor node. To determine the schedulability of a set of tasks, LSA introduces the concept of energy variability characterization curve (EVCC), which captures the dynamics of the energy source. More specifically, the LSA uses an offline schedulability test that, given the EVCC of the energy source, the capacity of the energy storage, and the maximum power requirement of a running task, determines whether all the deadlines of a given set of tasks can be met or not. LSA suffers from several drawbacks. For instance, in realistic application a task actual energy consumption does not depend on the worst case energy demand, but rather on factors including the sensor operational state and the circuitry used to perform the task. Furthermore, LSA does not consider dependency among tasks. Finally, the performance of LSA is highly dependent on the accuracy of predicted available energy, which is challenging and prone to errors.

The *STAM-STFU* protocol by Audet et al. [118] combines the operation of two scheduling algorithms, namely, Smooth to Average Method (STAM) and Smooth to Full Utilization (STFU), for scheduling a set of tasks offline, with the aim of reducing the total task deadline violations. STAM-STFU introduces the concept of virtual tasks to smooth out the energy consumption in the long run. Each real (physical) task has a corresponding virtual task that has the same arrival time, but equal or longer duration, and equal or smaller energy demand. Virtual tasks are distributed over a longer execution time than their real counterparts, but each consumes the same amount of energy as its corresponding real task, such that any scheduling for virtual tasks that meets the deadline constraints will not violate the deadline of any real task. STAM-STFU smooths out real task consumption to approximately the average power required by all tasks and then schedules them by using the Earliest Deadline First algorithm. Simulation results show that the performance of STAM-STFU are similar to that of LSA, with the additional benefit of not requiring an energy prediction model. However, STAM-STFU is only suitable for offline scheduling, which requires that tasks and their deadlines are known in advance.

The goal of the *multi-version scheduling algorithm* [119] is to execute the most important and valuable periodic tasks while meeting all the timing and energy constraints. Each task is assumed to have multiple versions, each with different characteristics and reward. “Easier” versions of a task execute faster, require less energy, and produce less accurate and valuable results. This static (offline) scheduling solution determines the best task versions and their execution speeds that maximize rewards. Selection is based on worst case scenario assumptions, i.e., the worst-case task execution times, worst-case number of speed changes, minimum harvesting rate, and worst-case battery discharging rates, are assumed and known in advance. However, a system does not always consume or harvest energy as in the worst-case, and often time the selection of tasks is not optimal. To obviate to this problem, the authors propose dynamic algorithms according to which the node periodically check the current energy storage and accordingly reschedule the tasks.

In [120] EL Ghor et al. describe an on-line scheduling algorithm, called *EDeg* (Earliest Deadline with energy guarantee), a variant of the Earliest Deadline First algorithm. EDeg maintains energy neutrality by making sure that before a task is started sufficient energy is in storage for all future occurring tasks. This protocol assumes that future task arrival times are known. Task execution is delayed until recharging has produced enough energy to meet the task deadline. When the stored energy drops below a threshold EDeg stops the current tasks and starts recharging the battery up to a level that support task completion. Thus, tasks never run in absence of enough energy. The requirement to know in advance the arrival times, the deadlines, and the energy demands of the tasks, seriously limits the applicability of this algorithm in real-life application scenarios.

Steck et al. [121] present a *task utility scheduling* protocol with two main goals: First, given a certain level of utility, determine the expected execution time and energy consumption of a set of tasks. Second, given a time constraint, find the maximum achievable utility for the set of tasks. This algorithm schedules the tasks by balancing task utility and execution time subject to an energy constraint aimed to ensure the energy neutrality of the system. The relationship among the tasks is assumed to be known and modeled by a Directed Acyclic Graph (DAG). In addition, the task execution times, past energy harvesting information, tasks qualities, and utility relationships are given in advance. For most applications, the utility is modeled as accuracy and as a function of the task priority. A task with higher priority is executed with the higher utility.

In [122], an energy-aware DVFS (EA-DVFS) scheduling algorithm is proposed that dynamically matches its schedules to the stored energy and harvestable energy in the future. Specif-

ically, tasks are executed at full speed if the stored energy is sufficient. Execution speed is slowed down when the stored energy is not sufficient. This work has been extended further in [123] by the adaptive scheduling and DVFS algorithm (AS-DVFS). AS-DVFS adaptively tunes the operation voltage and frequency of a node processor whenever possible while maintaining the time and energy constraints. The goal of AS-DVFS is to reach a system-wide energy efficiency by scheduling and running the tasks at the lowest possible speed and allocating the workload to the processor as evenly as possible. Moreover, it decouples the timing and energy constraints, addressing them separately. A harvesting-aware DVFS (HA-DVFS) algorithm is proposed in [124] to further improve the system performance and energy efficiency of EA-DVFS and AS-DVFS. In particular, the main goals of HA-DVFS are to keep the running speed of the tasks always at the lowest possible value and avoid wasting harvested energy. Based on the prediction of the energy harvesting rate in the near future, HA-DVFS schedules the tasks and tunes the speed and workload of the system to avoid energy overflow. Three different time series prediction techniques, namely regression analysis, moving average, and exponential smoothing, are used for predicting the harvested energy. Similar to AS-DVFS, HA-DVFS decouples the energy constraints and timing constraints to reduce the complexity of scheduling algorithm. Another *DVFS-based task scheduling* algorithm is presented in [125]. The basic DVFS ideas are combined with a linear regression model. The model is used to associate the number of tasks and their complexity to the execution time, energy consumption, and data accuracy. The main objectives of this protocol are maximizing system performance given the current energy availability, increasing the efficiency of energy utilization, and improving task accuracy. The protocol is deemed specifically suitable for structural health monitoring applications, since the events generated by this kind of applications concern mostly periodic tasks instead of sporadic externally triggered events.

---

## PRO-ENERGY: AN ENERGY PREDICTION MODEL FOR ENERGY-HARVESTING WSNs

Environmentally-powered networks have to deal with the variable behavior of ambient energy sources, which results in different amounts and rates of energy available over time. For instance, solar-powered nodes experience significant changes in the power harvested over time, due to the diurnal cycle in solar energy, varying weather conditions, monthly trends and seasonal patterns. Moreover, the position of the nodes and the orientation of their solar cell strongly impact the energy intake: even if two nodes are physically co-located, often their harvesting rates significantly differ [126, 26].

The uncertainty in the energy availability provided by ambient sources raises new challenges in developing reliable and energy-efficient power-management solutions. Many works assume that accurate predictions about the future energy intake are available to the system, either by simply looking at the past history [127] or by employing more sophisticated energy predictors [128]. Knowledge about the behavior of energy sources over short and medium time frames is often needed to optimize the system, and some solutions even rely on it to work well [129]. In general, having no such knowledge available will result in an under-performing system, in which nodes have no possibility to plan in advance how to spend the energy they will harvest in the near future. Predictions about the future energy availability also help to minimize the waste of energy. Nodes store the harvested energy in devices such as supercapacitors or rechargeable batteries, which are limited in both size and time, due to their limited capacity and to leakage and self-discharge, respectively. Developing energy predictors for WSNs that provide accurate future predictions over short (few minutes to half an hour) and medium (a few hours) time frames is very important, as they allow to exploit at best the available energy, minimizing the likelihood that important tasks are not executed due to lack of energy, and minimizing energy waste, i.e., cases in which the generated energy is neither used nor stored as the buffer is full.

So far, existing works, such as WCMA [109], have mainly focused on short-term predictions for solar energy harvesting. In WCMA, each day is discretized into  $N$  time slots and, at the end of each timeslot  $t$ , the energy prediction for timeslot  $t + 1$  is derived.

Our goal has instead been to develop a general framework for multi-source (i.e., solar and wind) energy-harvesting systems such as [31, 130], which is able to accurately predict energy for forecasting horizons that are dynamically chosen based on the application needs.

In this chapter, we make the following contributions:

- We present a novel energy prediction model, named Pro-Energy (PROfile Energy prediction model), which is able to leverage past energy observations to provide accurate estimations of future energy availability, for both solar and wind harvesting WSNs.

- We discuss a variation of our solution which combines multiple energy profiles in order to improve prediction accuracy for short and medium-term forecasting horizons.
- We provide a performance evaluation framework for energy prediction models. To validate our solution, we use real-life traces of energy availability obtained by interfacing Telos B nodes with photovoltaic panels and wind micro-turbines. We also exploit two additional solar and wind datasets from the US National Renewable Energy Laboratory [131]. Our results show that Pro-Energy performs up to 60% better than other prediction models, being able to provide higher accuracy than EWMA and WCMA.
- We perform a thorough analysis of how varying key parameters of our scheme impact on the prediction accuracy achieved for short and medium term prediction horizons.

The remainder of this chapter is organized as follows. In Section 2.1 we describe our prediction model, Pro-Energy. In Section 2.2 we discuss a variation of our scheme that may be employed to achieve better predictions accuracy for short and medium term predictions. We perform a comparative performance evaluation of Pro-Energy and other energy prediction models proposed in the literature in Section 2.3. In the same section, we also evaluate the impact of critical parameters on the performance of our prediction scheme. Finally, we present our conclusions in Section 2.4.

## 2.1 PRO-ENERGY

In this section, we discuss a new energy prediction algorithm for wireless sensor networks, which uses past-days' observations to derive predictions on the future energy intake for both short (few minutes to half an hour) and medium (a few hours) predictions horizons.

To reduce the time and memory overhead of the prediction model, each day is discretized into a given number  $N$  of equal-length timeslots, and predictions are performed once per slot. The main idea of our energy prediction algorithm is to make use of harvested profiles representing the energy intake available during different types of "typical" days. For instance, days may be classified into sunny, cloudy or rainy, and a characteristic profile may be associated to each of these categories.

The energy received during the current day is stored in a vector,  $C$ , of length  $N$ , containing the energy obtained during each of the past timeslots. A pool of energy profiles observed in the past is also maintained in a matrix  $E$ , of size  $D \times N$ . These profiles represent the energy obtained during a given number,  $D$ , of typical days. Such energy profiles are used by Pro-Energy to forecast future energy intake over short and medium term time frames: Once per timeslot, Pro-Energy delivers energy predictions by looking at the stored profile that is the most similar to the current day. For each of these profiles, the similarity with the energy profile observed during the current day is computed as their mean absolute error (MAE), taking into account the last  $K$  energy observations. More formally, the stored profile,  $E^d$ , that, among the  $D$  typical profiles stored, is the most similar at timeslot  $t$  to the current day,  $C$ , is defined as follows:

$$E^d = \min_{E^d \in E} \sum_{i=t-K}^t \frac{1}{K} |C_i - E_i^d| \quad (2.1)$$

Figure 2.1 shows an example of the application of the Pro-Energy algorithm over 4 days of solar predictions. During the initial timeslots of Oct 23, the first stored profile is selected among the typical ones, as it is the most similar to the portion of the current day observed so far. As the day goes on, the shape of the profile is scaled and adapted according to the new observations. Two other different profiles are used for predictions during days 2 and 3.



Table 2.1: Pro-Energy: Table of notations

Symbol	Explanation
$N$	Number of timeslots in a day
$D$	Number of energy profiles stored in the memory
$E$	Matrix of energy profiles ( $D \times N$ )
$E_t^d$	Harvested energy observed during timeslot $t$ of day $d$
$C$	Power harvested during the current day
$C_t$	Power harvested during timeslot $t$ of the current day
$K$	Number of past observations used to compute profiles similarity
$\hat{E}_{t+1}$	Predicted energy at timeslot $t + 1$ on the current day
$\alpha$	Weighting factor for short-term prediction
$F$	Prediction horizon (number of time slots)
$G$	Correlation parameter
$P$	Number of energy profiles combined for energy predictions
$WP$	Weighted profile (combination of $P$ profiles)
$\gamma$	Weighting factor for short and medium-term predictions
$MAE$	Mean Absolute Error
$MAPE$	Mean Absolute Percentage Error

Then, on the fourth day, the first profile is selected again as the most similar to the current observations.

If the weather conditions change during the current day, e.g., a sunny morning followed by a cloudy afternoon, we expect the most similar profile to be one of those stored which corresponds to a sunny day in the morning, and a cloudy one in the afternoon. In such cases, considering only the last  $K$  observations in Equation (2.1) has the effect of lowering the probability of choosing the wrong profile, while reducing at the same time the computational overhead of Pro-Energy.

Pro-Energy is made up of three components:

1. The **prediction module** delivers future predictions for short and medium term prediction horizons;
2. The **profile analyzer** selects, among the stored profiles, the one that is the most similar to the current day;
3. The **profile pool refresh** updates the pool of energy profiles, taking into account the age of profiles and their similarity.

### 2.1.1 SHORT-TERM ENERGY PREDICTIONS

When delivering energy predictions, Pro-Energy tries to match the observations of the current day with one of the typical profiles stored in its pool.

Specifically, Pro-Energy computes the predicted value for the next timeslot based on a combination of the value for the next timeslot reported in the stored profile and the energy observed in the last timeslot,  $C_t$ . More formally, being  $E^d$  the stored profile that is the most similar (up to timeslot  $t$ ) to the current day, the predicted energy intake for the next slot,  $t + 1$ , of the current day is computed as:

$$\hat{E}_{t+1} = \alpha \cdot C_t + (1 - \alpha) \cdot E_{t+1}^d \quad (2.2)$$

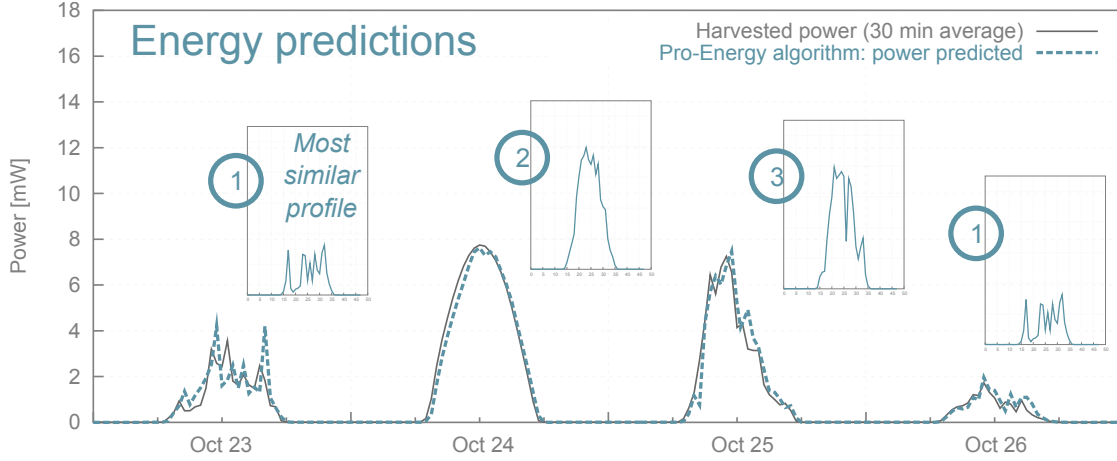


Figure 2.1: Pro-Energy: harvesting profiles representing energy observations from past days are used to predict the future energy availability.

where:

$\hat{E}_{t+1}$  is the predicted energy intake in timeslot  $t + 1$  of the current day;  
 $E_{t+1}^d$  is the energy harvested during timeslot  $t + 1$  on the stored day  $d$ ;  
 $C_t$  is the energy harvested during timeslot  $t$  on the current day  $C$ ;  
 $\alpha$  is a weighting factor,  $0 \leq \alpha \leq 1$ .

The weighting parameter,  $\alpha$ , allows to combine the value reported in the stored profile with the current energy observation, i.e., the energy observed in the last slot,  $C_t$ .

### 2.1.2 MEDIUM-TERM ENERGY PREDICTIONS

When computing short-term predictions, considering the correlation between two consecutive timeslots usually helps increasing the prediction accuracy. This approach, however, is not as effective when delivering medium term predictions. In fact, the correlation between the energy observed at time  $t$  and the one observed at time  $t + \delta t$  generally decreases for increasing  $\delta t$ . To analyze such correlation, we discretized each day in 48 slots of 30 minutes duration and considered a given timeslot,  $t$ , which corresponds, in our example, to the 8:30 AM (results are similar for different timeslots). Figure 2.2 shows the Pearson correlation of the power observed during timeslot  $t$  and timeslot  $t + \delta t$ ,  $\forall \delta = \{0, \dots, 48\}$ , for both solar and wind harvested data. The Pearson correlation coefficient ranges from -1 to 1. An absolute value of 1 implies a linear relationship between the energy observed at two different timeslots, while a value of 0 means that there is no linear correlation between them. It is evident from the figure that, in the solar case, there is a *strong* correlation (i.e., correlation coefficient  $> 0.7$ ) between the harvested power observed at 8:30 AM and the energy intake during the successive 4 – 6 slots (2 – 3 hours) (Fig. 2.2(a)). On the contrary, wind energy observed at 8:30 in the morning shows *strong* correlations only with the successive 1 – 2 slots (30 minutes to one hour) (Fig. 2.2(b)).

Figure 2.3 shows an example of the power harvested by a solar cell and a wind micro turbine over 8 days in August, which highlights that the wind energy intake is generally much more variable than the solar one.

Knowledge of correlation can be exploited for better prediction accuracy. To this purpose, we introduce a new parameter,  $\gamma$ , which determines the influence of the last energy observation while deriving predictions for the next  $F$  future slots.

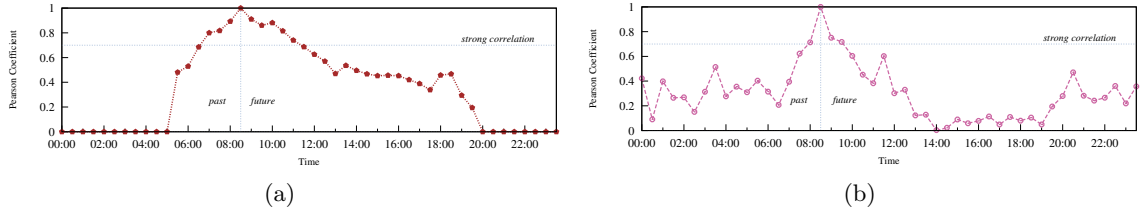


Figure 2.2: Pearson autocorrelation coefficient for (a) solar ORNL Dataset and (b) wind Bologna Dataset.

Assuming that two slots at a distance equal to or greater than  $G$  show only a weak correlation, the  $\gamma$  parameter to be used when predicting the energy intake for the future slot  $i$  is defined as:

$$\gamma_i = \begin{cases} \alpha \cdot \left(1 - \frac{i-1}{G}\right), & \text{if } i \leq G \\ 0 & \text{if } i > G \end{cases} \quad \forall i, 1 \leq i \leq F$$

where:

$\alpha$  is the weighting factor defined in Equation (2.2);

$i$  is the  $i^{\text{th}}$  timeslot in the future, with respect to the current slot,  $t$ ;

$G$  is the number of timeslots in the future which show a correlation above a given threshold with timeslot  $t$ ;

$F$  is the number of future timeslots for which Pro-Energy is delivering energy predictions.

The  $\gamma_i$  parameter plays a similar role in Equation (2.3) (defined in the following) as the weighting parameter  $\alpha$  in Equation (2.2): It allows to combine the energy value of the stored profile with the current energy observation. However, the weight associated to the value observed during the current slot progressively decreases when computing predictions for timeslots that are further away in time. For timeslots that are more than  $G$  slots in the future from timeslot  $t$ , such weight,  $\gamma_{t+G}$ , is set to zero, as there is little or no correlation between the energy value observed at timeslot  $t$  and that observed at timeslot  $t + G$ .

Having defined such  $\gamma_i$  parameter, the medium term predictions are then computed by using a generalization of the short-term version (Equation 2.2):

$$\hat{E}_{t+i} = \gamma_i \cdot C_t + (1 - \gamma_i) \cdot E_{t+i}^d \quad (2.3)$$

Indeed, short-term predictions are computed according to Equation 2.3, where the prediction horizon  $F$  is equal to 1,  $i = 1$  and  $\gamma_i = \alpha$ .

### 2.1.3 STORED PROFILES UPDATES

Pro-Energy maintains a pool of  $D$  typical profiles, each ideally representative of a different weather condition. In order to adapt predictions to changing seasonal patterns, this pool has to be periodically updated. At the end of each day, Pro-Energy decides whether to update the pool of stored profiles with the profile observed during the current day,  $C$ , or not. Specifically, it jointly implements two update strategies:

1. If there is a profile in the pool that was stored longer than  $A$  days ago, substitute it with the profile observed during the current day,  $C$ .
2. If there are two profiles  $E^{d_1}$  and  $E^{d_2}$  in the pool that are very similar, i.e., their MAE is below a given threshold, substitute with  $C$  the one among the two that is the most similar to the current day. In case of multiple pairs of similar profiles we select among these pairs the most similar to  $C$ .

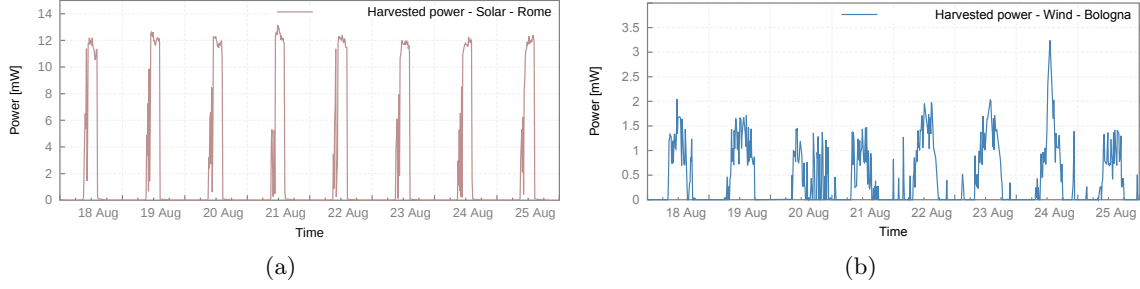


Figure 2.3: Power generated by our (a) solar cell and (b) wind micro-turbine over 8 days in August 2011.

The first strategy allows to discard profiles that have become obsolete, while the second strategy allows to maintain a pool of profiles that are ideally representative of different weather conditions, by discarding profiles that are very similar.

## 2.2 IMPROVING PREDICTION ACCURACY BY COMBINING MULTIPLE PROFILES

Pro-Energy predictions can be further improved through a technique which allows to combine multiple profiles together. Such method selects a set of  $P$  profiles, instead of a single one, among the  $D$  profiles stored in the  $E$  matrix and combines them to form a “weighted” profile  $WP$ .

The main idea behind the use of multiple profiles is to consider different possible evolutions of the current day. For instance, a sunny morning may be followed by a cloudy or rainy afternoon. While delivering medium and long term predictions, considering a single profile may lead to poor accuracy if significant variations occur in the weather conditions. On the contrary, considering multiple profiles allows to account for these potential changes, reducing the prediction error at the price of a small additional overhead.

Let  $E^{d_1}, E^{d_2}, \dots, E^{d_P}$  be the ordered list of profiles that are most similar to the current day  $C$ , i.e., profiles with the smaller Mean Absolute Errors. The weighted profile  $WP$ , for the future slot  $t + i$ ,  $i \in \{1, 2, \dots, F\}$ , is computed as:

$$WP_{t+i} = \frac{1}{P-1} \sum_{j=0}^P w_j \cdot E_{t+i}^{d_j} \quad (2.4)$$

where

$$w_j = 1 - \frac{MAE_k(E^{d_j}, C)}{\sum_{j=1}^P MAE_k(E^{d_j}, C)} \quad (2.5)$$

As for the previous case (Section 2.1.2), energy predictions for the future slot  $t + i$  are computed based on the value for such slot stored in the  $WP$  profile and on the energy harvested during the last time slot.

The predicted energy intake for the future slot,  $t + i$ , is then computed as:

$$\hat{E}_{t+i} = \gamma_i \cdot C_t + (1 - \gamma_i) \cdot WP_{t+i} \quad (2.6)$$

where:

$\hat{E}_{t+i}$  is the predicted energy in timeslot  $t + i$  for the current day;  
 $C_t$  is the harvested energy during last timeslot;

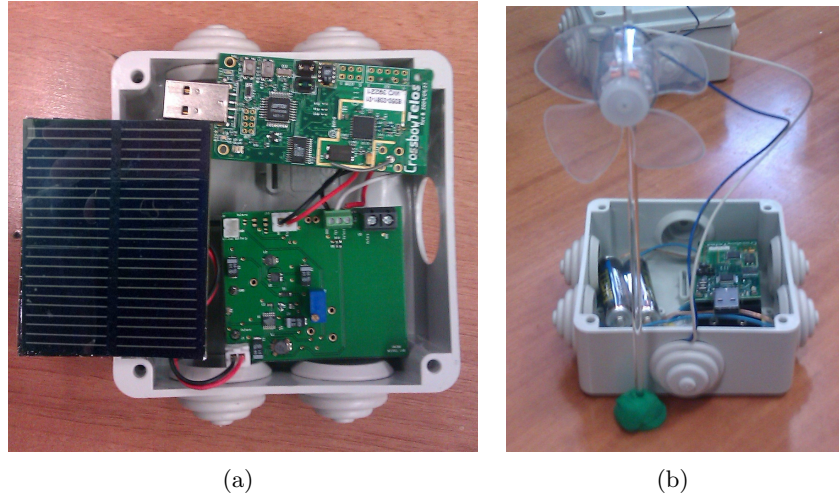


Figure 2.4: Telos B motes interfaced with (a) photovoltaic cell (b) and wind micro turbines.

$WP$  is the vector of the combination of timeslot  $t + i$  of the  $P$  profiles;

$\gamma_i$  is a correlation factor for prediction of slot  $t + i$ .

Equation (2.6) is a generalization of Equation (2.3). Specifically Equation (2.3) is obtained by Equation (2.6) by using only one profile for future energy predictions.

### 2.3 PERFORMANCE EVALUATION

We evaluated the accuracy of the Pro-Energy predictor in many different settings, by using four different types of harvested energy datasets: 1. real-life solar data obtained from a testbed in Rome, Italy; 2. real-life wind data obtained from a testbed in Bologna, Italy; 3. traces of solar availability obtained from the National Renewable Energy Laboratory at Oak Ridge, Tennessee [131]; and 4. traces of wind availability obtained from the same source.

We obtained real-life solar data by interfacing Telos B motes [23] with photovoltaic cells (Figure 2.4(a)). A dedicated TinyOS application was developed to track the amount of energy generated by the harvesters every 30 seconds. The monitoring motes were deployed close to the window of our university building in Rome for 46 days reporting data under variable weather conditions and in different locations. Ten nodes were deployed in different locations, inside and outside the windows, with windows selected in offices with different orientations (west/east/south). In general, due to varying weather conditions, seasonal patterns and different node positions and solar cell orientations, the amount of energy harvested varied significantly over time (3 – 220 J per day). Real-life wind harvesting data were obtained from an outdoor testbed, located in Bologna, Italy, of Telos B motes equipped with micro wind turbines (Figure 2.4(b)), collecting data for 75 days. The other two datasets were obtained from the National Renewable Energy Laboratory at Oak Ridge, Tennessee, and consist of 90 days of solar and wind data collected with a granularity of one per minute.

#### 2.3.1 ACCURACY OF SHORT AND MEDIUM TERM ENERGY PREDICTIONS

#### 2.3.2 PREDICTION ALGORITHMS EVALUATION

We evaluated the performance of Pro-Energy by comparing, for each timeslot, the amount of energy predicted with the energy actually harvested. The prediction error was calculated by using the Mean Absolute Percentage Error (MAPE) function [132]:

$$MAPE = \frac{1}{T} \sum \left| \frac{\bar{e}_t - \hat{e}_t}{\bar{e}_t} \right|, \quad (2.7)$$

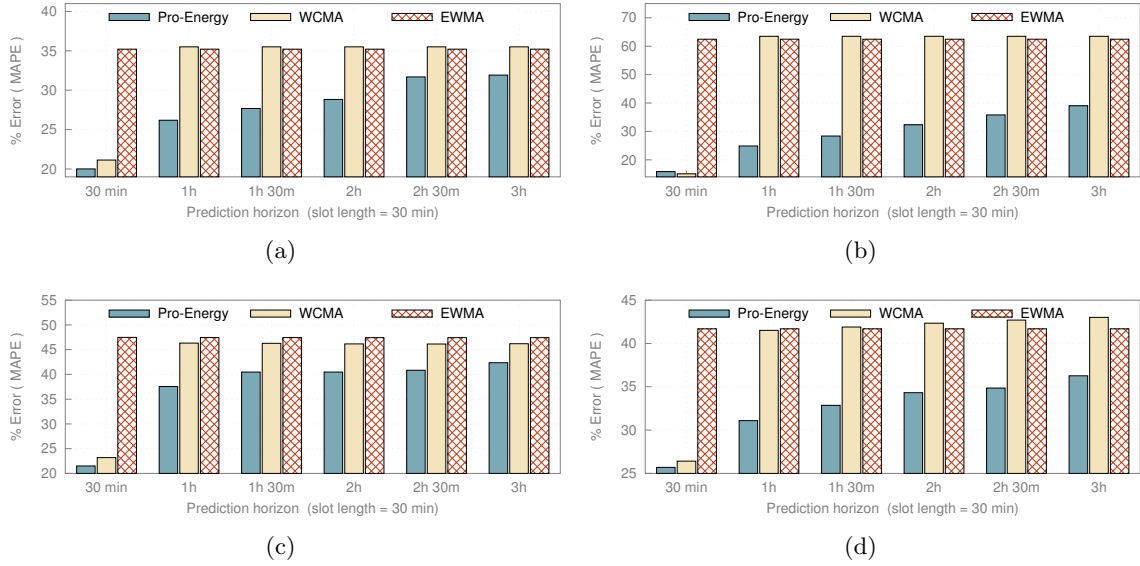


Figure 2.5: Short and medium-term energy predictions accuracy: comparison between Pro-Energy, WCMA and EWMA for (a) solar ROME dataset; (b) solar ORNL dataset; (c) wind BOLOGNA dataset and (d) wind ORNL dataset.

where:

$\hat{e}_t$  is the energy predicted for timeslot  $t$ ;

$\bar{e}_t$  is the actual energy harvested during timeslot  $t$ ;

$T$  is the total number of timeslots over which the MAPE error is computed.

In general,  $T$  is lower than the total number of timeslots in a given dataset. When computing the MAPE error, we only consider the timeslots in which the energy intake is meaningful to evaluate the prediction accuracy [109]. For this reason, we discard from the MAPE calculation the timeslots in which the harvested power is low, i.e., it is less than the 10% of the maximum peak power of the day.

We compare the performance of Pro-Energy with that of two energy predictors previously proposed in the literature, EWMA and WCMA. In our experiments, we set  $N = 48$ . Thus, a whole day is represented by a vector of 48 timeslots, each corresponding to a 30 minutes interval. In order to perform a fair comparison, we set the coefficient of each prediction model to their optimal value, i.e., the ones minimizing the overall MAPE error, using the same energy traces. Since WCMA is designed to only deliver predictions for the next timeslot, we needed to extend it to make it able to perform predictions for different time horizons. Specifically, we modified WCMA so that, when it is asked to predict the energy intake at timeslot  $t + \delta$ ,  $\delta > 1$ , it returns the average energy observed at timeslot  $t + \delta$ , computed over the last  $D_{wcma}$  days.

Figure 2.5 shows the prediction error of Pro-Energy, WCMA and EWMA for four different solar and wind datasets and for different prediction horizons. Specifically, we report here results about the accuracy of both short and medium term energy predictions. The prediction error shown in the figure is the MAPE (Equation (2.7)) between the amount of energy predicted and the one actually observed, computed over the whole dataset.

The results highlight that the characteristics of the energy source impact the accuracy of prediction. As can be seen, wind energy (Fig. 2.5(c)- 2.5(d)) is more difficult to predict than solar energy (Fig. 2.5(a)- 2.5(b)), since it is less stable over time.

Table 2.2: Solar Rome dataset: parameter settings and MAPE error of Pro-Energy, WCMA and EWMA for short and medium term predictions.

	Pro-Energy						WCMA				EWMA	
	<i>Error</i>	$\alpha$	$D$	$K$	$G$	$P$	<i>Error</i>	$\alpha$	$D$	$K$	<i>Error</i>	$\alpha$
30m	<b>20.00</b>	0.50	14	2	-	9	<b>21.12</b>	0.6	11	5	<b>35.21</b>	0.2
1h	<b>26.18</b>	0.40	14	2	5	9	<b>35.51</b>	-	10	7	<b>35.21</b>	0.2
1h30m	<b>27.68</b>	0.45	9	6	5	7	<b>35.51</b>	-	10	7	<b>35.21</b>	0.2
2h	<b>29.81</b>	0.45	14	1	6	9	<b>35.51</b>	-	10	7	<b>35.21</b>	0.2
2h30m	<b>31.68</b>	0.60	14	3	6	9	<b>35.51</b>	-	10	7	<b>35.21</b>	0.2
3h	<b>31.92</b>	0.55	18	3	7	9	<b>35.51</b>	-	10	7	<b>35.21</b>	0.2

As can be expected, the prediction error of Pro-Energy increases for longer prediction horizons. In fact, correctly estimating the energy trend of the current day becomes much more difficult as the forecasting horizon increases. Pro-Energy however consistently outperforms EWMA and WCMA for both short and medium term solar energy predictions. In case of solar energy predictions with a prediction horizon of 1 hour, Pro-Energy performs  $\approx 25\%$  better than EWMA and WCMA (Fig. 2.5(a)). The parameter setting in such scenario is summarized in Table 2.2. More generally, for both short and medium-term energy predictions, Pro-Energy achieves a 5% – 26% reduction of the overall MAPE with respect to WCMA. The reduction of the MAPE error with respect to EWMA is between 9% – 43%.

Such an improvement is even more significant in the solar-ORNL dataset (Fig. 2.5(b)). For energy predictions within a prediction horizon of 1 hour, Pro-Energy performs 60% better, by exhibiting a MAPE error that is almost one third of that of EWMA and WCMA. For medium-term energy predictions, Pro-Energy achieves an average reduction of the overall MAPE error of almost 50% with respect to WCMA and EWMA. In case of short-term predictions, the performance of Pro-Energy is comparable with that of WCMA while it is 75% better than EWMA's.

Differently from the other predictors, Pro-Energy achieves a good accuracy also when performing wind harvesting forecasting. For the Wind-Bologna dataset (Fig. 2.5(c)), Pro-Energy leads to a 7% – 19% lower MAPE error than WCMA. The improvement is between 9% and 54% in case of EWMA. Figure 2.5(b) shows the improvement of Pro-Energy over WCMA and EWMA in the wind-ORNL dataset. The overall MAPE error achieved by Pro-Energy is 3% – 25% lower than WCMA and 13% – 38% lower than EWMA.

Figure 2.5 shows that EWMA is the worse performing predictor even if its performance are constant and do not depend on the prediction horizon. The reason is that EWMA does not use information about the current energy intake in slot  $t$  to adjust prediction in future slots  $t + \delta$ . At the end of each slot  $t$ , the only prediction that is updated is the one relative to the same slot  $t$ , which will be used for energy predictions on the next day. WCMA performs very well in delivering accurate short-term term energy predictions. Its prediction accuracy, however, degrades when handling medium term predictions. This is due to the fact that WCMA, being designed to only deliver predictions for the next timeslot, does not exploit the current energy observation and the correlation between current observation and future ones to adjust future energy predictions over medium-term forecasting horizons. The remarkable improvement achieved by Pro-Energy over WCMA highlights the importance of considering the correlation between the current conditions and the future time slots for accurate medium term prediction.

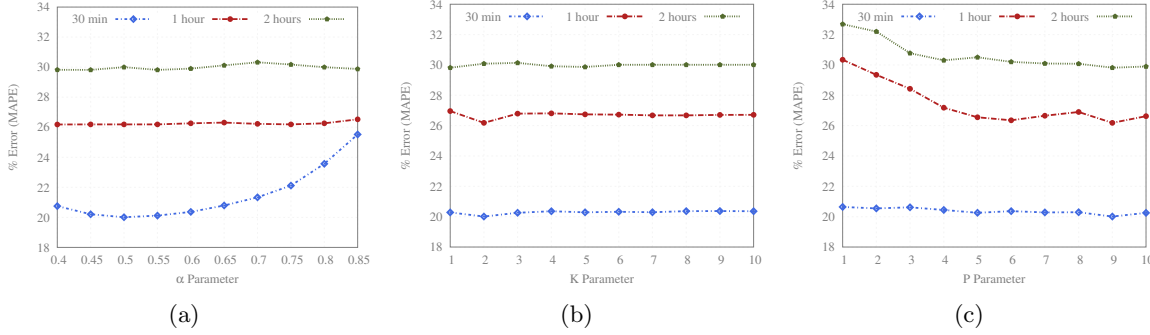


Figure 2.6: Impact of varying Pro-Energy parameters on the overall MAPE error for 30 minutes, 1 hour and 2 hours prediction horizons: (a)  $\alpha$  parameter; (b)  $K$  parameter and (c)  $P$  parameter.

### 2.3.3 ACCURACY OF ENERGY PREDICTIONS FOR VARYING PARAMETER SETTINGS

The last part of our analysis is focused on the impact of varying parameter settings on the accuracy of the energy predictions. We focus our evaluation on the solar-ROME dataset, which well represents a practical application scenario. Due to space restrictions, we restrict our analysis considering three different predictions horizons: 30 minutes, 1 hour and 2 hour. We performed three sets of experiments, varying the value of the parameters  $\alpha$ ,  $K$  and  $P$ . While fixing a parameter, the value of the other parameters have been set so as to minimize the overall MAPE error (Table 2.2).

Figure 2.6(a) displays the impact of varying the  $\alpha$  parameter on the prediction accuracy of Pro-Energy, for 30 minutes, 1 hour and 2 hours energy prediction horizons. Figure 2.6(a) shows that the  $\alpha$  parameter has a high impact on the total MAPE error in case of short-term predictions. In such case, the total error, computed over the whole solar dataset, is minimized for  $\alpha = 0.5$ . This corresponds to a balanced contribution between the energy value reported in the stored profile  $E_{t+1}^d$  and the last energy observation made during the current day,  $C_t$ . Higher values of the parameter, i.e., values of  $\alpha > 0.75$ , lead to performance degradations: The MAPE error increases of up to 5 percentage points. This is because in such settings Pro-Energy strongly relies on the energy trend expressed by the typical profiles, without effectively adapting them to the current weather conditions. When considering prediction horizons of one and two hours, instead, the performance of Pro-Energy are quite stable with respect to variations of the  $\alpha$  parameter, as varying it changes the MAPE error only up to 0.5 percentage points. This is due to the fact that, for such prediction horizon, the value of the  $G$  parameter has a stronger impact than in the previous cases on the overall MAPE error.

Figure 2.6(b) shows that the value of  $K$  does not deeply influence the accuracy of energy predictions of short term energy prediction. In fact, for  $K$  parameter ranging from 1 to 10, the MAPE error increases only up to  $\approx 0.5$  percentage points. Such results suggest that, to characterize the future energy intake during the current day, it is enough to consider the energy harvested in the last few timeslots. In fact, the information collected during timeslots that are further away in time does not provide significant improvement in the accuracy of energy predictions. This characteristic allows Pro-Energy to use small values of  $K$  while performing MAE computations, thus reducing the overhead of computing similarity between different profiles.

Figure 2.6(c) shows how varying the number of profiles used by Pro-Energy impacts on the overall MAPE error. The overall trend is that increasing the number of profiles that Pro-Energy takes into account tends to reduce the prediction error. However, in case of short-



Table 2.3: Overhead of Pro-Energy, WCMA and EWMA (solar-Rome dataset)

Prediction Algorithm	Number of multiplications
Pro-Energy (1 profile)	4369
Pro-Energy (2 profiles)	12917
Pro-Energy (3 profiles)	17047
Pro-Energy (4 profiles)	21081
Pro-Energy (5 profiles)	25019
WCMA	27931
EWMA	4416

term predictions, combining multiple profiles together does not have a very strong impact, as it improves the prediction accuracy only up to 0.5 percentage point. This means that the overhead of the Pro-Energy algorithm may be reduced in such case by choosing a small values of  $P$ , with limited impact on performance. On the contrary, the effect of the  $P$  parameter is much more evident for medium term predictions, as using a combination of multiple profiles can reduce the overall MAPE error up to  $\approx 4$  percentage points with respect to the setting in which a single profile is used.

#### 2.3.4 PRO-ENERGY OVERHEAD

Table 2.3 compares the overhead of Pro-Energy with that introduced by other solutions, in terms of number of multiplications performed by each scheme, computed over the solar-Rome dataset. The values reported in the table refer to a setting of parameters in which  $D = 10$  (number of energy profiles stored),  $K = 7$  (number of slots used for comparing profiles),  $F = 1$  (prediction horizon) and  $P$  (number of combined profiles) varies in  $\{1, 2, 3, 4, 5\}$ .

## 2.4 CONCLUSIONS

In this chapter, we have presented Pro-Energy a novel energy prediction model for multi-source energy harvesting WSNs, which is able to provide accurate predictions for short and medium term forecasting horizons. We have performed extensive validation of Pro-Energy using real-life traces of the harvested energy we have obtained by interfacing Telos B nodes with photovoltaic panels and wind micro-turbines. We have also exploited two additional solar and wind datasets from the US National Renewable Energy Laboratory. Our results show that Pro-Energy performs better than previous solutions such as EWMA and WCMA, with improvements in prediction accuracy which can be as high as 60%.



---

## ADAPTIVE RECTIFIER DRIVEN BY POWER PREDICTIONS FOR WIND EHWSNs

Research in power aware systems has gained increasing interest in recent years, pushing the exploration of new ultra low-power, energy autonomous hardware architectures and the investigation of new algorithms for power generation, estimation, profiling, prediction and management. Energy harvesting is a key component of such self-powered systems. Many works have explored power scavenging opportunities from sources such as vibrations [133], electro-magnetic fields and heat [134], which can provide power densities in the microwatt range. Solar light, however, remains the most investigated energy source [135, 136, 137], thanks to the fact that even small solar cells are able to deliver power densities in the milliwatt range. Another very attractive ambient source, especially in application scenarios in which solar light is unavailable or too scarce, is air-flow, which can also provide energy in the order of milliwatts under favorable conditions. The small micro-wind turbine used in [138] and [139], for example, with a diameter of just 6.3 cm can generate power in the range 10 - 100 mW.

The architecture of air-flow energy harvesters typically consists of an initial rectifier stage to convert the AC output of the turbine into a more suitable DC signal, and of a second regulation stage to perform MPPT, store the energy and supply the user system [138, 139, 140]. Typically, the rectifier circuits used in ultra-low power applications are divided into two categories, namely *passive* and *active*.

*Passive* rectifiers, which are usually realized through a diode full wave bridge, are the simplest and commonly used topologies. However, they are also the least efficient, due to the high voltage drop across the diodes during the forward polarization (about 0.6 - 0.7 V using common Silicon Diffused Junction diodes, 0.2 - 0.3 V using Schottky diodes).

*Active* rectifiers improve the conversion efficiency by replacing diodes with MOSFETs, which significantly reduce the voltage drop in the ON state. Such additional efficiency, however, increases the complexity and the cost of the system, due to the presence of control circuitry for the MOSFETs. When the micro-wind turbine generates low voltage levels (e.g., <1.8 V), such that the control circuit is switched off, the conversion is performed by the parasitic diodes of the transistors. This means that there is a transition threshold between the passive and the active operating modes, and therefore between a lower and a higher efficiency AC-DC conversion. The *active* rectifier optimizes the efficiency when the wind speed generates an input power greater than the transition threshold, but whenever the incoming power falls below the transition threshold the conversion efficiency is the same as a classical full wave bridge. In this latter case, a Schottky rectifier would perform much better.

In this chapter we present the design of a hardware and software power management technique to improve the efficiency of the rectifier stage. The block diagram of the proposed system is shown in Fig. 3.1. It features a hybrid adaptive rectifier stage that exploits both the *active*

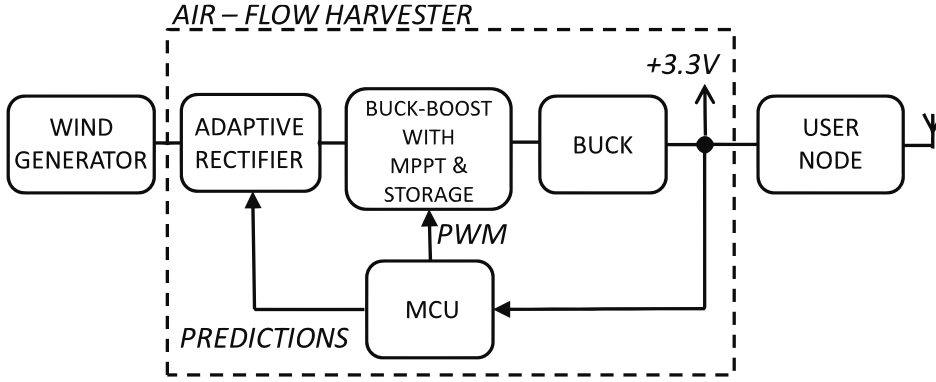


Figure 3.1: Block diagram of the proposed air-flow energy harvester

and *Schottky-passive* topologies to achieve the maximum efficiency over the whole range of air-flow speed. In addition, an efficient power management stage, controlled by an ultra-low power microcontroller, converts and stores the incoming energy. The microcontroller elaborates periodically the prediction of the power intake from air-flow data, delivers estimations about the energy availability in the near future, and determines which topology of rectifier is the most efficient under certain air-flow speed conditions. To show the benefits of the adaptive AC-DC converter in a real-life scenario, the practical case of a WSN deployed in an underground tunnel is considered, where nodes are able to harvest energy from air-flows. More in detail, real-life air-flow data have been collected for 33 days by instrumenting a tunnel of the *Metro B1* line in Rome, Italy, with Telos B motes equipped with wind micro-turbines. Then, the usable power obtained from passing trains is estimated for each rectifier by considering the efficiency values previously calculated. In such scenario, the average energy harvested per day by using the adaptive converter is up to 18% higher than that harvested by the passive-Schottky-only topology and up to 22% higher than that harvested by the active-only topology.

The underground tunnel environment is almost totally predictable, as underground trains generally transit with a regular schedule and with approximately the same speed. By exploiting such regularity, a power management technique that is specifically tailored to the underground tunnel scenario is devised. It allows to reduce the overall overhead of the system, rated as the average number of sampling performed per day by a node using a given power management policy, of up to 93%, without impairing the energy harvesting process.

The rest of the chapter is organized as follow: Section 3.1 gives an overview of the state of the art on the architecture of air-flow harvesters, rectifiers design and power management and prediction algorithms. Section 3.2 presents a detailed description of the hybrid system and the energy harvester adopted. Section 3.3 is dedicated to the analysis of air-flow data collected during tunnel monitoring, while Section 3.4 discusses the power management algorithms. Finally, results are discussed in Section 3.5, followed by conclusions in Section 3.6.

### 3.1 RELATED WORKS

One of the first prototypes of air-flow harvesters was developed with the aim of extending the lifetime of a WSN for wind speed sensing [140]. The same anemometer used to perform measurement is connected to a small alternator to harvest energy, while a buck-boost converter operated in DCM provides the regulated voltage to recharge a battery. Furthermore, the power transfer is optimized by biasing the alternator, maintaining constant the input resistance of the converter. The resistance emulation approach to perform MPPT in energy harvesting systems is discussed in depth by Paing *et al.* in [141]. They proposed a theoretical method to estimate the power consumption of the most common topologies of DC-DC

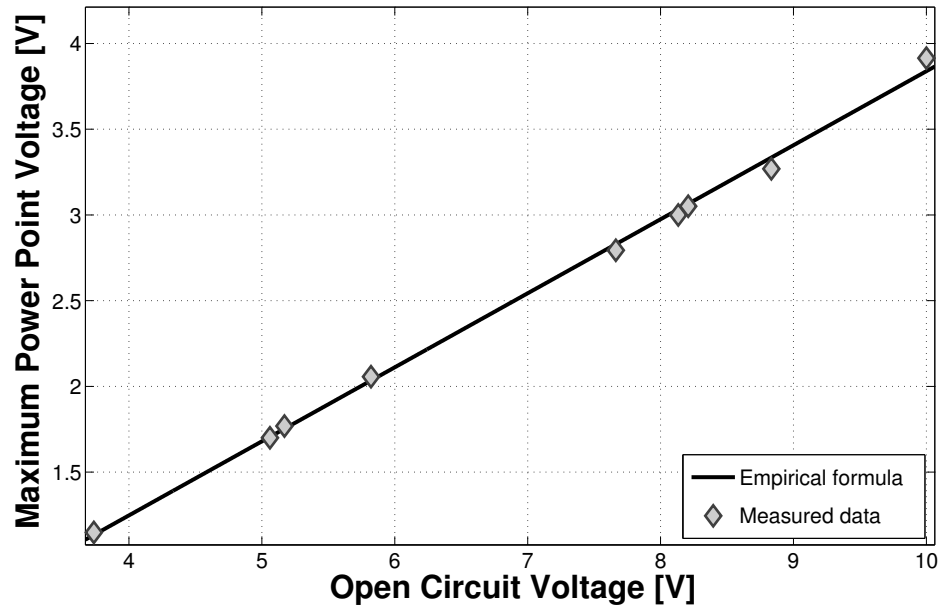


Figure 3.2: Relation between open circuit voltage and maximum power point voltage of the micro-turbine. The solid line represents the empirical formula while the dots the measured data.

converter as a function of critical parameters such as switching frequency and duty cycle, concluding their work with an example of buck-boost converter suitable for wind harvesting. Such technique was later elaborated and exploited in several recent works, such as [138], where the authors modeled and characterized a micro-wind turbine with a sinusoidal output signal and a diameter of 6 cm. The AC signal is rectified by a full wave Schottky-bridge and the design method of a buck-boost converter optimized to achieve a high conversion efficiency is presented. A similar wind generator is used in [139] for delivering energy to a self-powered node. The conversion circuit consists of an active full wave rectifier followed by a boost converter with resistance emulation capability combined with a micro-controller to perform MPPT. The active rectifier, realized with off-the-shelf components, increases the efficiency up to 70% when compared to a Silicon Diffused Junction diode-passive rectifier with a low input voltage of 1.2 V, reaching peak values of about 80%. Nevertheless, this solution exploits the bulk parasitic diodes of the MOSFETs as alternative way to perform rectification when the control circuit cannot work, resulting in a significant loss of efficiency.

The design of an efficient rectifier is challenging in energy harvesting applications, especially when dealing with micro-watt sources. Several works presented in literature are based on the principle of replacing the passive elements (the diodes) with active ones, usually called active diodes as they work as diodes but need control circuitry. Moreover, to achieve higher efficiency the majority of researchers have investigated only integrated solutions. For example, the circuit proposed in [142] exploits linear-region operated MOSFET to emulate diodes and the control circuitry is directly powered from the input signal. Such system, simulated and realized in 130 nm technology can extract up to 90% of the maximum power from an ideal piezoelectric device. In [143] an integrated bridge fabricated in 0.35  $\mu\text{m}$  CMOS process is described, in which the four diodes are replaced by two cross-coupled pMOS transistors and two active diodes driven by two 4-input comparators. Such configuration matches a zero-threshold diode and effectively eliminates the reverse current increasing the overall efficiency up to 90%.

Another widely explored method to design rectifier is the voltage multiplying technique. The active voltage doubler presented in [144], realized in 5 V CMOS STMicroelectronics technol-

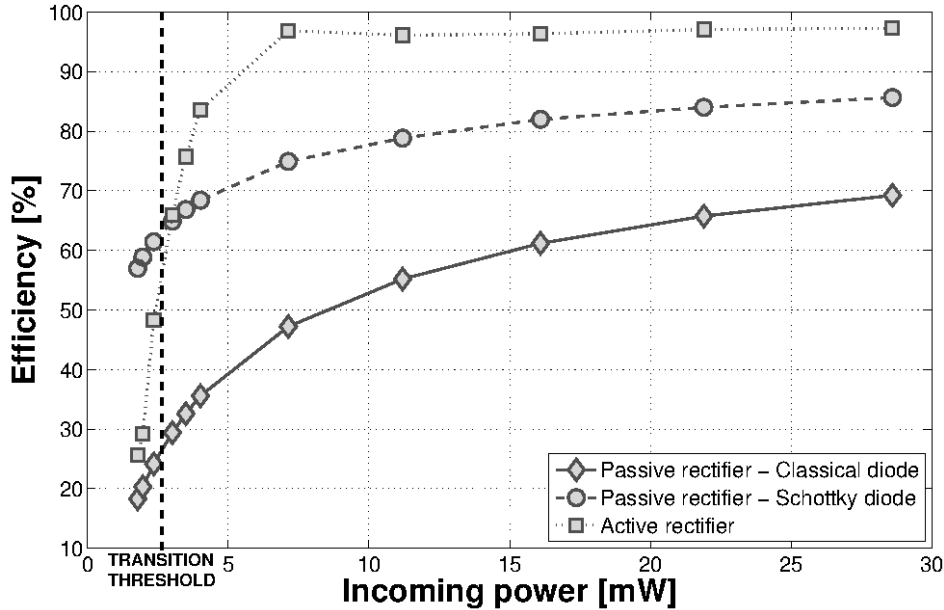


Figure 3.3: Efficiency comparison of the simulated passive, passive-Schottky and active rectifiers. The efficiency is calculated at the optimal load resistance of  $560 \Omega$ . The vertical dashed line shows the efficiency transition threshold.

ogy, uses two switching MOSFETs driven by operational amplifiers instead of comparators and shows an efficiency between 75% and 95%. Finally, Cheng *et al.* propose an active voltage doubler [145] and an  $8\times$  active voltage multiplier [146] exploiting active diodes technique and using off-the-shelf components. The voltage doubler can reach more than 80% efficiency for input voltage amplitudes greater than 0.25 V while the  $8\times$  multiplier can recharge a 3.7 V lithium battery with over 80% efficiency.

All the mentioned active rectifiers are optimized to work in piezoelectric or RF harvesting applications and are designed to maximize the efficiency with very low input voltage and power because it is crucial to avoid power wasting in the *microwatts*. Complex systems, featuring a very low start-up voltage and high conversion efficiency are fundamental in these conditions. The hybrid solution presented in this chapter is realized with off-the-shelf components and represents a cost effective design suitable for environmental sources which produce *milliwatts*, as air-flows. In these conditions, the proposed solution is simpler and achieves performance comparable to the on-chip rectifiers.

We tested our architecture in the specific scenario of a WSN deployed in an underground tunnel, harvesting energy from the air-flows generated by passing trains. Deployments of WSNs in tunnels have been described and discussed in previous works [147, 148, 149, 150, 151, 152]. In [147], Ceriotti *et al.* report on a deployment in which a WSN is a key component of a control system for adaptive lighting in road tunnels. In [148], Stajano *et al.* discuss their experience with a WSN testbed composed of 26 nodes deployed in a London Underground tunnel on the Jubilee Line to measure changes in displacement, inclination, temperature and relative humidity. In [149], Mottola *et al.* presents two WSN deployments in an operational road tunnel and in a nonoperational one. They compare the wireless topology in the two scenarios, in terms of reliability, stability, and asymmetry of links, providing results about the impact of such topologies on MAC and routing layers. In [150] the development and deployment of a WSN to monitor a train tunnel during adjacent construction activity is described. Such works, however, focuses on connectivity issues in tunnel scenarios and none reported the deployment of WSN nodes with energy harvesting capabilities in underground

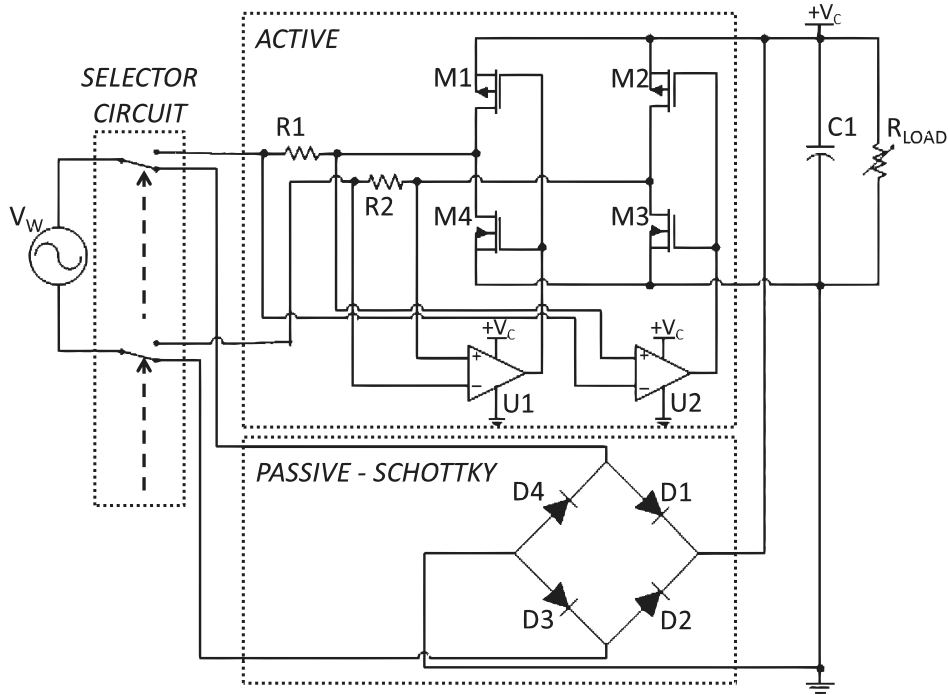


Figure 3.4: Schematic of the adaptive hybrid rectifier. The selector circuit chooses between the active and passive topology according to the air-flow conditions.

tunnels.

## 3.2 ARCHITECTURE OF THE ENERGY HARVESTER

The adaptive rectifier presented in this chapter was originally designed to improve the efficiency of the air-flow path of the multi-source energy harvester discussed in [153]. This air-flow harvester consists of a two-stage architecture, more precisely a passive-Schottky-diode full wave rectifier followed by a buck-boost converter which recharges a supercapacitor used as a local energy buffer. In this work the passive rectifier is combined with an adaptive one. As shown in Fig. 3.1 an ultra low-power MCU performs power management, namely it selects the optimal rectifier and performs the MPPT algorithm to maximize the conversion efficiency. Finally, an output buck converter provides the regulated power supply to the micro-controller and to the supplied platform.

### 3.2.1 WIND GENERATOR

The air-flow transducer used in this work is a small plastic four-bladed horizontal axis micro-wind turbine, which produces a sinusoidal power signal, whose amplitude and frequency is dependent on the air speed. The maximum power transfer is reached when a load in the range 500 - 700  $\Omega$  is applied. Experiments show that the optimal load value is 560  $\Omega$ . An exhaustive characterization of this micro-turbine with simulations and experimental results is given in [138] and [153]. In addition, some experiments were conducted to derive the following empirical formula:

$$V_{MPP} = V_{OC} \times 0.4319 - 0.48 \quad (3.1)$$

that shows the relation between the open circuit voltage ( $V_{OC}$ ) and the maximum power point voltage ( $V_{MPP}$ ) of the micro-turbine. This relation will be used during data analysis discussed in Section 3.3. In Fig. 3.2, the measured data compared with the empirical formula are proposed.



Figure 3.5: Snapshot of nodes deployed in a tunnel of the Metro B1 line in Rome.

### 3.2.2 HYBRID FULL-WAVE RECTIFIER

The schematic, in Fig. 3.4, shows in detail the design of the adaptive rectifier. The passive stage is a full wave bridge implemented with four Schottky diodes, while the active stage uses P-channel MOSFETs M1-M2 and N-channel MOSFETs M3-M4 as rectifying elements, while the control circuit exploits two fast-switching ultra low-power comparators U1, U2. During the positive half-wave M1 and M3 are switched ON, forming a conductive path to the filter capacitor C1 and ground, respectively, while M2-M4 are switched-OFF. Vice-versa M2-M4 are in conduction during the negative half-wave and M1-M3 are OFF. The control circuit, powered by the voltage  $V_C$  across the filter capacitor C1, continuously monitors the AC source current by means of the sensing resistors R1, R2. Comparators U1, U2 are used to generate the proper gating signals for M1-M4. A thorough discussion about the benefits of this current-sensing approach is given by Tan *et al.* in [139].

The performance of both rectifiers is evaluated individually by means of SPICE simulations, using a variable resistor as a load. The results are plotted in Fig. 3.3, which compares the efficiency of the active and passive-Schottky rectifiers. For the sake of completeness, the efficiency of a passive rectifier realized with common Silicon diodes is also reported in the figure. It is clear that, due to the high voltage loss across diodes, the latter is a totally inefficient configuration. The Schottky diodes, with their 0.2 - 0.3 V voltage drop in conduction mode, are a very attractive solution in case of low power intake. As shown in Fig. 3.3, there is a transition threshold which delimits two operating areas: with an input power in the range 0 - 2 mW the Schottky rectifier (dashed line marked with circles) performs conversion with an efficiency of 60% - 70%, outperforming the Silicon diode bridge (solid line with rhomboid markers) by 20% - 40%. Moreover, in the same range, it is better than the active rectifier (dotted line marked with squares) because the efficiency is 10% - 40% higher than the active topology. Finally, when the power intake exceeds the threshold of 2 mW the active rectifier is the most efficient topology to use with a peak of 96% of efficiency.

Thus, for each operating region there is an optimal solution. When the input power is below the transition threshold the Schottky rectifier is preferable, while the active topology is much better with input power above the threshold. The design allows to dynamically select the most suitable topology by means of the selector circuit, thus power management policies will adjust adaptively to the optimal configuration as described in detail in Section 3.4.

### 3.2.3 MPPT CIRCUIT AND OUTPUT STAGE

To achieve maximum power transfer the conversion circuit has been designed to emulate an equivalent input resistance discussed in Section 3.2.1. The present work exploits a buck-boost converter, implemented with off-the-shelf components and operated in Fixed Frequency-



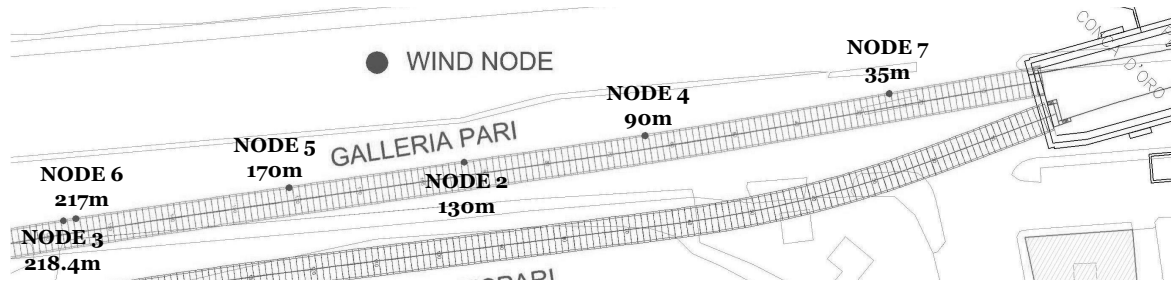


Figure 3.6: Position of the nodes deployed in the tunnel and their distances from the train station. (Site plan courtesy of Roma Metropolitane and Tre Esse Engineering, FP7 GENESI project).

Discontinuous Current Mode (FF-DCM) to emulate the optimal input impedance value of  $560\Omega$  and stores the converted energy in a 1 F, 5.5 V supercapacitor. The PWM gating signal is generated by an ultra-low power micro-controller according to the formula:

$$R_{IN,eq} = \frac{2LT}{t_1^2}, \quad (3.2)$$

where L is the value of the inductor L1 and T and  $t_1$  are the period and the duty cycle of the PWM signal, respectively. In Eq. (3.2) the input equivalent resistance is the only constraint to satisfy, thus the remaining three degrees of freedom are used to size the inductor value, the frequency and the duty cycle by solving a system of equations which minimizes the converter losses [138].

Finally, an output stage consisting of an integrated buck converter provides regulated 3.3 V supply for the micro-controller and the powered system.

### 3.3 REAL-LIFE AIR-FLOW DATA COLLECTION

This section is dedicated to the analysis of the air-flow conditions of the underground tunnel used as test scenario. The data collection was performed in a tunnel of the new Underground *Metro B1* line in Rome and took place after the construction phase of the tunnel was completed. More specifically, air-flow data were recorded in the pre-testing and testing phases of the new tunnel during which trains, as well as other vehicles used in construction works, were operated for testing purposes. Six Telos B nodes [23] equipped with a wind micro-turbine were used to instrument 220m of tunnel with the aim to collect air-flow data generated by passing trains (and vehicles) for 33 days. Figure 3.6 shows the nodes deployment in the tunnel and their distance from the *Conca D'Oro* train station. A dedicated TinyOS [154] application has been developed to track the voltage of the supercapacitor every 2 s. Whenever the measured voltage was higher than 3 mV, the collected data was stored in the node flash memory and marked with a time-stamp corresponding to the local time of the node. These voltage values were converted to the respective maximum power point voltage values in post processing by using Equation (3.1).

The nodes deployed in the tunnel of the *Metro B1* line were placed all at the same height along one side of the tunnel. The distance between consecutive nodes was variable, to allow to test air-flow data correlation in different conditions. Figure 3.5 shows a snapshot of two deployed nodes.

#### 3.3.1 COLLECTED AIR-FLOW DATA

Nodes were deployed in an Underground tunnel of the Metro B1 line in Rome for 33 days, from April 16<sup>th</sup>, 2012 to May 19<sup>th</sup>, 2012.

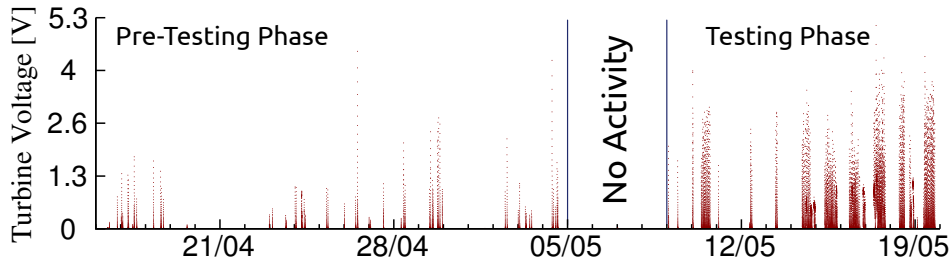


Figure 3.7: Turbine open circuit voltage detected during the three phases of the train test in the tunnel on the Metro B1 line. Data are those collected by the node with id 7.

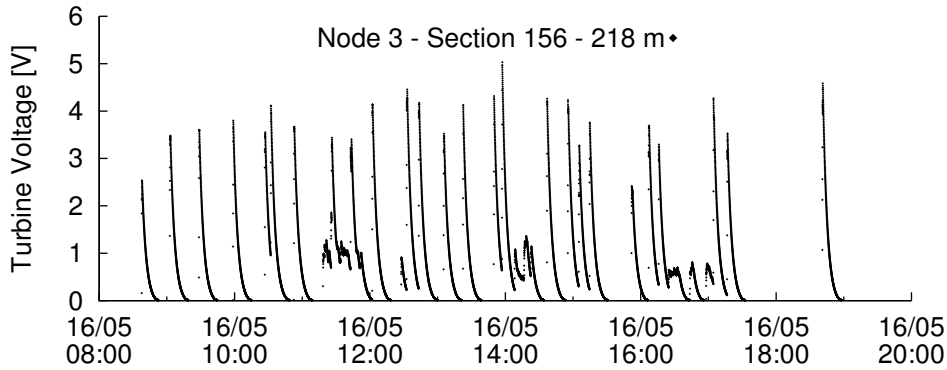


Figure 3.8: Data collected by node 3 on the 16<sup>th</sup> of May 2012.

Fig. 3.7 shows the three distinct phases of the Metro B1 train test during the period in which data were collected:

- (i) A pre-testing phase, in which most of the detected events were related to the movement of vehicles used in construction work.
- (ii) A phase of no activity, during which no passage in the tunnel was detected.
- (iii) A testing phase in which passing trains were detected.

Fig. 3.8 shows an example of data collected over one day by node 3, highlighting how harvesting events occurred fairly regularly.

### 3.3.2 TRAINS PASSAGE DETECTION

The detection of train passage events has been performed by considering the changes in the measured voltage of the micro-turbines over time. More in details, the detection algorithm works as follows:

1. Whenever the voltage generated by the micro-turbine starts increasing, a potential event is detected and its start time  $t_s$  is annotated;
2. The end time of the event is the instant of time  $t_e$  after which the voltage generated by the turbine starts decreasing and keeps dropping for at least 30 seconds<sup>1</sup>;
3. The energy generated in the period  $[t_s; t_e]$  is computed as explained in Section 3.3.3. If the total energy intake in such period is below a minimum detection threshold, the event is discarded, as it is likely not related to a train passage, but rather to wind blowing in the tunnel.

<sup>1</sup>Such 30 seconds interval is used as guard time, because during train passage events the voltage of the turbine does not monotonically increase or decrease, but it rather fluctuates depending on the train speed and on the position of the node with respect to the passing train.

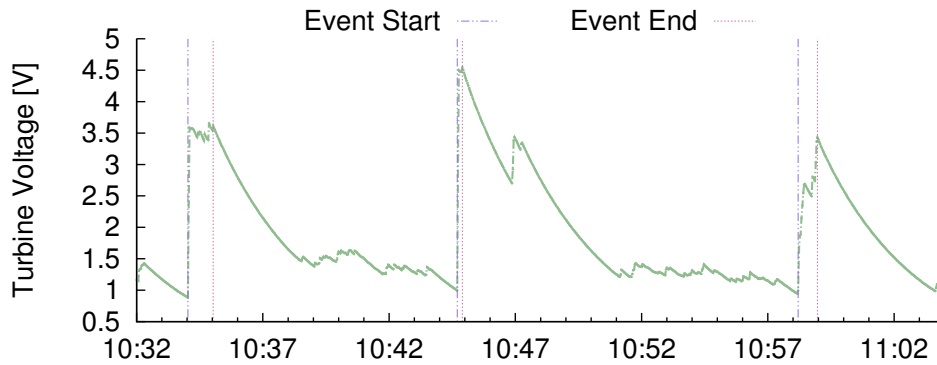


Figure 3.9: Detection of train passage events performed by node number 3. Dashed lines mark the time interval in which the event has occurred.

Table 3.1: Statistics about train passage events detected during the period 14-18 May: number of trains detected by each node, mean interarrival time (MIT) and standard deviation between the passage of two consecutive trains at daytime; average duration and standard deviation of each harvesting event.

Node	Detected trains	MIT (m:s)	$\sigma$ (m:s)	Duration (s)	$\sigma$ (s)
7	143	11:58	06:13	20	19.84
4	141	12:47	06:00	26	21.30
2	141	12:47	06:00	24	24.26
5	143	12:49	06:13	25	16.76
6	142	12:50	05:56	27	13.85
3	142	13:04	06:09	29	16.34

Fig. 3.9 shows an example of detection of train passage events. The measured turbine voltage is shown in the y-axis, while in the x-axis time is reported. Dashed lines mark the time interval in which the event has occurred. As shows in the figure, three train passage events were detected, with an average train inter-arrival time of 12 - 30 min. Table 3.1 reports the complete statistics about all the train passage events detected during the period 14 - 18 May 2012 by the six nodes deployed in the tunnel. More in details, the table shows, for each node, the total number of train passages detected, the mean interarrival time (MIT) and the standard deviation between the passage of two consecutive trains at daytime, and the average duration and standard deviation of each recharging event.

Such statistics are important because they are used by the nodes to estimate when the future energy recharging event is going to occur and for how long it is expected to last, thus allowing to devise pro-active strategies to plan in advance the energy usage. As reported in the table, results are quite similar for different nodes. Node 7 detects an average interarrival time lower than the other nodes. This is due to the fact that it is the node closest to the station, thus it is more exposed to air-flows that are not generated by trains passing in the tunnel. The average duration of its recharging events is also lower than that of other nodes, because trains decelerate when approaching the station.

### 3.3.3 ENERGY INTAKE CALCULATION

To calculate the energy intake generated by the micro-turbine during each train passage event, the open circuit voltage measured by the nodes has been converted to the voltage at maximum power point (as explained in sec. 3.2.1). Fig. 3.10 shows the voltage conversion performed for node number 3.

During train passage events, the capacitor voltage measured by the nodes alternates between increasing and decreasing periods (an example is shown in Fig. 3.9). When the voltage

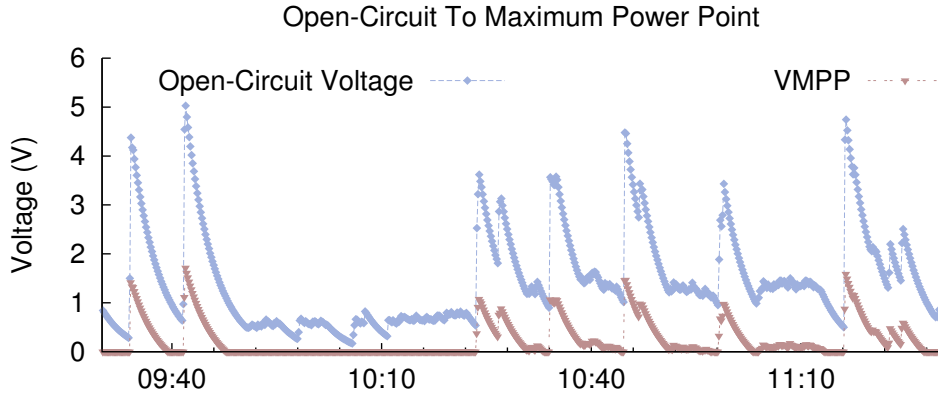


Figure 3.10: Open-circuit voltage to  $V_{MPP}$  conversion performed according to the empirical Equation (3.1). Plot refers to the data collected by node number 3.

increases, the harvested power is calculated according to a look-up table which relates voltages at MPP and actual power values. When the capacitor voltage decreases, however, the actual power that is being harvested by the node can not be known exactly. To estimate the actual voltage of the micro-turbine during such decreasing periods we defined three different heuristics:

- **Best:** the power harvested is computed by considering the voltage measured at the end of the last increasing period;
- **Worst:** the harvested power is assumed to be zero;
- **Average:** the power harvested is computed by considering a value equal to half of the voltage measured at the end of the last increasing period.

Fig. 3.11 shows an example of application of such heuristics. The Worst heuristic is the most pessimistic one, as it assumes the voltage of the micro-turbine during voltage decreasing periods to be zero. The Best heuristic, instead, assumes that during decreasing periods the voltage of the micro-turbine remains constant, thus leading to the most optimistic estimation of the harvested power. Finally, the Average heuristic is a balance between the other two.

Another possible approach to estimate the voltage of the micro-turbine during capacitor voltage dropping periods is to use interpolation techniques to approximate the decreasing trend. However, the duration of such events is usually quite limited (4 - 10 seconds or 2 - 5 voltage samples), making it difficult to obtain good results by interpolating the empirical data. Thus, the heuristic-based technique is the estimation method that best suits the data collected from the nodes deployed in the underground tunnel.

### 3.4 POWER MANAGEMENT ALGORITHM

This section deals with the power management algorithms to determine how to choose the proper rectifier bridge so as to maximize the power harvested by the node with minimal overhead.

#### 3.4.1 ADAPTIVE AND ADAPTIVE-F STRATEGIES

The first and simplest power management strategy considered is the one called *adaptive*. Such strategy constantly keeps track of the power generated by the micro-turbine over time and dynamically selects the rectifier to be used such as to maximize the efficiency of the conversion to be performed. More in details, the *adaptive* strategy uses the passive-Schottky topology when the harvested power is lower than 2 mW and the active topology when the

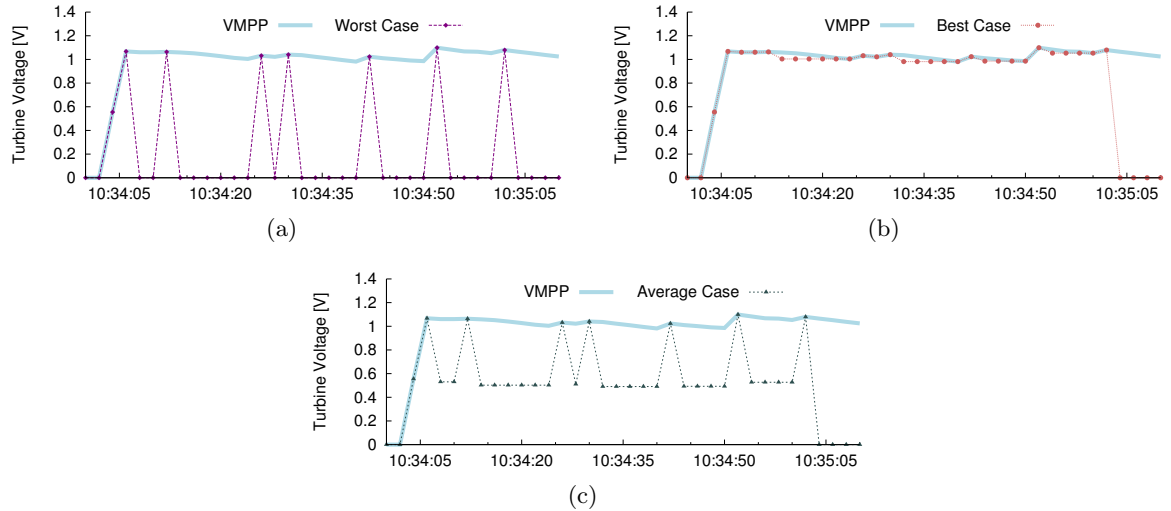


Figure 3.11: Turbine voltage estimation during voltage dropping periods using the (a) Worst, (b) Best and (c) Average heuristics.

harvested power is equal to or greater than such threshold (Fig. 3.3). Since it always selects the most efficient rectifier bridge, the *adaptive* strategy achieves the best results in terms of harvested energy. However, it also suffers from the highest overhead among the possible power management strategies, as it needs to monitor the power generated by the turbine constantly.

To reduce such overhead, a natural approach is to periodically monitor the power generated by the micro-turbine every  $f$  seconds, instead of performing continuous sampling. Every time that a sample is collected, the rectifier topology to use is dynamically selected by comparing the sampled value with the threshold of 2 mW discussed in Section 3.2.2. Once selected, such topology is then used until a new sample is collected. We call this strategy *adaptive- $f$* , where  $f$  is the sampling frequency in seconds. Based on the sampling frequency, such strategy clearly reduces the overhead of the system, at the cost of potentially not selecting the most efficient rectifier bridge at any given time  $t$ .

### 3.4.2 SMART STRATEGY

Since the tunnel scenario is almost totally predictable, knowledge of the environment may be exploited to further reduce the overhead of the system. To this end, a third strategy, called *smart*, is proposed. It specifically targets the underground tunnel scenario. The *smart* strategy is similar to the *adaptive- $f$*  approach, as it samples the power generated by the micro-turbine every  $f$  seconds and dynamically selects the rectifier to be used. However, differently for the *adaptive- $f$*  strategy, every time a sample is collected the *smart* approach tries to estimate the expected power intake during the next  $f$  seconds. The rectifier topology to use is selected based on such estimation, such as to maximize the conversion efficiency of the *expected* power. To forecast the expected power in the next  $f$  seconds, regression analysis, a statistical technique widely employed for prediction, is used. In the employed model, a simple linear regression is used in which the prediction variable is the time, denoted by variable  $t$ , and the response variable is the estimated power at time  $t$ , denoted by  $p^t$ . Given the set of the last  $n$  power observations,  $\{(t_{i-n}, p_{i-n}^t), \dots, (t_i, p_i^t)\}$ , the goal of simple linear regression is to find the equation of the straight line which would provide the best fit for the observed data points. Such equation can be found by minimizing the sum of squared residuals of the linear regression [155].

Moreover, in addition to power forecasting, the *smart* strategy also implements two specific

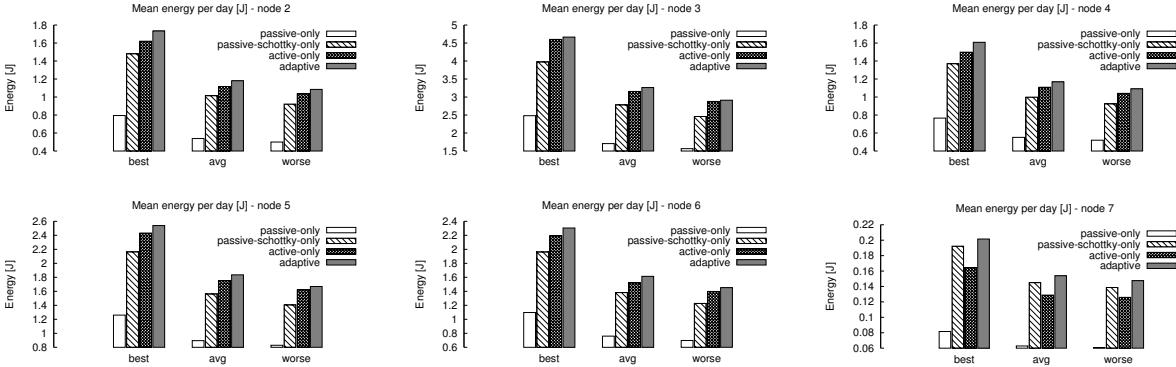


Figure 3.12: Comparison of the average amount of energy harvested per day by each node, when using the passive, passive-Schottky, active or adaptive rectification techniques

optimizations for the tunnel scenario, namely: 1) sampling is not performed at night time, as no trains passed in the tunnel during the train test phase between 8:10 PM and 8:15 AM, and 2) whenever a train passage is detected, no sampling is performed for the next six minutes, which is the minimum expected inter-arrival time between two consecutive train passages (Table 3.1). To detect train passage events, we used the algorithm detailed in Section 3.3.2.

### 3.5 EXPERIMENTAL COMPARISON OF POWER MANAGEMENT POLICIES

This section discusses the results of the performance evaluation of the power management techniques described in Section 3.4, as well as the passive, passive-Schottky and active topologies detailed in Section 3.2.2. For each rectification strategy, the metrics considered in each evaluation are: 1) average energy harvested per day by each node, and 2) overhead of the system, in terms of the average number of sampling performed per day by a node using a given strategy.

Fig. 3.12 shows the average energy gathered per day by each node in the tunnel scenario, based on the rectification technique used by the nodes. Energy is computed as follows: the voltage measurement recorded by the node is converted to the voltage at maximum power point according to Equation (3.1). To estimate the actual voltage of the micro-turbine during capacitor voltage dropping periods, the heuristics described in Section 3.3.3 are used. Once the micro turbine voltage has been estimated, the power harvested by the node is computed according to a look-up table which relates voltages at MPP and actual power values. The final value of the harvested power is then obtained by taking into account the efficiency of the rectification strategy used (Fig. 3.3).

Results are plotted for the *adaptive* rectification techniques and for the passive, passive-Schottky and active topologies. As can be seen from Fig. 3.12, the energy harvested per day varies significantly for different nodes, depending on their position in the tunnel. In particular, node 7, being deployed very close to the train station, harvests significantly less energy than the other nodes. For all the nodes, the *adaptive* technique consistently outperforms the passive-only, passive-Schottky-only and active-only topologies, resulting in significant increment in the amount of energy harvested. More in detail, the average energy harvested per day by using the adaptive strategy is, depending on the considered node, up to 146% higher than that harvested by the passive-only topology, up to 18% higher than that harvested by the passive-Schottky-only topology, and up to 22% higher than that harvested by the active-only topology. When considering all the nodes, the average harvested energy increase of

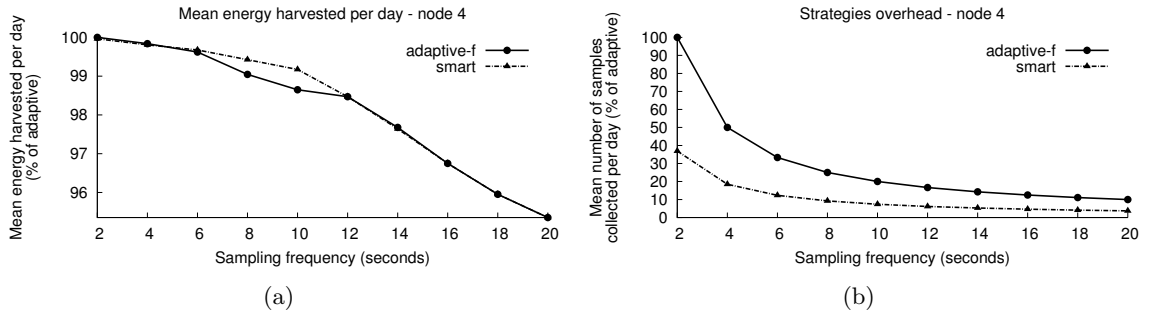


Figure 3.13: Comparison between *smart* and *adaptive-f* strategies for varying sampling frequency: (a) average energy harvested per day, as a percentage of the energy harvested by the *adaptive* strategy, and (b) strategies overhead in terms of average number of samples collected per day, as a percentage of the overhead introduced by the *adaptive* strategy.

the *adaptive* strategy with respect to the passive-only, passive-Schottky-only and active-only topologies is of 112%, 15% and of 7%, respectively.

As mentioned before, the *adaptive* strategy always achieves the best results in terms of harvested energy, but it suffers from the highest overhead. The second set of results shows the trade-off between the energy harvested by the nodes and the overhead introduced by managing the adaptive rectifier. The performance of the *adaptive-f* and of the *smart* strategies are thoroughly studied in terms of harvested energy and system overhead, for varying sampling frequency. Fig. 3.13(a) shows the average energy harvested per day by both the *adaptive-f* and the *smart* strategies, as a percentage of the energy harvested by the *adaptive* strategy, which represents indeed an upper bound on the energy harvestable by using the topologies described in Section 3.2. Fig. 3.13(b) shows the overhead introduced by the *adaptive-f* and *smart* strategies, in terms of the average number of sampling performed per day, as a percentage of the overhead introduced by the *adaptive* strategy. As it can be seen in Fig. 3.13(b), the *smart* strategy significantly reduces the overhead with respect to the *adaptive-f* approach, without impairing the capability of the nodes to harvest energy from air-flows. The number of sampling performed by the *smart* strategy is almost one third of that performed by *adaptive-f*. At the same time, the average energy per day collected by the *smart* strategy is always greater or equal to that of the *adaptive-f* strategy (Fig. 3.13(a)). For instance, by performing a sampling every 10 seconds the *smart* strategy is able to harvest an amount of energy per day that is more than 99% of that harvested by the *adaptive* strategy, introducing an overhead that is only  $\approx 7\%$  of that of the *adaptive* strategy. When using the same sampling frequency, the *adaptive-f* strategy harvests slightly less energy than the *smart* strategy, but its overhead is almost three times greater than that introduced by the *smart* strategy. Finally, the passive-Schottky-only and active-only topologies do not introduce any additional overhead, but they harvest only 93% and 85% of the energy obtained by the *adaptive* strategy.

### 3.6 CONCLUSIONS

In this chapter we presented a power management technique for improving the efficiency of harvesting energy from air-flows generated by trains passing in an underground tunnel. The key feature of the proposed solution is the adaptive AC-DC converter, a hybrid voltage rectifier which exploits both passive and active topologies combined with power prediction algorithms. Such combined approach significantly outperforms other rectification topologies, resulting in an increase of efficiency between 10% and 30% with respect to the only-passive and the only-active solutions. To evaluate the effectiveness of the presented approach, a data collection campaign has been conducted in a tunnel of the new Underground *Metro B1* line in Rome. Six Telos B motes equipped with wind micro-turbines are used to instruments

220m of tunnel and collected air-flow data for 33 days. We found that, by using the adaptive AC-DC converter, nodes deployed in the tunnel can harvest up to 22% more energy than that harvested by using the active-only or the passive-only rectifiers. Finally, we proposed a *smart* power-management strategy which exploits the predictable tunnel scenario to significantly reduce the overhead of the system. Such strategy performs an average number of sampling per day that is only 7% of that of the *adaptive* strategy and almost one third of that of the *adaptive-f* strategy. At the same time, the average energy per day collected by the *smart* strategy is always greater or equal of that of the *adaptive-f* strategy.



---

## SENSOR-MISSION ASSIGNMENT IN RECHARGEABLE WIRELESS SENSOR NETWORKS

Field and environmental monitoring are common applications of wireless sensor networks. In a typical scenario, the nodes of a WSN are placed in a region for collecting measurements about some phenomenon. The number of active nodes in the network (i.e., those currently performing their sensing and communication tasks) determines the accuracy and precision of the collected data and the number of tasks that can be completed successfully. There is a tradeoff between accuracy, the number of tasks performed, and the longevity of the network. Since WSNs are usually intended to last for long periods of time, the number of active nodes should be carefully managed. Recent works [156, 157, 158] have addressed selective activation of nodes, i.e., sensing tasks are allocated only to a group of sensor nodes over time, allowing the other nodes in the network to go to sleep and save energy. Many applications, however, may require the network to achieve multiple, simultaneous missions, potentially competing for the sensing resources of the nodes. A natural example is a surveillance network in which nodes are equipped with pan-tilt-zoom cameras, which can be rotated to point in a direction of interest. The same camera can not thus be used by two different missions monitoring two distinct targets located in the opposite regions of a field [18]. A similar scenario is a network deployed to perform concurrent localization and intrusion detection tasks using directional acoustic sensors that can be assigned to only one mission at a time [18]. More generally, sensor nodes, together with other information sources, may be part of a collection of intelligence, surveillance, and reconnaissance (ISR) assets that should be allocated to support the objectives of a mission [159, 160].

In these scenarios, a sensor selection scheme is no longer sufficient, because it is necessary not only to decide which nodes in the network are active, but also to assign each active sensor to the mission it may serve best. This is a non trivial task, because a given node may offer support to different missions with different levels of accuracy and fit (*utility*). Meanwhile, missions may vary in importance (*profit*) and amount of resources they require (*demand*). They may also appear in the network at any time and may have different durations. A mission is executed if enough sensors are assigned to it, based on its demand and on the quality of contribution that the assigned sensors can provide to it. In this scenario, the goal of a sensor-to-mission assignment algorithm is to assign available nodes to appropriate missions, maximizing the profit received by the network for mission execution.

Different constraints on the assignment decision lead to different versions of this problem, depending on whether missions arrive over time [18, 19, 21] (dynamic case) or they are all available when network operations start [20, 19, 21] (static case). Other variants concern whether the network has a predefined target operational lifetime [21] or must last as long as possible [19]. Some prior solutions are energy aware, in the sense that they take into account

nodal residual energy to decide mission assignments. In doing so, however, they make the specific assumption that energy is monotonically decreasing, as is typical with a battery, and therefore residual energy is the only criterion for assigning missions.

In EHWSNs, sensor nodes mount devices such as energy harvesters and supercapacitors, which draw new energy from the environment surrounding a node and store it, respectively. For these nodes, new paradigms for mission assignments are needed, which take into account that nodes currently having little or no energy left might have enough in the future to carry out new missions. These solutions should also consider that energy availability is time-dependent and that energy storage is limited in size and time (due to self-discharge). So energy usage should be carefully planned to minimize energy waste.

In this chapter we are concerned with the practical case of WSNs that run applications requiring the network to be operational for a given amount of time, serving missions that arrive dynamically in the network (*dynamic assignment with a time horizon*). We study this case with sensor nodes that have energy harvesting capabilities. We refer to the given amount of time the network is expecting to be operational, i.e., accepting and completing missions, as the *target lifetime* of the network.

We make the following contributions:

- We model the problem of optimum mission assignment in energy harvesting WSNs. Our model selects which missions to execute and the nodes that should execute them so that the profit throughout the network operational lifetime is maximized. By addressing scalability issues of previous approaches, we provide a MIP formulation that can be solved for real-life-sized instances, consisting of hundreds of nodes and with target lifetimes of several months. At the same time, our MIP model captures the details of the behavior of a typical energy harvesting subsystem, by modeling several advanced real-life characteristics such as: hybrid storage systems consisting of multiple energy storage devices; supercapacitor and battery non-idealities (limited storage size, charging and discharging efficiency); variations in the power consumption of the node; capability of using the harvested energy directly, when possible. The mathematical model we propose provides an upper bound to the maximum profit achievable by the networks, considering both energy and assignment constraints. Thus it serves as a benchmark for more realistic, distributed protocols. We demonstrate that considering buffer non-idealities significantly reduces overestimations of the available energy, providing a tighter bound on the optimal solution.
- We provide the first ENergy harvesting-aware sensor-Mission ASSignmEnt distributed algorithm (denoted EN-MASSE). In order to decide whether to bid for a given mission or not, an EN-MASSE node considers not only the nodal residual energy, but also the energy it expects to harvest in the future (using a harvester-based energy prediction model) and the expected profit and demand of missions to come. Since our approach is general, EN-MASSE may be combined with any energy prediction model. Additionally, we propose a simple yet effective long-term energy prediction algorithm, based on historical weather data, that can be integrated with EN-MASSE to further improve its performance and to fine-tune its behavior over longer timeframes.
- We provide a simulation-based performance evaluation framework for energy harvesting WSNs. In our experiments, we use traces of the availability of solar energy that we obtained by interfacing TelosB nodes with solar cells, collecting data for several months under variable weather conditions and in different locations. We also validate our approach by using four additional solar datasets obtained from the US Climate Reference Network (USCRN). Specifically, we considered one year of solar datasets from four different weather stations, located in Santa Barbara, CA, Boulder, CO, Durham, NH and

Darrington, WA. We implemented EN-MASSE as well as the major existing mission assignment schemes in such simulator.

- We perform a comparative performance evaluation of EN-MASSE, the schemes proposed by Johnson et al. in [21], as well as an upper bound on the optimum mission profit computed by our analytical model. We evaluate the impact of critical parameters, such as the target lifetime, the types of sensors embedded in the nodes (and their energy consumption), the supercapacitor size and the mission arrival rate, on the performance of the different schemes in twenty distinct scenarios. Our results confirm that EN-MASSE is able to significantly outperform previous schemes in terms of profit achieved, efficient usage of the harvested energy, capability to support critical missions over time, performance stability and robustness. More specifically, we show our solution perform up to 160% better than other energy-aware assignment methods in terms of achievable profit. EN-MASSE exhibits better performance in terms of profit stability and robustness to the variability of the environmental source, as well as graceful battery depletion and better usage of the renewable energy. Furthermore, the profit earned by EN-MASSE are remarkably close to optimum, i.e., between 0.54% and 11.29% below the upper bound provided by our MIP model.
- We implemented our proposed solution in TinyOS and experimentally validate its performance in a real-life testbed of solar-powered Telos B motes equipped with cameras.

The remainder of this chapter is organized as follows. We discuss related work in Section 4.1. In Section 4.2 we formulate the mission assignment problem for energy harvesting WSNs and provide an analytical model that maximizes network profit. We present EN-MASSE in Section 4.3 and compare it to previous solutions and the upper bound derived by the model in Section 4.4. In Section 4.5 the experimental validation of EN-MASSE is presented, reporting results obtained from a testbed of Telos B motes interfaced with directional video sensors. Finally, we present our conclusions in Section 4.6.

## 4.1 RELATED WORK

The general problem of sensor-mission assignment, being a key issue in the intelligence, surveillance, and reconnaissance (ISR) domain [159, 160, 161], has received considerable attention lately. Bar-Noy et al. introduced the Semi-Matching with Demands (SMD) in [20]. Their approach is based on different priorities and demands of each mission and on additive utility values for each sensor-mission pair. In the original SMD profits are awarded only if a certain utility threshold is met and the problem is defined only for a set of missions known a priori. SMD was extended in [19, 162], incorporating both a profit threshold in case of partial mission satisfaction and mission dynamics. The authors propose centralized and distributed approaches for maximizing the network profit by satisfying all missions available at a given time. They also provide an energy-aware assignment scheme for prolonging the network lifetime. However, the case in which the network operates for a finite target lifetime is not considered. A variation of the sensor-mission assignment problem, motivated by frugality and conservation of resources, was addressed by Johnson et al. in [21]. The authors show that finding an optimal solution to the dynamic sensor-mission assignment problem is NP-hard. They then propose a heuristic where the assignment decisions depend on the sensors energy, exposing a trade-off between network lifetime and achievable profit. Rather than satisfying all missions available at a given time, this scheme allows the nodes to autonomously decide the missions in which they will participate based on their residual energy.

Other related problems with different assignment constraints have been studied. Pizzocaro et al. introduced the Sensor Utility Maximization (SUM) problem in [163], in which missions are associated with uncertain demands for sensing resource capabilities. In [161], Le et al.

consider missions than can be decomposed into a set of specific tasks and solve the sub-problem of sensor-task assignment, allowing sensors to be shared and reassigned between mission subtasks. Their work was extended in [164], by adding an adaptive negotiation mechanism in the allocation process. In [18], Rowaihy et al. describes two utility models where the contribution provided by multiple sensors to a mission may be combined not only additively, as in previous works, but also in more involved ways. They also introduce the concept of fuzzy location, which may be useful to preserve location privacy. Their work was later extended in [165], by turning the focus on maximizing the profit achieved by the network while preserving sensors' location privacy. Erol-Kantarci et al. considers in [166] a network of wireless rechargeable sensors powered by Radio Frequency (RF)-based energy transfer. Their goal is to optimize the placement of RF-based chargers such as that the nodes with replenished batteries participate in profit maximizing missions.

With respect to previous works discussed in Section 1.4, which targets task scheduling in energy harvesting networks, our approach has two fundamental differences. First, our primary goal is to maximize the network profit within a given time horizon, rather than enabling the network to operate perennially. Thus, requesting the nodes to achieve energy neutrality, such as in [36, 115, 116], may conflict with our goal, because some profitable missions may be rejected when the current harvesting rate is low. For this reason, we may want to violate energy neutrality when necessary to better serve important missions. Second, the problem we address is harvesting-aware *collective* task allocation at network level, i.e., how to assign nodes in the network to competitive tasks that may require the simultaneous contribution of multiple sensors. Such problem is quite different from the task scheduling problem tackled by other works, which instead focus on *individual* tasks scheduling at node level.

## 4.2 PROBLEM FORMULATION

In this section, we formulate the mission assignment problem for energy harvesting WSNs. In Section 4.2.1 we describe the architecture of a typical node with energy harvesting capability and give some details about non-ideal energy storage buffers. Section 4.2.2 discusses the general application scenarios for our model. In Section 4.2.3 we discuss the approach we take to provide an analytical model for the mission assignment problem in energy harvesting WSNs. Our MIP formulation of the assignment problem, whose solution provides an upper bound on the maximum achievable profit over a given target lifetime, is described in Section 4.2.4. Finally, in Section 4.2.5 we discuss hardness results for the sensor-mission assignment in energy-harvesting WSNs.

### 4.2.1 NODE ARCHITECTURE

Each node in the network is equipped with an energy harvesting subsystem, which includes one or more photo-voltaic panels<sup>1</sup> and a supercapacitor that acts as an energy buffer for the node. In our model and simulations, we try to capture the details of the behavior of a typical supercapacitor, modeling realistic characteristics such as the fact that it has a finite size  $C^{Max}$ , that it suffers from leakage and self-discharge, and that it has a charging efficiency  $\eta_c^C < 1$  and a discharging efficiency  $\eta_d^C < 1$ , which results in some energy being lost during charging and discharging. Nodes are also equipped with a non-rechargeable primary battery of capacity  $B^{max}$ , whose purpose is to guarantee a minimum lifetime in case no or little energy can be drawn from the environment. Similar to the supercapacitor, also the battery has a discharging efficiency  $\eta_d^B < 1$ .

The hybrid system of solar harvester, supercapacitor, and primary battery provides the energy to power the node and to support the sensing activity required for mission execution.

---

<sup>1</sup>Although we focus here on solar-based harvesters, our approach is general and can be applied to other energy sources as well.

An actual supercapacitor deviates from an ideal energy buffer in many ways. First, it has a finite size  $C^{Max}$  and therefore can hold only a finite amount of energy. Second, it suffers from leakage and self-discharge, through which energy is lost even if the supercapacitor is not in use. Finally, it has a charging efficiency  $\eta_c^C < 1$  and a discharging efficiency  $\eta_d^C < 1$ , i.e., some energy is lost while charging and discharging the supercapacitor. All these aspects have been explicitly accounted for in our models and solutions.

#### 4.2.2 APPLICATION SCENARIOS

We aim at providing a formulation of the sensor-mission assignment problem that captures several aspects of real-life systems, while providing enough flexibility to be applicable to a number of different scenarios.

Our model allows us to define:

1. an application-specific measure of how valuable the data generated from a particular node are for performing a given task (utility);
2. the minimum amount of resources needed by each task to successfully complete (mission demand);
3. the priority and importance of each task (mission profit).

The concept of utility provided by a sensor to a given mission is useful for defining several application-specific requirements of practical scenarios [167]. For example, a given camera node may be totally useless to a target-tracking application if its video sensor is not oriented in a given direction. At the same time, a microphone is more useful to the application if it is closer to the observed area.

The demand of a mission is another application-specific quantity strictly related to the aforementioned concept of utility. It can be used to simply indicate how many sensors should be assigned to a particular task, but also to evaluate the overall quality of contribution that the nodes assigned to a mission are able to provide to it. For instance, a mission to capture a 3D representation of a particular target will fail if only one camera is assigned to it, and the accuracy of the resulting image will depend not only on how many nodes are assigned to the mission, but also on their positions and orientations. In other scenarios, instead, it may be desirable to have as many nodes as possible monitoring the same target to increase the redundancy of the measurements and, thus, the robustness of the network to unpredictable events [168].

Finally, the profit of a task is an application-specific quantity that defines its level of importance. This quantity may be used to discriminate between routine (low-profit) missions, and critical, high-profit missions that can be triggered when measured values are above an alarm threshold or upon occurrence of specific events.

#### 4.2.3 ANALYTICAL MODEL

The mission assignment problem for wireless sensor networks equipped with an energy harvesting subsystem such as the one described in Section 4.2.1 is mathematically formulated as follows. The network consists of a set of energy-harvesting-endowed sensor nodes  $N_1, \dots, N_n$ , pre-deployed in a field. At any time, a mission may appear in the network at a specific geographic location. Let  $M_1, \dots, M_m$  be the set of missions that the network is asked to perform.

A mission  $M_j$  is a tuple  $(p_j, d_j, g_j, ts_j, te_j)$  where:

$p_j$  is the profit of the mission per unit time, indicating both its importance and the reward achieved by the network for its accomplishment;  
 $d_j$  is the mission demand, indicating the amount of sensing resources it needs;  
 $g_j$  is the geographic location of the mission in the field;  
 $ts_j$  is the time at which the mission arrives in the network;  
 $te_j$  is the time at which the mission terminates.

Missions usually last for multiple units of time, i.e.,  $te_j > ts_j$ . During mission execution,  $p_j, d_j, g_j$  remain constant over time.

A mission is executed only if a sufficiently good set of sensors is assigned to it, where sensor quality is mission-specific. We define  $e_{ij}$  as the utility received by mission  $M_j$  if node  $N_i$  is assigned to it. This utility is zero if the node cannot contribute to the mission, which happens, for instance, if the node is not close enough to the mission location or if the orientation of the directional sensor is not useful to the mission. Different values of  $e_{ij}$  can indicate the “quality of contribution” that a sensor can provide to a particular mission.

While missions can be performed by multiple sensors simultaneously, we assume that a node, being equipped with directional sensors, can be assigned to at most one mission at a time.

Let  $u_{jt}$  denote the total utility received by a mission  $M_j$  at time  $t$ . We express the total utility  $u_{jt}$  as the sum of the utilities provided by the sensors assigned to the mission  $M_j$  at time  $t$ . That is,  $u_{jt} = \sum x_{ijt}e_{ij}$ , where  $x_{ijt} = 1$  if and only if node  $i$  is serving Mission  $j$  at time  $t$ . In this model, utility from each node is independent of the other nodes assigned to a sensor. Although this weighted linear model does not capture the 3D representation example of Section 4.2.2, it does capture the inability of specific sensors to serve a mission as described in the same section. Our model represents utility models more complex than simple counting, as well as other scenario-specific utility functions defined by the user.

The total utility that a mission  $M_j$  requires is expressed by its demand  $d_j$ . If the total utility  $u_{jt}$  received by a mission is lower than its requested demand  $d_j$ , we say that the mission  $M_j$  is partially satisfied (at time  $t$ ) and we indicate its satisfaction level with  $y_{jt} = u_{jt}/d_j$  (in the range  $[0, 1]$ ).

Profits are received by the network for mission accomplishment, based on the satisfaction level of the mission. In this formulation of the mission assignment problem, profits can be awarded fractionally, but only if a minimum satisfaction threshold  $T_{sat}$  is met. We use a single satisfaction threshold for all missions, but the formulation would be essentially the same if the threshold varies by mission.

The profit achieved for executing mission  $M_j$  at time  $t$  depends on the satisfaction level  $y_{jt}$  of the mission at time  $t$ , as shown in Figure 4.1. The profit achieved by the network for mission execution is: zero if the minimum satisfaction threshold  $T_{sat}$  is not met; a fraction of the mission profit if the satisfaction threshold is met, but the mission is not fully satisfied; equal to the mission profit,  $p_j$ , if the mission is fully satisfied.

Since missions usually last for multiple units of time, the total profit received for executing mission  $M_j$  is the sum of the profits earned over the entire mission lifetime, i.e.,  $p_j = \sum_{t=ts_j}^{te_j} p_{jt}(y_{jt})$ .

Ideally, we seek an assignment of sensors to missions that always satisfies each mission’s demand at least to the given satisfaction threshold. However, satisfying all missions may not be feasible. Thus our goal is to maximize the total profit obtained by the network over a given target lifetime.

$$p_{jt}(y_{jt}) = \begin{cases} p_j, & \text{if } y_{jt} \geq 1 \\ p_j \cdot y_{jt}, & \text{if } T_{sat} \leq y_{jt} < 1 \\ 0 & \text{if } y_{jt} < T_{sat} \end{cases}$$

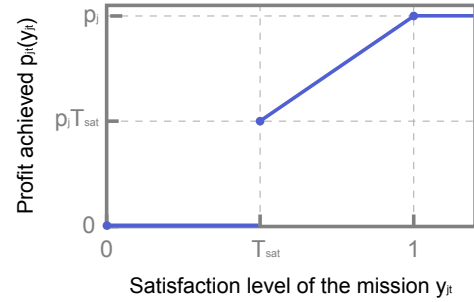


Figure 4.1: The profit achieved for mission execution is a function of mission satisfaction level

#### 4.2.4 SENSOR-MISSION ASSIGNMENT PROBLEM: MIP FORMULATION

In this section, we describe a MIP formulation for the sensor-mission assignment problem in energy-harvesting WSNs, whose solution provides an upper bound on the maximum achievable profit over a given target lifetime.

Previous works have proposed MIP formulation for sensor-mission assignment in traditional WSNs. For example, Johnson et al. considered battery-operated nodes that lose energy monotonically [21]. When nodes can harvest energy, however, the energy available to each node fluctuates over time. This characteristic adds significant complexity to the MIP problem, because it is necessary to update the energy level of the nodes with higher frequency to accurately represent the current energy availability. The model should also capture energy buffer non-idealities, such as limited capacity and charging/discharging efficiency, to avoid grossly overestimating the energy available to the nodes.

One possible solution to this problem is to divide time into discrete time epochs of small size and update the energy level of the nodes periodically [5]. Since the environmental energy strongly varies over time, such updates should be performed within seconds or minutes, with a tradeoff between an accurate representation of the energy variations and the model scalability. However, we found such an approach difficult to scale, especially when considering real-life instances with hundreds of nodes and target lifetimes of weeks or months.

We thus propose in this work more scalable approach to formalize the sensor-mission assignment in energy harvesting WSNs. Our idea is to divide time into discrete time epochs of relatively large size, and to compute off-line the variations in the energy level of the nodes within each of such epochs. More specifically, we define the set of time epochs in which the energy level of the node  $N_i$  is updated,  $\tau_i^c$  (where  $c$  stands for “check”), as the union of all times in which a mission starts or ends within its sensing range. In this way, when a new mission arrives and a decision has to be made about assigning a node to it or not, we ensure that the energy level of the node is up to date. Similarly, at the end of each mission the energy levels of the nodes that were assigned to it are updated considering the energy spent for its execution.. Figure 4.3 shows an example of  $\tau_i^c$ : missions  $M_i, M_j$  arrive within the sensing range of node  $N_i$  at different times. The energy level of  $N_i$  is updated at both their start and end times. The variations in the energy level of the nodes are not explicitly calculated in the model; instead, they are pre-computed off-line through simulations that account for both fluctuations in the environmental energy availability and non-ideal behaviors of the energy storage. These pre-computations are necessary because the energy available to the node fluctuates over time, according to the variability of the energy source. For this reason,

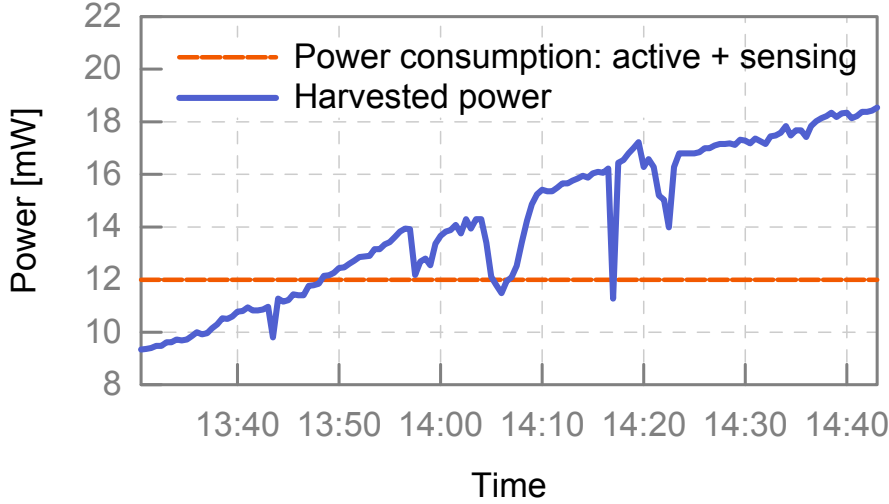


Figure 4.2: Power harvested by the node  $N_i$  during time epoch  $t$  and energy consumption required by the sensing activity.

considering a simple indicator, such as the average power, of the energy harvested during each time epoch is not enough to correctly represent the real energy availability. For instance, Figure 4.2 shows the power harvested by node  $N_v$  during a particular time epoch  $t$  spanning between 1:30PM and 2:40PM. During this period, the mean harvested power is around 14.20 mW, while the power consumption of the node is set to 12 mW, assuming  $N_i$  is executing some mission  $M_j$ . Despite the fact that the mean harvested power is higher than the power consumption of  $N_i$ , at the beginning of time epoch  $t$  the harvested power is not enough to directly power the node, thus requiring some energy from an external buffer to be supplied. To correctly model such situations, the MIP model should assign the node  $N_i$  to the mission  $M_j$  only if  $N_i$  has enough energy available in its battery and supercapacitor at the beginning of time epoch  $t$ .

Energy pre-computations allow us to identify such critical points in terms of energy availability and to make correct decisions for mission assignment, even when considering large time epochs during which the harvested energy may vary significantly. Moreover, these pre-computations are also used to simulate how the energy level of the supercapacitor will vary during each time epoch according to the power harvested, in order to capture features of realistic energy buffers, such as limited capacity and charging/discharging efficiency. More details about this approach are explained in Section 4.2.4.

Compared to fine-granularity updates of the energy level of the node, our solution provides a substantial reduction of the number of time epochs considered in the model, thus significantly improving the MIP problem scalability.

It is worth noting that we follow this approach only when computing an upper bound on the maximum achievable profit; our distributed heuristic, presented in Section 4.3, does not suffer from such scalability issues.

### MIP formulation

We model the sensor-mission assignment problem in energy harvesting WSNs as reported in the mathematical program (MP) 1. Please refer to Table 4.1 for notations.



**Mathematical program 1** Sensor-mission assignment problem in energy harvesting WSNs

$$\max \sum_{M_j} \sum_{t \in Tm_j} L_j(t) * p_j * y_{jt} \quad (4.1)$$

$$\text{s.t.} \quad \sum_{\substack{t' \in Tm_j: \\ t' \leq t}} \sum_{\substack{N_i: \\ j \in aM_i(t')}} x_{ijt'} * e_{ij} \geq d_j * y_{jt}, \quad \forall M_j, t \in Tm_j \quad (4.2)$$

$$\sum_{j \in aM_i(t)} \sum_{\substack{t' \in \tau_i: \\ ts_j \leq t' \leq t}} x_{ijt'} \leq 1, \quad \forall N_i, t \in \tau_i \quad (4.3)$$

$$x_{ijt} \leq \sum_{\substack{j' \in aM_i(t): \\ te_{j'} = t}} \sum_{\substack{t' \in \tau_i: \\ ts_{j'} \leq t' < t}} x_{ijt'}, \quad \forall N_i, t \in \tau_i, j \in aM_i(t) : ts_j < t \quad (4.4)$$

$$C_{it} \leq C_{it} + D_{it} + \Delta_{it}^I + \\ - (\Delta_{it}^I - \Delta_{it}) \sum_{j \in aM_i(t)} \sum_{\substack{t' \in \tau_i: \\ ts_j \leq t' \leq t}} x_{ijt'}, \quad \forall N_i, t \in \tau_i^c \quad (4.5)$$

$$B_{it} \leq B_{it} - D_{it}, \quad \forall N_i, t \in \tau_i^c \quad (4.6)$$

$$D_{it} \leq B_{it}, \quad \forall N_i, t \in \tau_i^c \quad (4.7)$$

$$C_{it} + B_{it} \geq \mu_{ijt} x_{ijt}, \quad \forall N_i, t \in \tau_i, j \in aM_i(t) \quad (4.8)$$

$$y_{jt} \leq z_{jt} \quad \forall M_j, t \in Tm_j \quad (4.9)$$

$$z_{jt} \leq 1 + y_{jt} - T_{sat} \quad \forall M_j, t \in Tm_j \quad (4.10)$$

$$x_{ijt} \in \{0, 1\}, \quad \forall N_i, t \in \tau_i, j \in aM_i(t) \quad (4.11)$$

$$0 \leq y_{jt} \leq 1 \quad \forall M_j, t \in Tm_j \quad (4.12)$$

$$z_{jt} \in \{0, 1\} \quad \forall M_j, t \in Tm_j \quad (4.13)$$

$$0 \leq C_{it} \leq C_{max} \quad \forall N_i, t \in \tau_i^c \quad (4.14)$$

$$0 \leq B_{it} \leq \eta_d^B B_{max} \quad \forall N_i, t \in \tau_i^c \quad (4.15)$$

$$0 \leq D_{jt} \leq \eta_d^B B_{max} \quad \forall N_i, t \in \tau_i^c \quad (4.16)$$

We seek an assignment of nodes to missions that maximizes the total profit obtained by the network (4.1). There are six sets of variables:

$y_{jt}$  is the satisfaction level of the mission  $M_j$  at time  $t$ ;

$z_{jt}$  indicates whether  $y_{jt}$  is 0 or in its continuous region;

$x_{ijt}$  indicates if the node  $N_i$  starts serving the mission  $M_j$  at time  $t$ ;

$C_{it}$  is the energy level of the supercapacitor of the node  $N_i$  at time  $t$ ;

$B_{it}$  is the energy level of the battery of the node  $N_i$  at time  $t$ ;

$D_{it}$  is the energy drained from the battery of the node  $N_i$  during time epoch starting at time  $t$ .

Table 4.1: Table of notations.

Symbol	Explanation
<i>Variables</i>	
$y_{jt}$	satisfaction level of mission $M_j$ at time $t$
$z_{jt}$	(binary) indicates whether $y_{ij}$ is 0 or in its continuous region
$x_{ijt}$	(binary) indicates if node $N_i$ starts serving mission $M_j$ at time $t$
$C_{it}$	supercapacitor energy level of node $N_i$ at time $t$
$B_{it}$	battery energy level of node $N_i$ at time $t$
$D_{it}$	energy drained from battery of node $N_i$ during time epoch starting at time $t$
<i>Parameters</i>	
$p_j$	profit of the mission $M_j$
$d_j$	demand of the mission $M_j$
$g_j$	geographic location of the mission $M_j$ in the field
$ts_j$	time mission $M_j$ arrives in the network
$te_j$	time mission $M_j$ terminates
$e_{ij}$	utility received by mission $M_j$ if node $N_i$ is assigned to it
$u_{jt}$	total utility received by the mission $M_j$ at time $t$
$T_{sat}$	minimum satisfaction threshold; if $y_{jt} < T_{sat}$ no profit is awarded for mission execution
$C_{max}$	supercapacitor size
$B_{max}$	battery size
$\eta_c^C$	supercapacitor charging efficiency, $\eta_c^C < 1$
$\eta_d^C$	supercapacitor discharging efficiency, $\eta_d^C < 1$
$\eta_d^B$	battery discharging efficiency, $\eta_d^B < 1$
$\tau_i$	set of time epochs in which node $N_i$ can start executing a mission
$\tau_i^c$	set of time epochs in which the energy level of the supercapacitor of the node $N_i$ is updated, i.e., $\tau_i^c = \bigcup_{j \in aM_i} \{ts_j \cup te_j\}$
$aM_i(t)$	set of missions node $N_i$ may serve at time epoch $t$ , i.e. $aM_i(t) = \{M_j : e_{ij} > 0 \wedge ts_j \leq t \leq te_j\}$
$aM_i$	set of missions node $N_i$ can serve, i.e. $aM_i = \bigcup_{t \in \tau_i} aM_i(t)$
$Tm_j$	set of time epochs in which a node may start executing mission $M_j$ i.e. $Tm_j = \bigcup_{N_i: e_{ij} > 0} \{t \in \tau_i : ts_j \leq t \leq te_j\}$
$\hat{t}$	next time epoch after $t$ , i.e., $S = (t_1, \dots, t, t_{i+1}, \dots, t_s)$ , $\hat{t} = t_{i+1}$
$L_j(t)$	length of the time epoch $t$ in the set $Tm_j$ , i.e., $L_i(t) = \min(\hat{t}, te_j) - t$
$\Delta_{it}$	variation in the energy level of the supercapacitor of the node $N_i$ during time epoch $t, t \in \tau_i^c$ , assuming the node is executing a mission
$\Delta_{it}^I$	variation in the energy level of the supercapacitor of the node $N_i$ during time epoch $t, t \in \tau_i^c$ , assuming the node is not executing a mission
$\mu_{it}$	minimum energy level reached by the supercapacitor of the node $N_i$ during time epoch $t, t \in \tau_i^c$
$\mu_{ijt}$	minimum energy level reached by the supercapacitor of the node $N_i$ if $N_i$ starts executing $M_j$ during time epoch $t, t \in \tau_i^c$

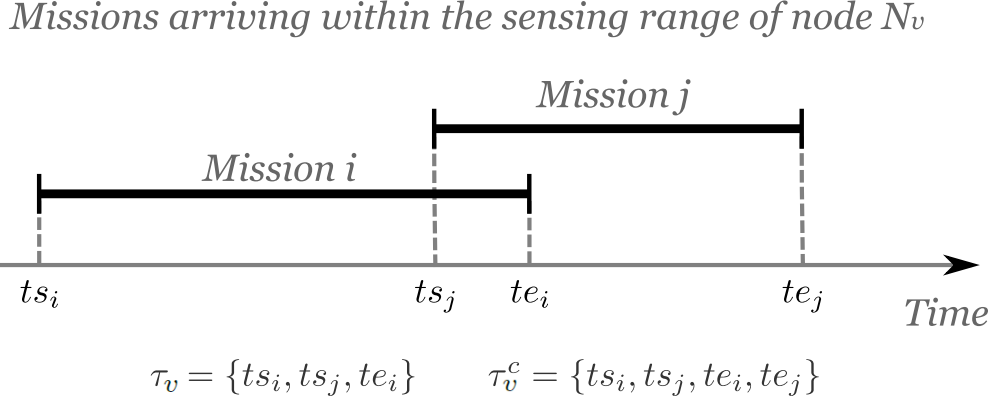


Figure 4.3: Missions  $M_i$  and  $M_j$  appear at different times within the sensing range of node  $N_v$ .  $N_v$  can start executing mission  $M_i$  at time  $ts_i$ . It can start executing missions  $M_j$  either at time  $ts_j$  or  $te_i$  (if it was executing mission  $M_i$  before  $M_j$  arrived). Thus,  $\tau_v = \{ts_i, ts_j, te_i\}$ . The energy level of node  $N_v$  is updated before each mission's start and end times;  $\tau_v^c = \{ts_i, ts_j, te_i, te_j\}$ .

The  $x_{ijt}$  variables are the only decision variables. The others are determined by the  $x_{ijt}$  variables, the other constraints, and the objective function.

The satisfaction level  $y_{jt}$  of the mission  $M_j$  at time  $t$  depends on the utility received by the mission with respect to its demand (4.2). The variable  $y_{jt}$  is effectively a semi-continuous variable, which either must take a value between  $T_{sat}$  and 1, or it must be zero ((4.12) enforces the upper and lower bounds). We implement this using the binary helper variables  $z_{ij}$ . If  $z_{ij} = 0$ , then  $y_{ij} = 0$  by constraints (4.9). Constraints (4.10) ensure that  $z_{ij}$  is not allowed to be 1, and hence  $y_{ij}$  is not allowed to be non-zero, until  $y_{ij} \geq T_{SAT}$ . We consider the case in which preemption between missions is not allowed : a node may be assigned to at most one mission at a time and, once assigned to it, it runs the mission until completion (4.3). A node can only start executing a mission either when it arrives in the network or when another mission that the node was executing ends. Thus, nodes are forbidden to start a mission at an arbitrary time within its duration. The problem constraint (4.4) implements this rule: it does not allow a node to start serving a mission that already started, unless another mission that the node was serving just terminated.

Constraint (4.5) updates the energy level of the capacitor after each time epoch, both in the case the node is executing a mission, or it is idle. When a node starts executing a mission, it must have enough energy stored in its capacitor and in its battery to run it until completion (4.8). More details about the problem constraints (4.5) and (4.8) are given in Section 4.2.4.

Constraint (4.6) updates the level of the primary battery when the node drains some energy from it. For every node and every time epoch, the energy drained from the battery must not exceed the available energy (4.7). Finally, nodes can not be fractionally assigned to a mission (4.11) and both the supercapacitor and the battery have a finite size (Variable definitions (4.14) and (4.15)). Since the primary battery has a discharge efficiency strictly lower than one,  $\eta_d^B < 1$ , the maximum battery capacity is scaled by a factor equal to  $\eta_d^B$ . Since the battery is non-rechargeable, no charging efficiency is modeled for it.

The supercapacitor, too, has a charging and discharging efficiency,  $\eta_c^C$  and  $\eta_d^C$ , strictly lower than one. However, these efficiency factors have not been explicitly modeled in the MIP problem because we account for them during energy simulations (Section 4.2.4).

### Supercapacitor non-idealities

Based on current energy-harvesting node prototypes [130, 36], we model energy harvesting subsystems with the following real-life characteristics:

1. If the current energy consumption is greater than (or equal to) the energy currently harvested, then the node can directly use the harvested energy to (partially) fulfill its power requirements. This is the most efficient way of using the environmental energy, because there is no energy loss due to buffer inefficiency and self-discharge [36].
2. If the amount of energy harvested is greater than the current energy consumption, some energy is directly used to sustain the node's operation, while excess energy is stored, if possible, in the supercapacitor for later use.

Because both the charging and discharging efficiency of the buffer are strictly less than one, only a fraction  $\eta_c^C \cdot \eta_d^C$  of the excess energy is available after storing (and retrieving) it. Furthermore, because of the finite size of the buffer, some energy may be lost if there is not enough space left in the supercapacitor to store it.

We account for those non-idealities in our energy pre-computations, by allowing the node to consume the harvested energy directly, when possible, and by storing in the supercapacitor only a fraction  $\eta_c^C \cdot \eta_d^C$  of the excess energy.

For each node  $N_i$  and for each time epoch  $t, t \in \tau_i^c$ , we simulate both  $N_i$  executing a mission and being idle. In fact, during energy pre-computations, it is not possible to know if, according to the solution of the optimization problem, node  $N_i$  will be assigned to a mission  $M_j$  during time epoch  $t$ .

In order to track the current energy level of the node, and to ensure that the energy required to a execute mission is available before assigning the node to the mission, we define the following parameters:

$\Delta_{it}$  is the change in the energy level of the supercapacitor of node  $N_i$  during time epoch  $t, t \in \tau_i^c$ , assuming the node is executing a mission;

$\Delta_{it}^I$  is the change in the energy level of the supercapacitor of node  $N_i$  during time epoch  $t, t \in \tau_i^c$ , assuming the node is not executing a mission;

$\mu_{it}$  is the minimum (relative) energy level reached by the supercapacitor of node  $N_i$  during time epoch  $t, t \in \tau_i^c$ , if the node is executing a mission.

$\Delta_{it}$  and  $\Delta_{it}^I$  represent the *change* of the energy level experienced by the supercapacitor of node  $N_i$  during time epoch  $t$ . As during energy pre-computations the energy level of the supercapacitor at the beginning of each time epoch  $t$  is not known, we assume it to be 0 at the beginning of each simulation.

To clarify the definition of  $\Delta_{it}$ ,  $\Delta_{it}^I$  and  $\mu_{it}$  parameters, we give a simple example. Figure 4.2 shows the power harvested by node  $N_i$  during time epoch  $t$  and the power consumption required by the sensing activity and to keep the node active. Specifically, in this scenario such power consumption is 12 mW. If node  $N_i$  is executing some mission  $M_j$  during this time epoch, its supercapacitor level will increase when the power harvested by the solar cell is higher than the power consumption of the node being active and sensing; it will decrease or remain constant otherwise. Figure 4.4 shows the variation in the energy level of the supercapacitor during the same time epoch  $t$  (obtained by simulation) and it demonstrates how the parameters  $\Delta_{it}$ ,  $\Delta_{it}^I$  and  $\mu_{it}$  are defined.  $\Delta_{it}^I$  is computed by assuming that node  $N_i$  is not executing any mission at time  $t$ . Thus, since during this time epoch node  $N_i$  is harvesting

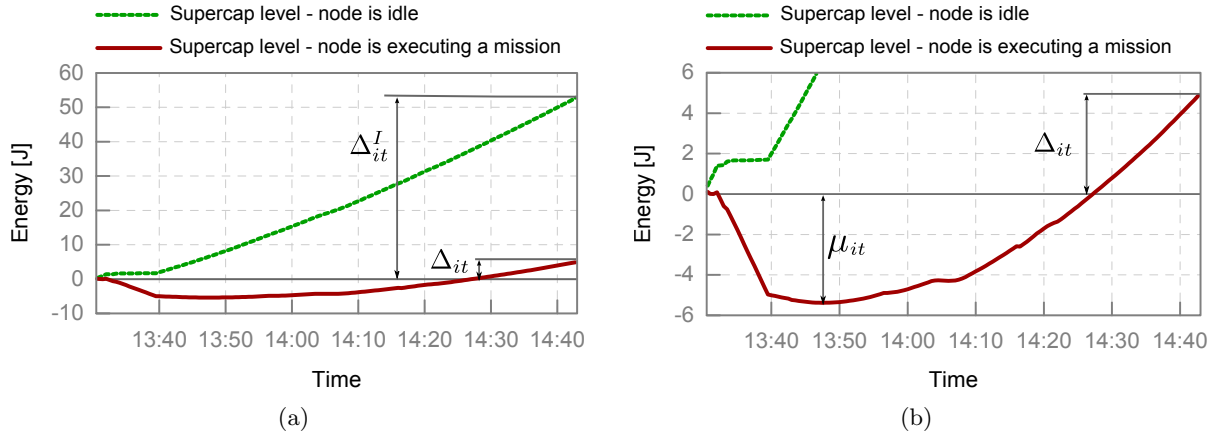


Figure 4.4: (a) Variation in the energy level of the supercapacitor during time epoch  $t$ ; (b) Same figure, zoomed and annotated with the value of  $\mu_{it}$ .

energy from the environment (Figure 4.2), the energy stored in its supercapacitor is expected to increase during this particular time epoch. This is clearly shown by the  $\Delta I_{it}$  curve in Figure 4.4(a) which monotonically increases. On the contrary, if node  $N_i$  is executing some mission  $M_j$ , the energy level of its supercapacitor will decrease as long as the harvested power is lower than the power consumption required by the sensing activity, i.e., until 1:50PM, and then it will increase after the harvested power exceeds this threshold. The parameter  $\mu_{it}$  is defined as the minimum energy level reached by the supercapacitor of node  $N_i$  during time epoch  $t$ . For example, in Figure 4.4(b) such a minimum energy level is reached shortly before 13 : 50.

The  $\mu_{it}$  parameter represents the energy reservoir that the node must have available before executing a mission during time epoch  $t$ : in fact, as computed through energy simulations, the node is expected to experience an energy deficit equal to  $\mu_{it}$  during this time epoch. A mission usually spans multiple time epochs and the value of  $\mu_{it}$  for each of these time epochs should be considered while computing the total energy needed. To this end, we define  $\mu_{ijt}$  as the minimum energy level reached by the supercapacitor of node  $N_i$  if  $N_i$  starts executing  $M_j$  during time epoch  $t$ ,  $t \in \tau_i^c$ :

$$\mu_{ijt} = \max(\mu_{it_1}, \mu_{it_2} - \Delta_{it_1}, \dots, \mu_{it_k} - (\Delta_{it_1} + \Delta_{it_2} + \dots + \Delta_{it_{k-1}})),$$

where  $te_j = t + k - 1$  and, for simplification of the expression,  $t_i = t + i - 1$ . Thus, there are  $k$  intervals from time  $t$  to time  $te_j$  inclusive. Parameter  $\mu_{ijt}$  represents the amount of energy a node must have as a reservoir to accept a given mission  $M_j$  at time  $t$ . Since  $\mu_{it}$  parameters are positive (absolute) values,  $\mu_{ijt}$  is defined as a maximum. In order to explain the definition of  $\mu_{ijt}$ , it is useful to keep in mind that once assigned to a mission a node runs it until completion. For this reason, when computing the energy reservoir required for the node to run during the time epoch  $t_2$ , we also take into consideration the supercapacitor energy change during the previous time epoch. For example,  $\Delta_{it_1}$  represents the change in the energy level of the supercapacitor of node  $N_i$  during the time epoch  $t_1$ . Thus,  $\mu_{it_2} - \Delta_{it_1}$  is the real minimum level reached by the supercapacitor of node  $N_i$  during time epoch  $t_2$ .

For node  $N_i$  to start executing mission  $M_j$  at time  $t$ , i.e.,  $x_{ijt} = 1$ , the energy stored in its capacitor at time  $t$ ,  $C_{it}$ , plus the energy stored in its battery,  $B_{it}$ , must be at least  $\mu_{ijt}$ . This is expressed by constraint 4.8:

$$C_{it} + B_{it} \geq \mu_{ijt}x_{ijt}, \quad \forall N_i, t \in \tau_i, j \in aM_i(t)$$

Finally, the  $\Delta_{it}$  and  $\Delta_{it}^I$  parameters are used to update the energy level of the supercapacitor at the end of each time epoch (constraint 4.5):

$$C_{i\hat{t}} \leq C_{it} + D_{it} + \Delta_{it}^I - (\Delta_{it}^I - \Delta_{it}) \sum_{j \in aM_i} \sum_{\substack{t' \in \tau_i: \\ ts_j \leq t' \leq t}} x_{ijt'}, \quad \forall N_i, t \in \tau_i^c$$

This constraint updates the energy level of the supercapacitor whether the node is executing a mission or it is idle during the current time epoch. If the node is executing a mission, the sum  $\sum_{j \in aM_i} \sum_{\substack{t' \in \tau_i: \\ ts_j \leq t' \leq t}} x_{ijt'}$  will be equal to 1 and the energy level of the supercapacitor will be updated with the energy change  $\Delta_{it}$ , i.e., constraint (4.5) becomes:

$$C_{i\hat{t}} \leq C_{it} + D_{it} + \Delta_{it},$$

where the variable  $D_{it}$  is the energy drained from the battery of node  $N_i$  during the time epoch starting at time  $t$ .

On the contrary, if the node is idle, the parameter  $\Delta_{it}^I$  will be considered when computing the new energy level  $C_{i\hat{t}}$ . In this case,  $\sum_{j \in aM_i} \sum_{\substack{t' \in \tau_i: \\ ts_j \leq t' \leq t}} x_{ijt'}$  is equal to zero and constraint (4.5) becomes:

$$C_{i\hat{t}} \leq C_{it} + D_{it} + \Delta_{it}^I.$$

Variable  $D_{it}$  will be greater than zero if the energy change computed for time epoch  $t$  is negative (i.e.,  $\Delta_{it} \leq 0$  or  $\Delta_{it}^I \leq 0$ , depending on whether the node is executing a mission or not) and the capacitor level  $C_{it}$  can not supply the energy needed.

On the contrary, if the energy change computed for time epoch  $t$  is positive or zero, no energy will be needed from the battery and the supercapacitor will be recharged. Objective function pressure ensures no unneeded transfer of energy between the battery and the supercapacitor unless they come at no penalty.

The definition of the variable  $C_{it}$  in (4.14) ensures that the supercapacitor is never charged beyond its maximum size.

The formulation of the sensor-mission assignment problem that we propose can capture the idle consumption of real-life systems and some non-ideal behaviors of energy buffers, namely the fact that energy storage has a finite size, and that the charging and discharging efficiency is lower than 1.

The assumption that the supercapacitor is empty at the beginning of each time epoch may lead to an overestimate of the energy available to the node. In fact, if the supercapacitor level is greater than 0, it may charge to its capacity sooner, and thus may lose some energy it cannot store because it is at capacity. However, since our goal is to obtain an upper bound on the optimal solution, we allow for such an overestimation in order to avoid adding complexity to the model.

In our current formulation, supercapacitor self-discharge is not modeled. In fact, including realistic models of leakage and self-discharge in the analytical formulation would significantly increase its complexity, impairing scalability. Despite that, our formulation succeeds in providing an upper bound to the optimal solution. In fact, since self-discharge negatively impacts energy availability of the nodes, the profit obtained by the optimal solution is necessarily lower than the one provided by our MIP model.

We accounted, however, for supercapacitor self-discharge in our experiments and performance evaluation (Section 4.4). Moreover, we evaluate these models of super capacitor characteristics in Section 4.5.

#### 4.2.5 SENSOR-MISSION ASSIGNMENT PROBLEM IN ENERGY HARVESTING WSNs

As a final note, we briefly discuss hardness results for the sensor-mission assignment in energy harvesting WSNs problem.

Bar-Noy et al. introduced in [20] Semi-Matching with Demands (SMD), which is a version of the sensor-mission assignment problem in which the set of missions to be executed is known, there is no time dimension in the problem and no energy restriction limits sensor-mission assignments. Specifically, an instance of SMD is a weighted bipartite graph  $G = (N, M, P, E)$  where  $N = \{N_1, \dots, N_n\}$  is a collection of nodes,  $M = \{M_1, \dots, M_m\}$  is a collection of missions,  $P = \{p_1, \dots, p_m\}$  is a collection of positive mission profits, and  $E$  is a collection of non-negative weights (utilities) for the edges  $N \times M$ . The demand of each mission is assumed to be 1. Missions can not be partially satisfied, i.e.,  $y_j \in \{0, 1\}$ . The goal of SMD is to find a semi-matching  $F \subseteq E$  in which  $\sum_{M_j \in A} p_j$  is maximized, where  $A \subseteq M$  is the set of missions satisfied by  $F$ . The corresponding decision problem is to determine, given an instance of SMD and a value  $b$ , if there exists a semi-matching  $F \subseteq E$  such that  $\sum_{M_j \in A} p_j \geq b$ .

Bar-Noy et al proved that SMD is NP-hard and as hard to approximate as Maximum Independent Set. Such hardness results also apply to sensor-mission assignment in energy harvesting WSNs. We give a polynomial-time reduction from a given instance of the SMD problem to an instance of the sensor-mission assignment in energy harvesting WSNs problem.

**Proposition 1** The sensor-mission assignment problem in energy harvesting WSNs is NP-hard and at least as hard to approximate as SMD.

*Proof.* Given an instance of SMD, an instance of the sensor-mission assignment in energy harvesting WSNs decision problem is created as follows.

The set of nodes  $N'$  of the new instance is the same as  $N$ . For each mission  $M_j$ , create a new mission  $M'_j$  with profit  $p'_j = p_j$  and demand  $d'_j = 1$ . The duration of each mission  $M'_j$  is set to one timeslot and the start time of the new missions is set so that as each mission  $M'_j$  starts at the beginning of timeslot  $t_1$ , i.e., missions are all overlapping. The utility  $e'_{ij}$  provided by node  $N'_i$  to mission  $M'_j$  is the same as in the SMD instance, i.e.,  $e'_{ij} = e_{ij}$ . The mission satisfaction threshold  $T_{sat}$  is set to 1, i.e., the demand of a mission must be fully met in order for it to be satisfied. The battery energy of each node is set such as to potentially execute all the missions, i.e.,  $B_{max} = ec_s$ , where  $ec_s$  is the energy consumed by the node in one timeslot of sensing. Finally, we assume that no energy is harvested by the nodes and that their supercapacitor is not in use, i.e.,  $C_{max} = 0$ . This reduction requires time polynomial in the size of the SMD instance. The corresponding decision problem is to determine if there exists a sensor-mission assignment such that the total profit achieved by the network at least  $b$ .

The SMD decision problem instance has a positive answer if and only if the constructed sensor-mission assignment decision instance in energy harvesting WSNs has a positive answer.  $\square$

Furthermore, generalizing the analysis in [21] to energy-harvesting wireless sensor networks, it can be proven that the online version of the sensor-mission assignment in energy harvesting WSNs problem can not be solved with any finite competitiveness guarantee.

**Proposition 2** There is no constant-competitive algorithm for the online sensor-mission assignment problem in WSN with energy harvesting, even assuming that each mission lasts only for one timeslot, that missions are not overlapping and that no energy is harvested by the nodes.

*Proof.* In the following, we denote with  $ec_s$  the energy consumed by the node to perform one timeslot of sensing, while  $ec_i$  is the energy required to stay idle for one timeslot.

We first consider the case in which all nodes have only limited amount of battery energy, which allows them to execute a mission for just one timeslot and to stay idle for another timeslot, i.e.,  $B_{max} = ec_s + ec_i$ . Since we are assuming that no energy is harvested by the nodes, the supercapacitor is empty and not in use, i.e.,  $C_{max} = 0$ . Suppose that at time 1 a mission  $M_1$  arrives in the network. Such mission has a profit  $p_1 = \epsilon$  and necessarily requires a given sensor  $N_i$  to be assigned to it in order to be satisfied. The online deterministic assignment algorithm must assign  $N_i$  to  $M_1$ , as there may be no further missions and refusing  $M_1$  could lead to an infinite competitive ratio. However, at time 2 a mission  $M_2$  may arrive in the network, having profit  $p_2 = 1$  and requiring sensors  $N_i$  as well. But the remaining energy would be not enough to execute  $M_2$ , so the total profit obtained by the online deterministic assignment algorithm would be  $\epsilon$ . The optimum assignment algorithm, instead, will ignore  $M_1$ , staying idle during timeslot 1, and then it will assign sensor  $N_i$  to  $M_2$  when it arrives, for a profit of 1. Now suppose that the battery energy of the nodes allows them to execute a mission for two timeslots and to stay idle for another timeslot, i.e.,  $B_{max} = 2ec_s + ec_i$ . We are still assuming that no energy is harvested by the nodes. Then consider the following sequence of missions arrival: at time 1 missions  $M_1$  arrives with profit  $p_1 = \epsilon$ , at time 2 missions  $M_2$  arrives with profit  $p_2 = exp(\epsilon)$  and at time 3 missions  $M_3$  arrives with profit  $p_3 = exp(exp(\epsilon))$ .  $M_1, M_2$  and  $M_3$  all require sensor  $N_i$  to be assigned to them in order to be satisfied. The online deterministic assignment algorithm must assign  $N_i$  to  $M_1$  at time 1, as there may be no further missions. At time 2,  $N_i$  must be assigned to  $M_2$  for the same reason. At time 3, there will not be enough energy left to execute  $M_3$ , thus leading to a total profit of  $\epsilon + exp(\epsilon)$ . The optimum assignment algorithm, instead, will ignore  $M_1$  and assign sensor  $N_i$  to  $M_2$  and  $M_3$  when they arrive, for a profit of  $exp(\epsilon) + exp(exp(\epsilon))$ . This construction can be extended to arbitrary  $B_{max}$ .  $\square$

### 4.3 EN-MASSE

In this section we introduce a decentralized heuristic for sensor-mission assignment in energy-harvesting wireless sensor networks, called EN-MASSE. EN-MASSE is able to handle hybrid harvesting systems consisting of multiple energy storage devices (supercapacitor and battery) and to adapt its behavior according to the current and expected energy availability of the node, efficiently using harvested energy. To this end, both mission characteristics (profit, demand, lifetime) and the current and expected energy available at the node (current harvesting rate, energy stored by the supercapacitor and the battery, energy that the node is expected to harvest in the near future) are considered by EN-MASSE when making assignment decisions. Our heuristic makes use of energy prediction models (Sections 4.3.4 and 4.3.4) to estimate the future behavior of the environmental energy source, in order to heuristically optimize assignment decisions over short and longer time frames.

The rest of this section is organized as follows:

- In Section 4.3.1 we describe the communication protocol used by the nodes in the network to disseminate information about mission arrivals and assignment decisions;
- In Section 4.3.2 we detail the behavior of our distributed scheme and the rationale for our proposed approach;



- In Section 4.3.3 we describe the algorithm used by the mission leader to decide sensors-to-missions assignments;
- In Section 4.3.4 we describe the energy prediction model used by EN-MASSE and the solar energy datasets that we use in Section 4.4.

#### 4.3.1 COMMUNICATION PROTOCOL

Each mission arrives in the network at a specific geographic location  $l_i$ . In EN-MASSE the sensor node closest to  $l_i$  is selected as the *mission leader* and coordinates the assignment of nodes to missions. Mission leaders may be selected either by the sink in a centralized fashion or using geographic routing techniques. We selected the communication protocol described in [21, 19] for exchanging information between the mission leader and the nearby nodes. We recap it here for clarity. Each time a new mission arrives in the network, the leader advertises mission information, including the mission's location, profit, demand, and duration to its neighbors. When a nearby node hears such an advertisement message, it makes a decision either to bid for the mission and become eligible for selection by the leader or to ignore the advertisement. If the node is already assigned to a mission, it ignores the advertisement message. Bidding decisions are taken autonomously by each node in the neighborhood, based on the *bidding scheme* they use (Section 4.3.2). Such decisions may be based on a number of different factors, including the contribution to the mission that the node is potentially offering, the residual energy of the node, the current time with respect to the target lifetime, etc. Bidding nodes then communicate their availability to the mission leader, which greedily selects which of the available sensor nodes to assign to the mission (Section 4.3.3), based on their offered contribution, until either the mission is fully satisfied or all nodes which have bid for it have been assigned to the mission. To avoid wasting energy resources, sensor nodes are actually allocated to missions only if such missions can be satisfied immediately.

#### 4.3.2 BIDDING SCHEME

On the reception of a mission advertisement message sent by the leader, nodes autonomously decide to bid for participation in the mission or not. Bidding decisions are based on the following factors:

1. the current energy level of the node battery and capacitor;
2. the energy cost of the mission;
3. the future energy availability, obtained through a solar energy prediction model<sup>2</sup> ;
4. the profit of the mission with respect to the maximum profit;
5. the utility offered by the node with respect to the mission demand, and
6. the target lifetime of the network.

A node uses the first three factors in the list to classify the incoming mission according to the impact that its execution would have on the energy reservoir of the node. More specifically, missions are classified into one of the following four classes:

**Free missions** are those arriving when the node super-capacitor is full and their energy cost is expected to be fully sustained by the energy harvested during their duration. The energy prediction model estimates the amount of energy that will be harvested in the near future.

**Recoverable missions** are those whose energy cost can be sustained using the energy stored in the supercapacitor. Such energy cost can be recovered through harvesting in a small period of time, according to the prediction of future energy availability.

<sup>2</sup>See Section 4.3.4 for additional details about the solar energy prediction model we use.

**Capacitor-sustainable missions** occur if the total energy cost of the mission can be sustained using only the supercapacitor but this cost is not expected to be recovered through harvesting in the near future.

**Battery-required missions** are those whose energy cost must be totally or partially supplied by the battery.

Such classification is used by the node to decide whether to bid for a mission or not. Nodes always accept *free* missions. The energy needed by such missions can be directly provided by the harvesting subsystem. Ideally, executing a mission of this class should not affect the energy reservoir of the node at all. Moreover, in this situation there is no reason for saving energy: Because the capacitor is full, any excess energy harvested from the environment would be wasted if not used. If the incoming mission is *recoverable* or *capacitor-sustainable*, the node evaluates how profitable the mission is, based on the profit of the mission with respect to the maximum profit and the utility offered by the node with respect to the mission demand. In more detail, a sensor compares the partial profit it can provide by participating in that mission with the *expected partial profit*  $\bar{p}$  of a typical mission, which is computed based on the distribution of mission profit and demand and the expected utility contribution that a node can offer to a typical mission in its range:

$$\bar{p} = \frac{E[u]}{E[d]} \times \frac{E[p]}{P},$$

where  $E[u]$  is the expected utility contribution,  $E[d]$  and  $E[p]$  are the expected demand and the expected profit of a typical mission, learned by the nodes based on previous history or obtained at design time based on the application characteristics, and  $P$  is the maximum mission profit.

The partial profit  $p^*$  achievable by the node  $N_i$  by participating in the incoming mission  $M_j$  is defined as:

$$p^* = \frac{e_{ij}}{d_j} \times \frac{p_j}{P} \times w, \quad (4.17)$$

where  $e_{ij}$  is the potential utility contribution that the node  $N_i$  can provide to the given mission,  $d_j$  and  $p_j$  are, respectively, the mission demand and profit,  $P$  is the maximum mission profit and  $w$  is the weight associated to the mission's classification (higher for recoverable missions, thus giving a higher chance to those missions to be accepted over capacitor sustained missions). The value  $p^*$  is then compared to  $\bar{p}$ , to have an indication of how profitable the mission is. A node will bid for a given mission only if  $p^* \geq \bar{p}$ .

To decide which missions are classified as recoverable, nodes estimate the missions' interarrival time and set the recoverable time interval dynamically, so that its duration is at most the expected time before the next mission arrives. In this way, choosing to execute a recoverable mission is not likely to affect the node's ability to bid on the next mission.

*Battery required* missions are those with the lowest weighting factor. In fact, we want the network to be able to reach a given target lifetime, so we choose to use precious battery energy only to execute missions with higher relative profits.

---

**Algorithm 1** EN-MASSE bidding scheme

---

**Data:** $B_{it}$  the battery energy level of node  $N_i$  at time  $t$  $C_{it}$  the supercapacitor energy level of node  $N_i$  at time  $t$  $M_j = (p_j, d_j, g_j, ts_j, te_j)$  the incoming mission  $M_j$  $MT_j$  the class of the mission  $M_j$  $EC_j(t)$  the amount of energy required to execute mission  $M_j$  from time  $t$  until its end time $\bar{p}$  the expected partial profit of a typical mission $P$  the maximum mission profit $e_r(t)$  the amount of energy the node expects to need to function to the target lifetime**Result:** 1 if the node bids at time  $t$  for participation in the mission  $M_j$ , 0 otherwise.**if**  $MT_j == Free$  **then**| **return** 1; // Always accepts Free missions**end**// Compute the partial profit achievable by participating in  $M_j$  $p^* = e_{ij}/d_j \times p_j/P$ ;// Weight  $p^*$  based on mission's classification**switch**  $MT_j$  **do**| **case** *Recoverable*|  $p^* = p^* \times w_{recoverable}$ ; // Compute  $p^*$ , Recoverable mission| **case** *Capacitor-sustainable*|  $p^* = p^* \times w_{capacitor}$ ; // Compute  $p^*$ , Capacitor-sustainable mission| **case** *Battery-required*| // Separately evaluate the energy contribution of the supercapacitor  
| and the battery|  $p_{capacitor}^* = p^* \times w_{capacitor-sustainable}$ ; // Compute  $p_{capacitor}^*$ |  $p_{battery}^* = p^* \times w_{battery-required} \times B_{it}/e_r(t)$ ; // Compute  $p_{battery}^*$ |  $p^* = C_{it}/EC_j(t) \times p_{capacitor}^* + (1 - C_{it}/EC_j(t)) \times p_{battery}^*$ ;**endsw**

// Decide whether to bid for the mission, based on how profitable it is

**if**  $p^* \geq \bar{p}$  **then**| **return** 1**else**| **return** 0**end**

---

If the mission is *battery-required*, the node separately evaluates the energy contribution provided by the supercapacitor and the battery. If the capacitor is not empty, its  $p^*$  is computed as in the capacitor-sustainable case and then weighted with the fraction of the requested energy that will be provided by the supercapacitor if no energy is harvested. The same approach is taken to compute the partial profit  $p^*$  associated with the battery contribution. However

in this latter case we use an additional factor when computing  $p^*$ , defined as follows:

$$w_e = \frac{e_a}{e_r},$$

where  $e_a$  is the amount of energy available at the node, i.e., its current battery level, and  $e_r$  is the amount of energy the node deems to be necessary to reach a given network target lifetime.

Let  $t_e$  be the *expected occupancy time*, i.e., the fraction of time the node expects to be serving missions in the future. This value is computed based on estimates of the mission arrival rate, the expected mission duration, the probability that a given mission is within the node's sensing range and the probability  $\gamma$  that a sensor's offer is accepted<sup>3</sup>. We denote with  $rtl$  the remaining target lifetime, i.e, the difference between the initial target network lifetime and the current time. We can then express  $e_r$  as:  $e_r = rtl \times t_e \times ec_s$ , where  $ec_s$  is the average mission sensing cost.

The factor  $w_e$  is then multiplied by  $w$  in the computation of  $p^*$ :

$$p^* = \frac{e_{ij}}{d_j} \times \frac{p_j}{P} \times w \times w_e,$$

The objective of  $w_e$  is to tune the eagerness of sensors to participate in new missions. It forces nodes to be more conservative in accepting missions as the energy they have gets low compared to what is expected to be needed to reach the target lifetime. On the other hand, it also makes the nodes act more aggressively as the target network lifetime approaches.

Algorithm 1 shows the pseudo code of the EN-MASSE bidding scheme.

### 4.3.3 TASK ALLOCATION TO SENSORS

Once the mission leader has collected bidding answers from nearby nodes, it performs the selection of nodes to assign to the mission. Nodes are ranked based on the utility they offer. The mission leader greedily assigns them to the mission, based on their ranking, until the mission is fully satisfied or there are no more sensors bidding for it. Once the minimum satisfaction threshold is reached, the leader may decide to stop short of full coverage if the next node to add would go way past the necessary utility, as there is no additional profit earned by the network if the required demand is exceeded. The mission (partially) succeeds if it reaches the success threshold  $T_{sat}$ ; if not, the leader releases all sensors. If the mission can be successfully started, an ACK message is sent to the nodes the leader chooses, to confirm they are assigned to the mission. When a mission ends, the leader sends out a message to announce that the mission has ended and all its assigned sensors are released.

Because the system is dynamic, the leaders of missions that have not reached their success threshold or are not fully satisfied after the first assignment process will retry to obtain more sensors when a nearby mission terminates and releases its sensors. Such information can be easily obtained by overhearing the message announcing the end of a mission.

---

<sup>3</sup>While all parameters can be easily learned or they are known a priori, the  $\gamma$  parameter is difficult to compute due to a feedback effect: to decide whether a node should bid for a mission we need to know the probability that a bid is accepted. The approach we have taken has been to experimentally tune the parameter  $\gamma$  so that profit performance of the selected scheme are maximized.

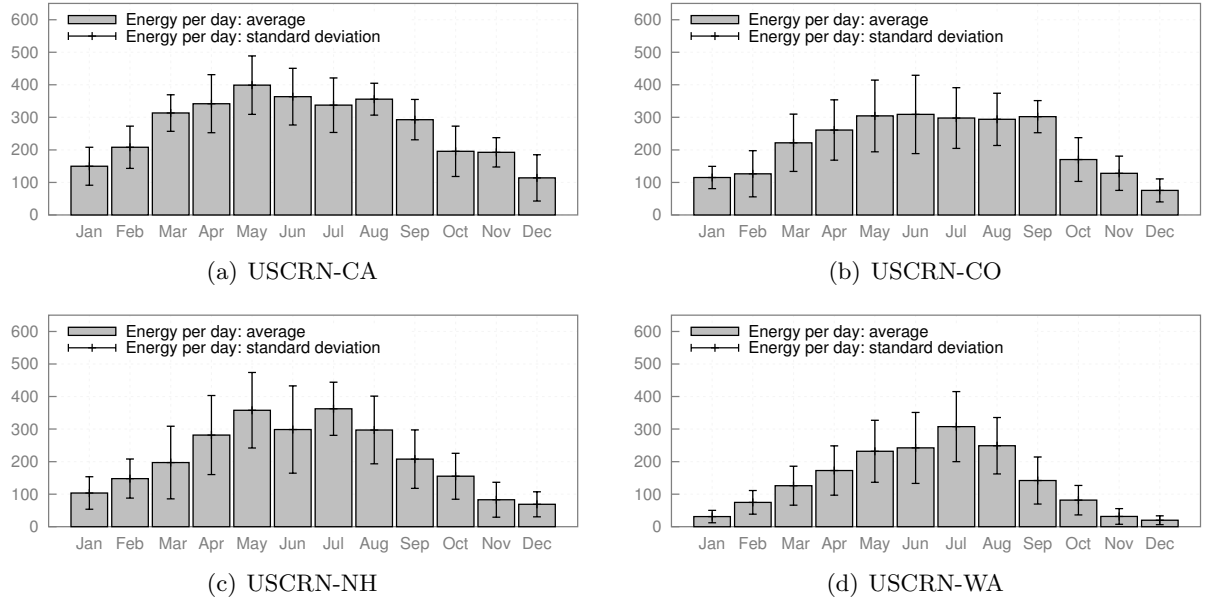


Figure 4.5: Harvested energy per day: average value in Joules and standard deviation for each month and each dataset.

#### 4.3.4 ENERGY PREDICTION MODELS AND SOLAR ENERGY DATASETS

##### Short term solar energy prediction model

EN-MASSE uses an energy prediction model in order to estimate the energy a node will receive from the ambient source. This prediction model allows us to classify missions, by estimating how much time will be necessary for the node to recover the energy requested by a mission through harvesting. Since these estimations are carried over a relatively small time frame (usually, half an hour to several hours), we refer to this prediction model as short term.

We specifically focused on three prediction models that have been previously proposed in the literature, namely EWMA, WCMA and Pro-Energy (Section 1.3). Based on an assessment of the prediction accuracy performed over real-life solar traces, we selected Pro-Energy as the short-term energy prediction model used by our bidding scheme, as it consistently outperforms the other predictors (Chapter 2).

##### Long term solar energy predictor

In order to further improve the performance of our solution, we also propose to add a long-term solar energy predictor to our scheme. The short term energy predictor allows EN-MASSE to classify incoming missions based on expected energy availability in the near future, but it does not take into account the long-term behavior of the energy source. However, in many scenarios it is quite easy to access historical data and statistics about past weather conditions. Our long-term predictor allows us to leverage such historical weather data, in order to further improve and to fine-tune the behavior of EN-MASSE over longer time frames. This predictor is lightweight and it only requires a limited amount of information to work: namely, the average energy harvested per day, for each month during which the network is expected to be operational. As an example, we obtained such historical weather data for the USCRN solar datasets we used in our simulator (Figure 4.5).

The long-term predictor works as follows: at the beginning of each month, it is used to compute a factor,  $LTP_m$ , indicating how much the average harvested energy per day is

expected to change during the next month with respect to the current month. Specifically, the  $LTP_m$  factor is:

$$LTP_m = \left( \frac{HE_{m+1}}{HE_m} \right)^\alpha \left( \frac{HE}{HE_m} \right)^\beta, \quad (4.18)$$

where:

$m$  is the current month;

$HE_m$  is the average energy per day harvested during the current month;

$HE_{m+1}$  is the average energy per day the node expects to harvest during the next month;

$HE$  is the mean of the average energy per day harvested during the whole target lifetime;

$\alpha, \beta$  are two weighting parameters,  $a, b \in [0, 1]$ .

The parameters  $HE_m, HE_{m+1}$  and  $HE$  are all computed based on historical weather data.

The first factor in Equation 4.18 represents how the amount of energy harvested per day is expected to change during the next month. If this ratio is greater than 1, we expect the average energy harvested per day to increase during the next month. In this case, EN-MASSE will be likely to use more energy from the battery during the current month than during the next one.

The second factor in Equation 4.18 is the ratio between the average energy harvested per day over the whole target network lifetime and the average energy harvested per day during the current month. If this ratio is bigger than 1, in the current month the average harvested energy per day is below the mean. We thus allow EN-MASSE to use more battery during the current month.

The  $LTP$  factor is used as a weighting factor in Equation 4.17, in order to fine-tune the eagerness of EN-MASSE nodes to accept battery-required missions. Only for this class of missions, the weight factor  $w_{battery}$  is updated every month  $m$  and becomes:

$$w_{battery} = \max\{w_{battery} * LTP_m, \text{max weight}\},$$

where  $\text{max weight}$  is the maximum weight that can be assigned to a battery-required mission, which should be lower than that assigned to the other mission classes.

$LTP$  allows us to estimate when the energy stored in the battery is more likely to be needed over the whole target lifetime, and to plan its usage accordingly. The  $LTP$  factor computed by the long-term predictor is only used to adjust the desirability factor of battery-required missions. Thus, it is not used for mission classification and it does not interfere with the general bidding strategy of the nodes. For this reason, different long term predictors may be seamlessly integrated into EN-MASSE.

### Solar energy traces

We use real solar data to evaluate the performance of sensor-mission assignment schemes in networks with energy harvesting capabilities. The solar energy profile was collected by using a Telos B mote [23] equipped with a XOB17-04x3 solar cell [169]. The motes were deployed in downtown Rome, for a total of 120 non-consecutive days at variable weather conditions and in different locations. A dedicated TinyOS application was developed to track the amount of energy generated by the cell at 30-second intervals.

### Additional solar datasets

We obtained extensive solar traces from the US Climate Reference Network [170], a network of climate stations deployed in the continental United States. The selected traces report the solar radiation in the period from January 2010 to December 2010, observed in four different weather stations: Santa Barbara, Boulder, Durham and Darrington. Solar data are recorded hourly, reported as an average of the solar radiation over each hour and expressed in  $W/m^2$ .

In order to use USCRN solar data in our simulations, we had to convert them and scale them down. We used the scaling method of [116], i.e., by using a scaling factor for the solar data equal to the ratio between the maximum peak power recorded in our solar traces and the maximum for each of the USCRN data sets.

Figure 4.5 shows how the amount of the harvested energy varies over time: for each month of the year and for each USCRN dataset, the average value and the standard deviation of the energy harvested per day is reported.

## 4.4 PERFORMANCE EVALUATION

In this section we evaluate our sensor-mission assignment scheme in several different scenarios and compare its performance with respect to other schemes proposed in the literature. For this purpose, we implemented a dedicated simulator in C++ which is the base of our evaluation framework for energy harvesting WSNs. It accurately models the energy harvesting subsystem of the nodes and allows the user to import solar trace datasets in different formats.

### 4.4.1 SIMULATION SETUP

In our simulations 500 nodes are randomly and uniformly scattered in a square area of  $400 \times 400$ m. The communication range of the nodes is set to 40m. The sensing range is 30m. The node energy model is that of ECO nodes [171, 172], an ultra-compact expandable wireless sensor platform, which has been used in combination with the Ambimax energy harvesting platform [31]. Specifically, ECO node active power consumption is 9mW, while its idle (sleep) power consumption is 0.006mW. The sensor node is also equipped with a supercapacitor, used as an energy buffer for the energy harvested by the solar cell. The reference supercapacitor we consider is the 25F ultracapacitor of Maxwell HC Power series [173]. It can nominally hold around 90J of charge, although the linear discharge exhibited by supercapacitors makes it usually impossible to fully use the energy they store. We set the charging and discharging efficiency of the supercapacitor to 95%, i.e.,  $\eta_c^C = \eta_d^C = 0.95$ , because ultracapacitors have typically high cycle efficiency, between 90% and 98% even under high current pulses [174, 175]. Finally, in our simulation we also modeled the leakage experienced by such supercapacitors. In general, the leakage suffered by a charged supercapacitor is a complex function, that increases when the energy stored is higher [30, 26]. To capture this behavior, we model the leakage,  $leak_i(t)$ , of the supercapacitor,  $C_i$ , of the sensor node  $N_i$  at time  $t$  by using a piecewise linear approximation of the empirical leakage pattern, as in [26]:

$$leak_i(t) = \begin{cases} a_1 \cdot C_i(t) + b_1, & C_{R_1} \leq C_i(t) < C_{R_2} \\ \vdots & \vdots \\ a_n \cdot C_i(t) + b_n, & C_{R_n} \leq C_i(t) < C_{R_{n+1}} \end{cases}$$

where  $B_{R_1}, \dots, B_{R_{n+1}}$  are the residual energy values in which the slope of the leakage curve change significantly and  $a_1, \dots, a_n, b_1, \dots, b_n$  are constants depending on the supercapacitor used, that represent the coefficients of the line segments used for the approximation.

The other parameters reported in Table 4.4.1 are related to the missions arriving in the network. Missions arrive in the network according to a Poisson arrival process and are

Simulation scenarios: default settings.

Parameter	Value
Nodes in the network	500
Simulation field	$400 \times 400$ m
Communication range	40 m
Sensing range	30 m
Average mission profit	10
Average mission demand	2
Average mission duration	1 hour
Satisfaction threshold	50% of the mission demand

assigned to a location randomly and uniformly selected in the deployment area. Mission duration is exponentially distributed with an average mission duration of 1 hour. The mission profit and demand also follow an exponential distribution with average equal to 10 and 2, respectively. We consider a mission satisfaction threshold  $T_{sat} = 50\%$ , i.e., in order for a mission to be successful, it must receive at least half of its demand from the sensors allocated to it. For simplicity, we define the utility that a sensor  $N_i$  can potentially offer to a mission  $M_j$  as a function of the distance  $D_{ij}$  between the location  $g_j$  of the mission and the position of the node  $N_i$ . The network target lifetime has been varied between 30 and 180 days.

Table 4.4.1 reports the parameters used in the simulation setup.

In our implementation of EN-MASSE, we set the weighting factors  $w$  associated with mission types equal to 0.95 for battery required missions, 1.05 for capacitor sustainable missions and 1.2 for recoverable missions.

Additionally, we set the time threshold within which the energy cost has to be recovered for the mission to be classified as recoverable equal to the mission inter-arrival time times the probability that the new mission falls in the node sensing range. Doing so, whenever a mission is recoverable bidding for it is not expected to compromise the node capability to serve future missions.

#### 4.4.2 BENCHMARK ASSIGNMENT SCHEMES

We compare the performance of our EN-MASSE assignment scheme with the three different energy harvesting unaware mission assignment schemes proposed in [21], namely the Basic Scheme, the Energy Aware Scheme and the Energy-Lifetime Aware Scheme. The Energy-Lifetime Aware Scheme is shown to perform very well in traditional scenarios (without harvesting) and with very limited network lifetimes (three days). In such cases, it outperforms the other assignment schemes, Basic and Energy Aware, achieving a total profit that is up to 22% higher.

Our benchmark assignment schemes are:

- **Basic Scheme:** Sensors propose to any mission within their range.
- **Energy Aware Scheme:** This scheme does not use any classification of missions or mechanism to account for the harvested energy. It also does not take the target lifetime of the network into account while taking bidding decisions. The Energy Aware Scheme evaluates how profitable a mission is by comparing the partial profit a node can achieve by participating in the incoming mission with respect to the expected partial profit of a



typical mission (as defined in Section 4.3.2). In order to take the current energy status of a node into account, the partial profit computed for the current mission is weighted by a factor equal to the fraction of residual battery energy available.

- **Energy-Lifetime Aware Scheme:** This scheme does not account for harvested energy, but it considers the target lifetime of the network while taking bidding decisions. It evaluates how profitable a mission is in a way similar to the Energy Aware Scheme, but it uses a different weighting factor. The partial profit computed for the current mission is weighted by a factor equal to the ratio between the time a node can be actively sensing, given its residual energy level and the target lifetime, and the expected occupancy time of the node.

Because these schemes were not initially designed for nodes with energy harvesting capabilities, we modified them so as to sum the contribution of both the capacitor and the battery when computing the residual and the maximum energy level of the node. The nodes are able to both directly use the energy obtained through harvesting, as well as store it in the supercapacitor for later use. All the bidding schemes we considered use the communication protocol described in Section 4.3.1 for the election of the leader and for exchanging information between the mission leader and the nearby nodes; the communication overhead of such a protocol is studied in [19].

#### 4.4.3 SIMULATION RESULTS

EN-MASSE, the Basic Scheme, the Energy Aware Scheme, and the Energy-Lifetime Aware Scheme have been compared in different scenarios, varying the target lifetime, the supercapacitor and battery size, the mission arrival rate, and the type of sensors embedded in the nodes (thus the energy cost associated to sensing). Here we first discuss results for a specific setting of such parameters taken from a practical case, and then we discuss how the relative performance of the four protocols changes when we explore the whole parameter space.

##### Reference scenario

Our first set of experiments refer to a scenario where node sensing cost is 4.5 mW, e.g., the power consumption of an ultra low-power vision sensor such as [176]. Each node is equipped with two solar cells and with a 25F Maxwell supercapacitor [173], which can store 90J of energy. The target network lifetime is set to four months (shown as a fine vertical line) and the simulations are run for 130 days. The arrival rate of missions in the network is 20 missions per hour. The solar dataset we use is the one of real-life solar data collected by using Telos B mote and XOB17-04x3 solar cells (Section 4.3.4). All other parameters are as detailed above.

We evaluate the performance of the different protocols with respect to the following metrics:

1. network profit achieved over time (Figure 4.6(a));
2. total profit achieved at the network target lifetime (Figure 4.6(b));
3. profit achieved per day: mean value and standard deviation (Figure 4.6(c));
4. fraction of nodes that have energy left in their battery over time (Figure 4.6(d)).

The first three metrics allow us to understand which bidding scheme is more profitable and whether a given scheme is able to provide a stable profit over the whole target lifetime or not. In particular, the third metric provides a good indication of the stability and robustness of the assignment scheme. The fourth metric deserves some discussions. Given the energy harvesting capabilities of the nodes, a node with empty battery is not considered dead, as it can execute missions using the energy harvested from the environment. However, a node with no residual battery suffers strongly from fluctuations of the environmental source. It is

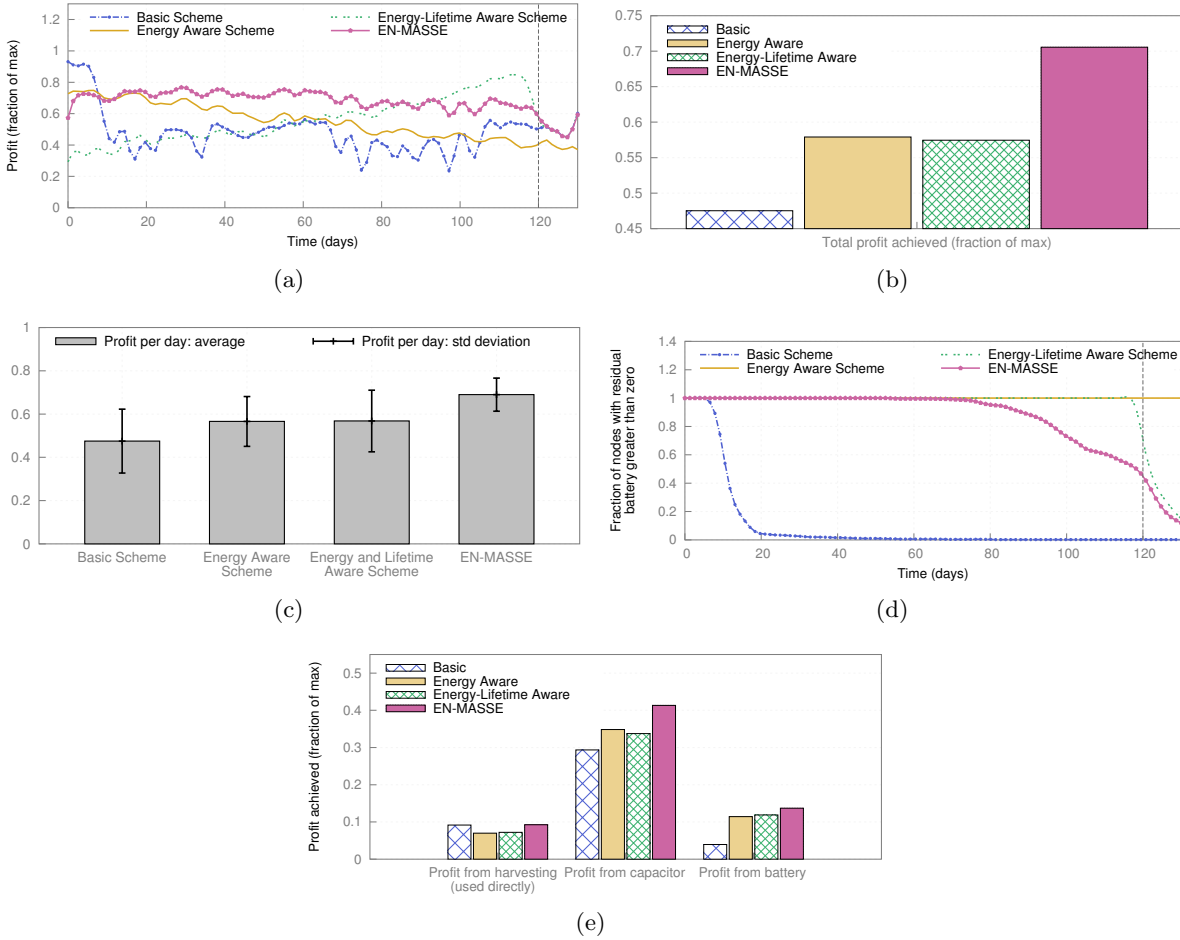


Figure 4.6: Simulation results for a sample scenario [Rome scenario, real-life solar traces dataset]: (a) fraction of achieved profit per time slot, (b) total profit achieved at target lifetime (as a fraction of maximum), (c) profit achieved per day: average value and standard deviation, (d) fraction of nodes with a residual battery greater than zero and (e) total profit achieved per energy source (as a fraction of maximum).

not able to execute important missions if there are limited energy harvesting opportunities when such missions come in. Therefore having a high percentage of nodes operating only based on the harvesting subsystem may compromise the capability of the network to execute critical missions and degrade the network profit.

We observe that EN-MASSE leads to the greatest total profit (Fig. 4.6(b)), and that is able to provide the highest profit (70 – 80% of the maximum achievable profit, defined as the profit that could be achieved if all missions were fully served) till the target network lifetime (Fig. 4.6(a)). Moreover, as shown in Fig. 4.6(c), EN-MASSE also provides the most stable profit over time among the considered bidding schemes, as the average profit it obtains per day is the least variable with respect to the other approaches. The fact nodes wisely exploit their resources to provide the needed support to arriving missions is confirmed by Fig. 4.6(d), which shows that no node has depleted its battery in the first 70 days. Then the fraction of nodes with no energy in their battery starts increasing, reaching 45% at the target network lifetime. The remaining nodes, as well as those that can be sporadically charged by the harvesting subsystem, are enough to serve arriving missions with very high profit. This is the desirable behavior for the network. The bidding scheme should not be too aggressive (as is the Basic Scheme) as this would mean that all nodes deplete their battery quickly, thus making the network profit significantly degrade over time. On the other hand, the bidding scheme

should not be too conservative, as the energy left in the nodes' batteries at the target network lifetime is wasted. Fig. 4.6(e) shows the sources from which EN-MASSE derives its increased profit. Its profit from energy harvesting (both directly and via the capacitor) is larger than the other two methods that are energy aware. Further tests showed that EN-MASSE received more than 40% higher profit than the other energy aware methods from free, recoverable and sustainable missions, indicating its direct consideration of the renewable energy source has large benefits.

The Basic Scheme achieves high profit at the beginning of the network operations. However, since sensors bid for any mission within their range, node batteries start dying rapidly. After 15 days of simulation more than half of the nodes have depleted their batteries and the profit falls below 50% of the maximum profit. After 30 days, less than the 1% of nodes in the network have some residual energy stored in their batteries. From here on, the profit achieved by the scheme shows a high variability (Fig. 4.6(c)), because the capability to serve missions now depends on the amount of harvested energy, which fluctuates as the environmental source does. Overall, as shown in Fig. 4.6(b), which reports the total profit achieved by each scheme over the target network lifetime, the total profit achieved by the Basic Scheme is less than half the maximum and 33% lower than the profit achieved by EN-MASSE.

In the Energy Aware Scheme, having no knowledge of the target network lifetime, each node tries to conserve its resources as long as possible, by becoming more conservative as the fraction of the residual battery energy decreases. This trend is clearly visible in Figure 4.6(a), which shows as the profit achieved by the Energy Aware Scheme decreases over time. Thanks to this mechanism, as can be seen in Fig. 4.6(d), no node has completely depleted its battery after 120 days of simulation. However, to achieve this the Energy Aware Scheme has to act conservatively and to ignore many missions. This is why its total profit falls below 60% of the maximum profit.

The Energy-Lifetime Aware Scheme tries to conserve node resources in order to reach the target lifetime. Since it does not exploit information on the harvesting subsystem or on the expected harvested energy, it tends to be overly conservative. This means that, in the first half of the target network lifetime, the support offered to missions (thus the network profit) is quite low. Then the scheme changes its behavior, becoming more aggressive as the target network lifetime approaches, and increasing its profit. For this reason, this scheme is not able to provide a stable profit over time: as shown in Fig. 4.6(c), the variability of the profit it achieves per day is the highest among all the bidding schemes. Overall, the total profit achieved during the target network lifetime is quite low: 57% the maximum and 20% lower than what achieved by EN-MASSE.

#### **Impact of the long-term energy predictor**

In this section we discuss the impact of the long-term energy predictor on the performance of EN-MASSE. We focus on the solar dataset collected in Darrington, WA, from September to December 2010. We use historical data of weather conditions in the past years, which are available for this scenario, to analyze the impact of the long-term energy predictor (LTP) described in Section 4.3.4 on the performance of EN-MASSE. In the setup we consider, all the simulation parameters (network topology, mission arrival rate, target lifetime, etc) are the same as described in Section 4.4.3.

Fig. 4.7 shows the comparison of the performance obtained by EN-MASSE with and without the use of the long-term predictor. As can be seen in Fig. 4.7(a), in this scenario, EN-MASSE without LTP is not quite able to provide a stable profit over time, as its performance degrades as the target network lifetime approaches; however, it outperforms the other assignment

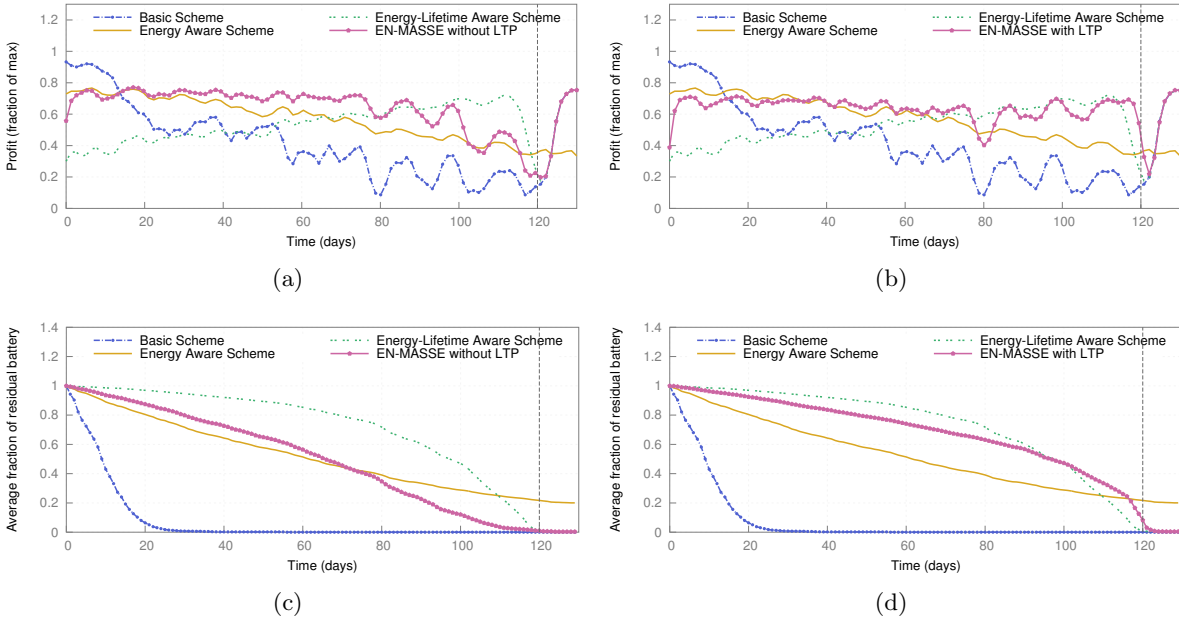


Figure 4.7: Impact of the long-term energy predictor on the performance of EN-MASSE [Darrington solar traces dataset, September-December 2010]: fraction of achieved profit per time slot without (a) and with (b) LTP; average residual battery energy over time without (c) and with (d) LTP.

schemes. This is due to the fact that, without using the long-term predictor, EN-MASSE tends to consume battery energy at approximately the same rate over time (Fig. 4.7(c)). However, as shown in Figure 4.5(d), in the four months during which the network is required to be operational, the average energy harvested per day significantly and steadily decreases, passing from 142 J in September to 20 J in December.

In EN-MASSE the long-term predictor is used to estimate how the harvesting trends are going to change from month to month, in order to decide when the energy stored in the battery is more likely to be needed. The effectiveness of this approach is confirmed by Figure 4.7(b), which shows how EN-MASSE with LTP is able to achieve a much stabler profit over time, by consuming energy from the battery at different rates in different months (Fig. 4.7(d)).

#### Impact of parameter variations on performance

We investigate how varying key parameters affect the performance of EN-MASSE and of the other considered mission assignment schemes. The parameters that have been varied is specified in the title of the following subsections. Unless otherwise specified, scenario and protocol parameters are as detailed in Section 4.4.1. Fig. 4.8 shows the ratio between the total profit achieved at target lifetime by EN-MASSE and the profit achieved by the other schemes. Each data point is obtained by averaging the results over 10 runs; for each run, the simulation is executed until the target lifetime of the network is reached. For each scenario, the performance improvement obtained by our EN-MASSE scheme with respect to the other assignment schemes is shown.

**Impact of target lifetime** As shown in Fig. 4.8(a), the gap in profit between EN-MASSE and the Energy Aware Scheme grows with the target lifetime. The same is true for the Energy-Lifetime Aware scheme. The reason is that for longer network lifetimes a higher percentage of missions are enabled by the harvested energy. This penalizes the Energy Aware and Energy-Lifetime Aware schemes, which do not use exploit information on future harvested energy

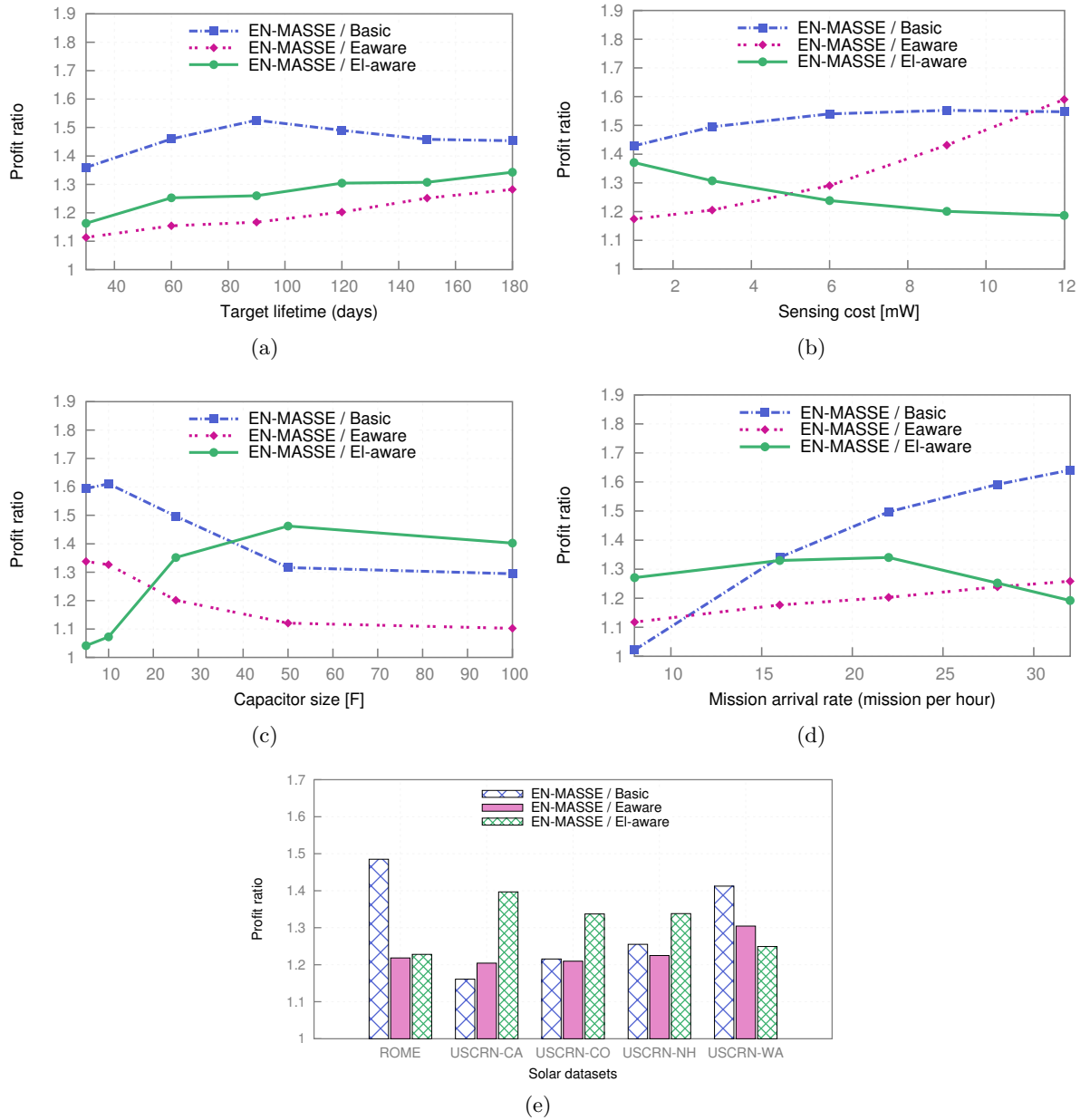


Figure 4.8: Simulation results: performance improvement for varying (a) target lifetime, (b) sensing cost, (c) capacitor size, (d) mission arrival rate and (e) harvesting scenarios.

and on the harvesting subsystem features to make their bidding decisions. Such schemes simply become more and more conservative, loosing in terms of profit, as battery becomes a critical resource, which can satisfy only a small percentage of missions.

The performance ratio of EN-MASSE over the Basic Scheme goes up to 1.5 when the target lifetime is set to 4 months. It then slightly decreases for longer lifetimes. EN-MASSE improved performance reflects the fact that our scheme uses the battery energy to serve missions that have a higher profit than those selected by Basic, and that it selects more profitable missions also when they are enabled by harvested energy. However, the gap in profit between missions satisfied by EN-MASSE and the Basic Scheme is less significant in case of energy harvesting operated missions. Harvested energy must be spent within a limited time frame, making it harder to achieve a high profit in this case. As the target lifetime increases a larger percentage of missions are sustained by energy harvesting, reducing the ratio between the profits achieved by the two schemes. However, the gap between the Basic Scheme and EN-MASSE remains significant. When considering target lifetimes of one year or longer, the Basic Scheme, despite outperforming the Energy-Aware and Energy-Lifetime-Aware schemes, achieves profits that are 10 – 15% lower than EN-MASSE.

**Impact of sensing cost** Fig. 4.8(b) shows how the performance of EN-MASSE and the other schemes is impacted by the sensors used and the associated energy consumption. A higher energy consumption for sensing (sensing cost) degrades the performance of the Energy-Aware Scheme. The ratio between EN-MASSE and this scheme can be as high as 1.65 for a sensing cost of 12mW. The reason is that when the sensing cost is high nodes deplete a considerable percentage of their battery energy quickly. In this case, the Energy-Aware Scheme becomes very conservative accepting only missions with very high profit. This would be a good strategy if nodes were equipped only with the battery, as already noticed. When harvested energy is a significant percentage of the overall energy available to the node, being overly conservative in accepting missions is a profit trap, since supercapacitor self-discharge and finite buffer size reward a fast use of harvested energy. EN-MASSE outperforms the Basic Schemes more significantly as the sensing cost increases. The higher the sensing cost, the higher the toll when making a wrong mission selection.

The performance improvement of EN-MASSE with respect to the Energy-Lifetime Aware Scheme shows a decreasing trend for increasing sensing costs, as this scheme has a finer mechanism to control nodes eagerness to bid for missions. Despite that, EN-MASSE still outperforms the Energy-Lifetime Aware Scheme, achieving a profit ratios between 1.35 (lower sensing cost) and 1.2 (higher sensing cost).

**Impact of capacitor size** As shown in Fig. 4.8(c), the performance improvement of EN-MASSE with respect to the Basic and Energy Aware schemes has a decreasing trend for increasing capacitor size. The Basic Scheme takes advantage of a bigger capacitor. Basic usually suffers from a dumb management of the supercapacitor energy buffer; when such buffer is larger this effect is less important. The Energy Aware Scheme shows a similar trend because, when making bidding decisions, it takes into account the ratio between the current residual energy (battery plus capacitor) and the maximum energy. The bigger the capacitor, the more aggressive the scheme is when harvested energy is available.

The performance improvement of EN-MASSE with respect to the Energy-Lifetime Aware Scheme instead increases for bigger capacitor sizes, demonstrating that our scheme better exploits recharge opportunities. We also observe that the relative performance of the assignment schemes does not show a significant variation when using a 100F capacitor instead of a 50F capacitor, because of its higher self-discharging rate.

**Impact of mission arrival rate** Fig. 4.8(d) shows how the performance of EN-MASSE varies with respect to the other schemes for different mission arrival rates. The performance improvement over the Energy Aware Scheme increases for higher mission arrival rates up to a ratio of 1.3. In fact, increasing the mission arrival rate has an effect similar to considering higher sensing cost, as it leads to heavier network workload. Thus, once again, the Energy-Aware Scheme becomes conservative and accepts only missions with high profit. Since nodes using the Basic Scheme propose to any mission within their range, while EN-MASSE selects missions with higher profit, the gap in profit between the two schemes grows up to a ratio of 1.65 as the mission arrival rate increases and more missions arrive in the network. Finally, the performance improvement over the Energy-Lifetime Aware Scheme slightly decreases for increasing mission arrival rates, but it remains between a ratio of 1.35 and 1.2.

**Impact of the harvesting scenario** Fig. 4.8(e) shows how the performance of EN-MASSE varies with respect to the other schemes when considering different harvesting scenarios, i.e., different solar datasets. The solar energy traces we consider here are the ones we collected in Rome (Section 4.3.4) and the ones from the US Climate Reference Network (Section 4.3.4), considering the first four months of the solar datasets.

As can be seen from the figure, our scheme, EN-MASSE, consistently outperforms the other assignment schemes by achieving a profit that is 16 – 49% higher.

The Basic Scheme is the scheme that depends the most on the harvested energy. In fact, by comparing the results shown in Fig. 4.8(e) with the statistics of the solar datasets reported in Fig. 4.5, it can be clearly seen that its performance increases for scenarios in which the average harvested energy per day is higher.

The performance of the Energy-Lifetime Aware Scheme also varies for different harvesting scenarios. This scheme does not exploit information about the harvested energy. For this reason, the higher the average harvested energy per day is, the more pronounced is the gap between the performance achieved by the Energy-Lifetime Aware Scheme and EN-MASSE.

The performance of the Energy Aware Scheme remains quite constant over all the different harvesting scenarios, but it exhibits the worst performance in the USCRN-WA scenario. This is due to the fact that, in this scenario, the energy harvested in the first couple of months is quite low. When running the Energy Aware scheme, nodes in the network have, on average, depleted more than 50% of their battery within the first 40 days. Since this scheme becomes more conservative as the fraction of the residual battery energy decreases, the Energy Aware Scheme starts refusing many missions and it is not able to take advantage of the fact that the average energy harvested per day was increasing during the last two months of the simulations.

We compare our solution to the optimal mixed integer programming (MIP) solution, obtained by solving the formulation of the problem described in Section 4.2.4. Solving this model provides an upper bound on the optimal solution for the sensor-mission assignment in wireless sensor networks with energy harvesting.

#### 4.4.4 COMPARISON WITH THE MIP SOLUTION

We consider a network of 200 nodes, deployed in a field of  $400 \times 400$ m; the arrival rate of missions in the network is 4 missions per hour. The battery size has been scaled accordingly, since the problem is less interesting if there is enough energy to execute almost all missions; the harvested energy and the power consumption of the node, both in idle (sleep) mode and when executing a mission, are the same as in the previous sections. To ease the computation, the satisfaction threshold,  $T_{sat}$ , has been set to zero for these instances.

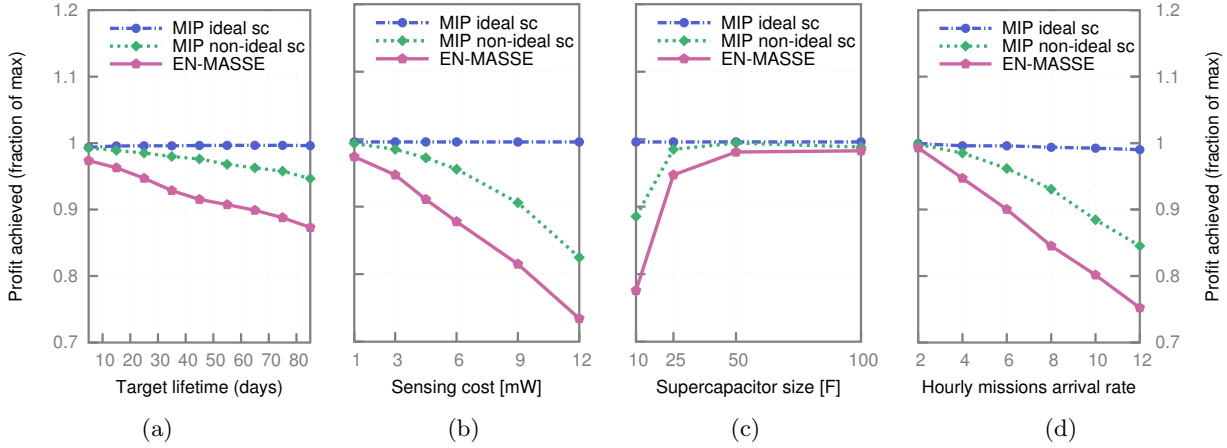


Figure 4.9: Performance of EN-MASSE with respect to the upper bound provided by our MIP models with ideal supercapacitors (MIP ideal sc) and with supercapacitor non-idealities (MIP non-ideal sc) for varying (a) target lifetime, (b) sensing cost, (c) capacitor size and (d) mission arrival rate.

In order to remain consistent with the problem formulation reported in Section 4.2.4, we consider in this section a slightly modified problem. In fact, in our MIP model the problem constraint 4.8 imposes that a node is only allowed to accept a mission if it has enough energy to run until completion. In the simulation results previously reported, instead, such constraints were not enforced. We have performed extensive simulations also for this more constrained scenario, which confirm the same trend discussed in Section 4.4.3. Fig. 4.9 shows the performance of EN-MASSE with respect to the upper bound provided by the optimal MIP solution for different target lifetimes, sensing costs, capacitor sizes and mission arrival rates. The  $y$ -axis shows the total profit obtained at target lifetime as a fraction of the maximum profit. The gap between our solution and the upper bound provided by our MIP model varies between 0.54% and 11.29% of the maximum profit, depending on the considered scenario, with an average gap of 5.55% of the maximum profit.

We also compare the upper bound provided by our MIP model, taking into account the non-idealities of supercapacitors (Section 4.2.4), with the upper bound provided by a similar formulation, which instead models *ideal* supercapacitors. An ideal supercapacitor stores any amount of energy without inefficiencies in charging and discharging, so that any energy that is harvested is stored and used later without losses. The MIP formulation of such ideal case is the same as detailed in Section 4.2.4, with  $C_{max}$  being unbounded and  $\eta_c^C = \eta_d^C = 1$ .

As shown in Figure 4.9, the gap between our model, which takes into account supercapacitors non-idealities, and the ideal model varies between 0.05% and 17.13% of the maximum profit, depending on the considered scenario.

We solved the MIP using the CPLEX commercial MIP solver version 12.3 on a Linux machine with 8 cores and 16 GB of RAM. Figure 4.10 shows the running times in hours of our MIP models for varying target lifetimes, sensing costs, capacitor sizes and mission arrival rates<sup>4</sup>. The running times of both our MIP model with supercapacitor non-idealities and of our MIP model with ideal supercapacitors are reported.

As shown in the figure, the running time of the model with ideal supercapacitor is significantly lower than that of the model with supercapacitor non-idealities. This is due to the fact that

<sup>4</sup> MIP is NP-hard in general, but commercial solvers have become so good that these solvers can quickly and reliably solve problems with millions of variables, depending on the structure. MIP has therefore become a workhorse technology for operations-research professionals solving difficult problems for industry [177].



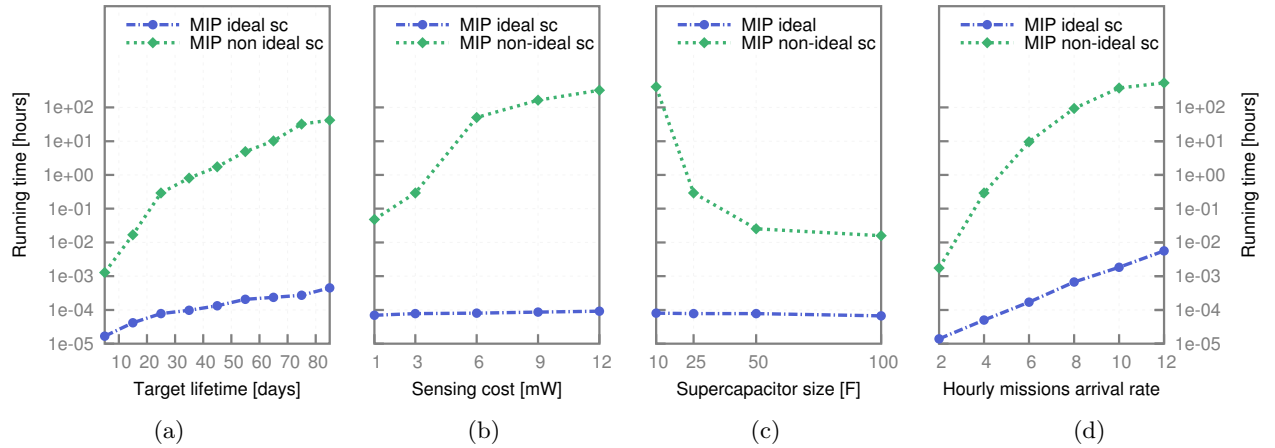


Figure 4.10: Running times in hours of our MIP model with ideal supercapacitors and of our MIP model with supercapacitor non-idealities for varying (a) target lifetime, (b) sensing cost, (c) capacitor size and (d) mission arrival rate.

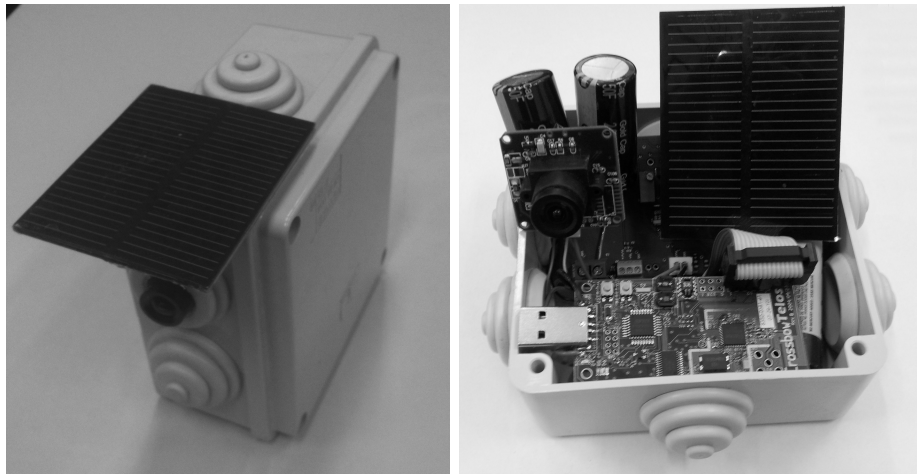


Figure 4.11: Telos B mote interfaced with a  $\mu$ CAM camera and powered by an hybrid harvesting subsystem composed of a solar panel, two supercapacitors and two AA primary batteries.

considering a supercapacitor with unbounded maximum size strongly eases the computation. In fact, since no energy may be lost due to the capacitor being full, it is no longer necessary to constantly keep track of the current energy level of the supercapacitor. To enforce the energy constraints in such a case, it is enough to ensure that, at any time  $t$ , the energy spent by each node is always equal or less than the sum of the energy harvested so far plus the energy initially stored in the battery.

The comparison between the ideal model and the non-ideal model shown in Figure 4.9 highlights the importance of considering buffer non-idealities when modeling energy-harvesting systems. In fact, provided a detailed formulation of realistic energy storages greatly reduces overestimations of the available energy, providing tighter bounds on the optimal solution with respect to the ideal case. Overall, the MIP model with ideal supercapacitors may be used to quickly obtain benchmark results on the achievable performance of a sensor-mission assignment algorithm. However, if a loose bound is not sufficient to assess the performance of the scheme, a more accurate bound should be derived by using the MIP model with supercapacitor non-idealities.

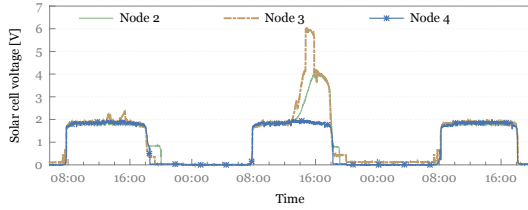


Figure 4.12: Solar data collected over three days of testbed run by three different nodes.

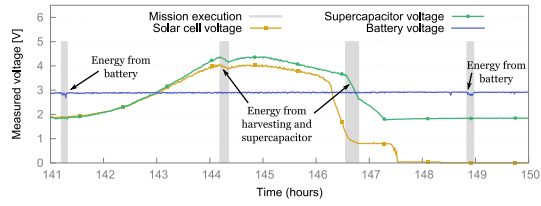


Figure 4.13: Snapshot of 9 hours of solar cell, supercapacitor and battery voltage measurements.

#### 4.5 EXPERIMENTAL TESTBED: IMPLEMENTATION AND VALIDATION

In order to validate our approach in a real-life application scenario, we interfaced six Telos B motes with directional video sensors (4D Systems  $\mu$ CAM [178] and Link Sprite Y201 [179] color cameras). Nodes power their camera on and turn them off by using a dedicated MOS switch controlled through the GI00 port located on the Telos B primary expansion connector.

We powered each node by using a harvesting system composed of a 0.5W solar panel, two 50F Panasonic Gold supercapacitors [180] and two AA primary batteries (Fig. 4.11). The two supercapacitors were wired in series to get a higher operating voltage, thus providing a total capacitance of 25F. Since operating the cameras is expensive in terms of energy cost (their power consumption being of  $\approx 200$  mW), the harvesting subsystem also implements a maximum power point controller (MPPC). The MPPC dynamically maximizes the harvesting efficiency, in order to get as much power as possible from the solar panel under any lighting condition. The voltage of the solar panel, the supercapacitor and of the batteries are periodically sampled and recorded by the nodes by using dedicated test points connected to the ADC input ports of the Telos B mote.

To validate our bidding scheme, we implemented EN-MASSE in TinyOS [154], together with the energy prediction model Pro-Energy (Chapter 2) that is able to deliver short-term solar predictions. We implemented the communication protocol outlined in Section 4.3.1, the EN-MASSE bidding scheme described in Section 4.3.2 and the missions allocation algorithm defined in Section 4.3.3 in TinyOS. To reduce the energy consumption of the communication activity, the CC2420 low power listening radio stack [181] was used.

In order to realize a fully functional system, we also implemented in TinyOS both a basic driver for the Link Sprite and the  $\mu$ CAM cameras and a simple state-of-charge estimator, based on direct voltage look up table, to determine the residual energy stored in the nodes' batteries.

We deployed our testbed outdoors, on the roof terrace of University of Rome “La Sapienza” CS Dept. building, which is located in downtown Rome. The test scenario we considered is that of a network deployed for intrusion detection. Missions were generated at random locations. The utility that a node was able to offer to a given mission was defined as a function of the distance between the camera of the node and the mission location. Each node assigned to a mission was required to turn its camera on and to periodically collect pictures until the end of the mission.

The data obtained while running the testbed has been used to validate the performance trends found by simulations. Moreover, for the whole test duration we also collected data about the harvested energy, the supercapacitor charge and discharge patterns and the battery utilization, in order to validate our energy model.

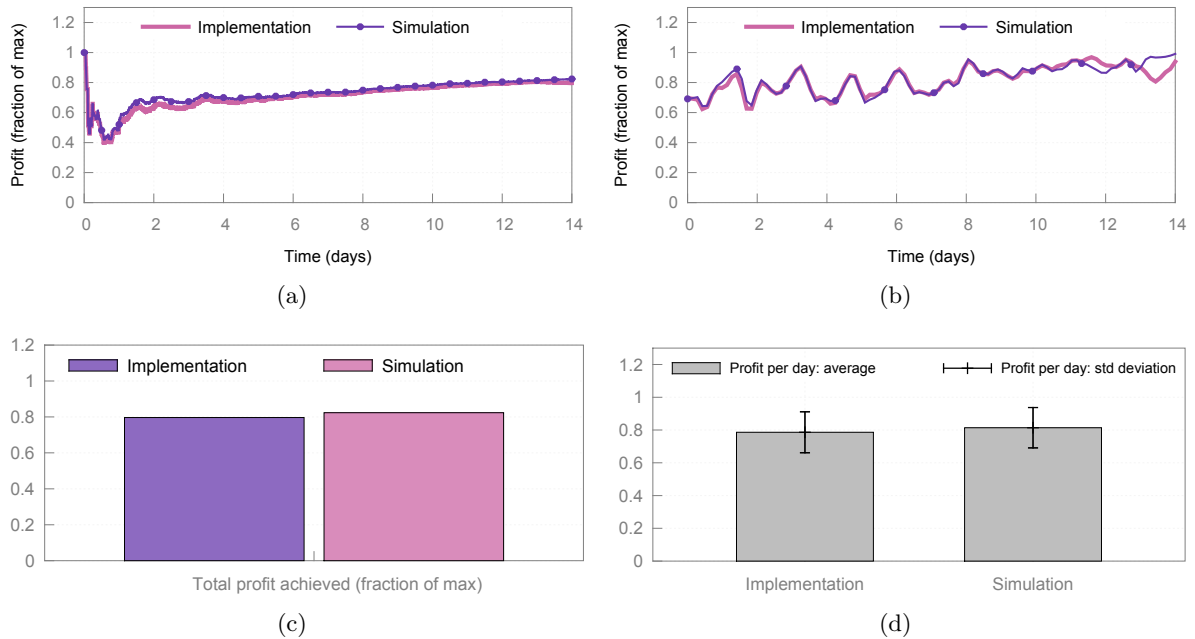


Figure 4.14: Comparison between experimental performance and simulation results: (a) *cumulative* profit achieved over time; (b) fraction of achieved profit per time slot; (c) total profit achieved at target lifetime (as a fraction of maximum) and (d) profit achieved per day: average value and standard deviation.

#### 4.5.1 EN-MASSE ASSIGNMENT SCHEME AND ENERGY MODELS VALIDATION

We deployed a testbed of six Telos B motes on Nov 8, 2012 at 02:40 PM. Five of such motes were sensing nodes equipped with video cameras, while the sixth node was the sink. Missions arrived in the network at random locations with an arrival rate of five missions per hour. The average duration of a mission was set to ten minutes and the target lifetime of the network was of two weeks.

After two weeks, we stopped the test and retrieved the logged data. The data was used to validate EN-MASSE simulations against the real deployment. To accurately reproduce the actual weather conditions experienced by the nodes, we used the solar data collected during the testbed run in our simulations. Figure 4.12 shows an example of solar data recorded by three different nodes over three days.

Fig. 4.13 shows a snapshot of 9 hours of solar cell, supercapacitor and battery voltage measurements, which highlights how different energy sources were used to power the nodes. Gray-shaded areas in the figure represent periods of time during which the node was executing a mission.

The comparison between EN-MASSE simulations results and real-life testbed traces is shown in Figure 4.14.

As can be seen from the figure, simulation results are remarkably close to experimental data. In fact, the difference between the total profit computed by simulation and the profit actually achieved by the testbed is less than 3% of the maximum profit. Such gap is due to the differences between the actual energy availability of the nodes and the estimates produced by the energy models we used in our simulations.

To further investigate this aspect, Figure 4.15 shows the comparison of the supercapacitor and the battery models used in simulations with the actual voltage measurements we gathered

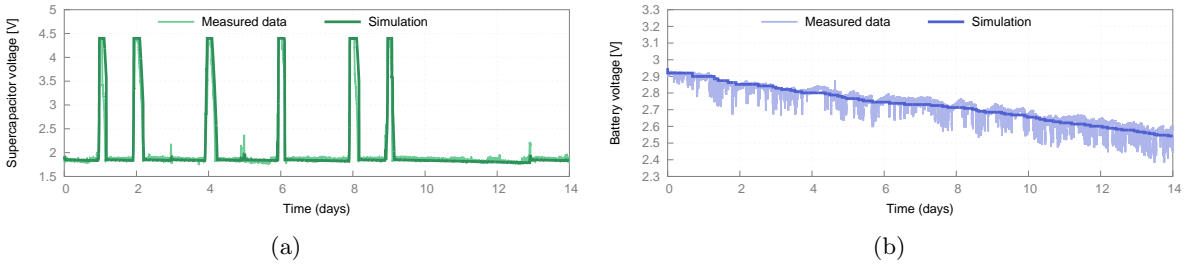


Figure 4.15: Energy model validation, comparison between measured data and simulation traces: (a) supercapacitor voltage and (b) battery voltage.

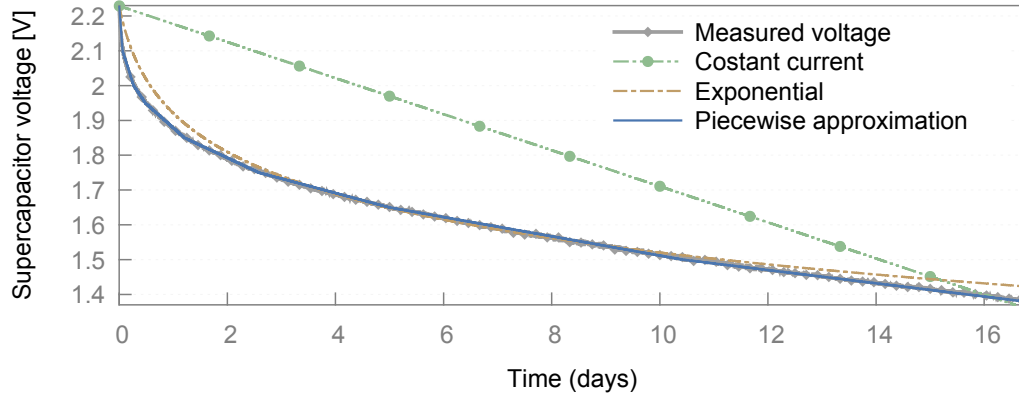


Figure 4.16: Supercapacitors self-discharge: comparison between empirical discharge pattern and different leakage models.

during the fourteen days of testbed experiments. Experimental supercapacitor data, shown in Fig. 4.15(a), confirms the accuracy of our model, which is able to capture the changes in the supercapacitor voltages that occur during supercapacitor charging and discharging and due to leakage and internal charge redistribution. A comparison between real-life battery voltage measurements and the data obtained through simulation is shown in Fig. 4.15(b). We found our battery model to be accurate enough to support mission bidding decisions, as it succeeds in reflecting the overall discharge patterns of the battery. However, our simple model does not capture the fine-grained behavior of battery discharge; dedicated models [39] should be employed if more accurate simulations are needed.

Finally, figure 4.16 shows the comparison between the empirical discharge pattern of two 50F Gold Cap supercapacitors wired in series and their self-discharge according to three different leakage models proposed in the literature.

To obtain the empirical data, we charged the supercapacitors to 2.3V for one hour, then disconnected them from the circuit. We collected self-discharge data for 17 days, by measuring the supercapacitors voltage drop once per minute.

Using such experimental data, we evaluated the accuracy of three different methods, in which the leakage experienced by the charged supercapacitors is modeled:

1. as a constant current [36];
2. as an exponential function of the current supercapacitor voltage [37];
3. by using a piecewise linear approximation of the empirical leakage pattern [26].

The parameters of all the models were set as to minimize the error between estimation and

actual data. As can be seen in the figure, the constant current model fails to capture the empirical discharge pattern of the supercapacitor, which is clearly not linear. The accuracy of the exponential model, instead, is quite good: its root mean squared error is around 24 mV. Finally, using the piecewise linear approximation model yields the best results, as shown by the root mean squared error which is less than 3.5 mV, i.e., one seventh that experienced when using an exponential model. This motivates the use of piecewise linear approximation in our simulations.

## 4.6 CONCLUSIONS

In this chapter we have presented an analytical model and a distributed solution, EN-MASSE, for sensor-mission assignment in WSNs with energy harvesting. We proposed a MIP formulation that captures advanced real-life details of the behavior of a typical energy harvesting subsystem, including supercapacitor and battery non-idealities, possibility to use the harvested energy directly when the current power consumption is higher than the harvested power, hybrid storage systems and variations in the power consumption of the node. We demonstrated that considering buffer non-idealities provides a tighter bound on the optimal solution, by reducing overestimations of the available energy. Moreover, we show that, by addressing scalability issues of previous models, our formulation is able to provide upper bounds on the optimal solution for real-life sized instances, consisting of hundreds of nodes and with target lifetimes of several months. Despite the theoretical difficulty of the general sensor-mission assignment problem, our distributed scheme, EN-MASSE, is shown to perform very closely to the optimum provided by the analytical formulation. Moreover, EN-MASSE significantly outperforms other harvesting-unaware assignment schemes. By comparing mission assignment schemes in several different scenarios we have demonstrated that traditional assignment algorithms cannot harness the full potential provided by the harvesting technology, which is instead taken into account efficiently by our proposed scheme. Finally, we experimentally validated our proposed scheme and the accuracy of the energy models we used in simulations in a testbed of Telos B motes powered by energy harvesting.



## EXPLOITING ENERGY HARVESTING TO SUPPORT DATA-CENTRIC ACCESS CONTROL IN WSNS

Health care and assisted living are two of the most notable application domains of wireless sensor networks in which emerging energy harvesting technologies can play a significant role. In fact, such scenarios presents a number of unique requirements that strongly challenge the limited energy resources of wireless sensor nodes [182]. Among them, privacy and security issues are of paramount importance, because of the sensitive nature of the data collected through patients monitoring.

The work presented in this chapter is motivated by the question of whether energy-harvesting techniques can be exploited to support powerful data access control solutions which would otherwise be too energy demanding to be feasible.

In the health care domain, access to sensitive data must be allowed only to a given set of privileged users, who can possibly belong to different institutions (multi-authority) and whose identities are not necessarily known a priori. In addition, different types of data (e.g., health data versus patient location versus environmental data) may be meant for different sets of users. Finally, the recipients of a given sensed information stream may further depend on the context, and change when the context does. For instance, consider a patient remotely monitored through sensing devices placed over her/his body. The gathered data (temperature, hearth rate, blood pressure, etc.) is generally not meant for a *specific doctor* (i.e., as an individual), but for someone having the *role* of doctor, whose identity may vary over time and may not even be known a-priori. Moreover, critical health conditions (as attested by anomalies in the gathered data) require prompt intervention. Such data should hence become suddenly accessible by emergency personnel not originally in charge of handling *normal* health parameters.

### DATA-CENTRIC ACCESS CONTROL

The problem of granting access privileges to given users is known as ‘data access control’, and it is traditionally addressed by dedicated server-based privilege management infrastructures. However, such infrastructures come along with several drawbacks in a scenario of pervasive deployment of wireless sensor networks, including the significant management burden posed to the WSN in terms of coordination and signaling.

Such drawbacks may be overcome by using different approaches, such as the novel category of Attribute Based Encryption (ABE) [183] schemes, which permit to address the access control problem through a completely different *data-centric* perspective. ABE permits a recipient to decrypt a given ciphertext only if she/he satisfies a given access control policy. ABE has been

designed in two flavors. In the original Key-Policy (KP-ABE) constructions [183, 184], an encrypted data is labeled with a set of descriptive attributes and the access control policies reside on the data recipients' terminals. An opposite approach is instead promoted by ABE schemes called Ciphertext-Policy (CP-ABE), originally proposed in [185]. With CP-ABE, access control policies (unlike attributes) are embedded in the ciphertext. Attributes are instead issued to users, possibly from multiple independent authorities (e.g., when using the construction in [186]). A user may decrypt the ciphertext only if the set of attributes she/he holds satisfies the access control policy embedded in the data. For instance, a monitored patient may freely decide that a given data may be accessed only by 'doctors AND nurses', or only by 'doctors OR personnel from a specific hospital'.

Embedding the access control policies inside the ciphertext, rather than having them enforced on external servers or policy enforcement points, makes CP-ABE schemes particularly well-suited for WSN scenarios. In fact, differently from KP-ABE, CP-ABE allows each sensor to dynamically and independently change the access control policies attached to the data, e.g., to promptly respond to a change of context or environmental conditions. This in turn gives full control to end users which can decide the access rules to their data and how they should evolve with context.

#### OUR CONTRIBUTION

Despite the appeal of CP-ABE schemes, there is considerable skepticism on their viability over battery-powered and resource-constrained sensors, especially when considering multi-authority schemes whose computational complexity and overhead scales at best linearly with the number of attributes involved in a policy. Indeed, to the best of our knowledge, our work is the first to document an implementation of a multi-authority CP-ABE scheme (actually, we are not even aware of previous works documenting "just" single-authority CP-ABE implementations over WSN nodes - works [187, 188] in fact report single-authority KP-ABE implementations), and our results show that performance appears still far from being practical for battery-powered nodes.

Our work stems from the observation that the ever increasing emergence of energy harvesting technologies for sensor nodes leads to a radical rethinking of energy efficiency strategies. In the traditional scenario of battery-powered devices, the only and obvious strategy to prolong the lifetime of a WSN was to reduce energy consumption as much as possible. This translated into believing that energy demanding operations (such as those mandated by some security schemes or cryptographic routines) were not feasible for energy constrained embedded devices. Conversely, energy harvesters opportunistically draw energy from the environment<sup>1</sup>. The result is an alternation between periods in which energy must be sparingly used, and situations in which there may even be an **excess of energy available**, energy which would be wasted unless used in the short term. Moreover, even if energy availability cannot be controlled, it can be predicted [4, 109, 36] to some extent, thus allowing the development of proactive energy management strategies. This opens up new opportunities: the question is no longer restricted to quantify how demanding an operation (say a costly CP-ABE encryption of a key using a given policy) is in terms of energy toll, but it extends to further understand *when* such an operation has to be performed and *whether*, and *to what extent* demanding computations can be pushed to periods where energy is harvested and is in excess.

This new area of "green wireless sensor network security", i.e., how to exploit the opportunities provided by energy harvesting for revisiting WSN security schemes, has so far been overlooked.

<sup>1</sup>In health-care applications using wearable medical devices, potential sources of energy harvesting include indoor light energy, mechanical energy produced by movements, and heat transfer between the human body and the ambient.



This work takes a first step in the direction of re-thinking WSN security schemes so as to exploit the opportunities provided by energy harvesting. Specifically, we make the following contributions:

- We assess the feasibility of CP-ABE in WSNs via an actual implementation in TinyOS for Telos B and Mica2 platforms. Such an implementation allowed us to determine its energy consumption, memory requirements and computational complexity and guided us through the development of specific optimizations aimed at reducing the large overhead of CP-ABE over resource-constrained motes. To the best of our knowledge, we are the first to fully implement a CP-ABE scheme (actually, the more complex multi-authority case) over sensor platforms.
- Around such multi-authority CP-ABE core, we have designed AGREE, an energy-harvesting-aware Access control framework for GREEN WSNs. AGREE mitigates the energy consumption of the CP-ABE scheme by pushing most of the costly encryption operations to energy harvesting periods, pre-computing and storing the CP-ABE encryption of as many keys as possible. Since the memory of the motes is clearly unable to hold all possible access control policies, AGREE implements a caching strategy designed to store information so as to minimize the need to invoke a CP-ABE operation before the next predicted energy harvesting phase occurs.
- We provide a simulation-based performance evaluation framework for EHWSNs. In our experiments, we use traces of the availability of indoor light energy that we obtained by interfacing TelosB nodes with photovoltaic cells, collecting data for a week in the student office of the CS Department building of Sapienza University of Rome. We also validate our approach by using two additional datasets obtained from the EnHANTs (Energy Harvesting Active Networked Tags) project of Columbia University.
- We performed a comparative performance evaluation of AGREE and of two other caching strategies which do not leverage information about the harvesting process and the dynamics of the application. Our validation clearly shows that AGREE is able to efficiently operate based on the excess harvested energy and that it significantly outperforms other harvesting-unaware caching strategies.

The remainder of this chapter is organized as follows. We discuss related work in Section 5.1. In Section 5.2 we review known results by giving an overview of the operation of CP-ABE schemes. We present our scheme, AGREE, in Section 5.3 and discuss in detail its operations and features. We evaluate our proposed approach in Section 5.4, discussing practical implementation challenges of CP-ABE schemes and presenting a simulation-based evaluation of AGREE. Finally, we present our conclusions in Section 5.5.

## 5.1 RELATED WORKS

Despite extensive research has been devoted to devise security solutions specifically tailored to traditional battery-powered WSNs [189, 190], so far only a few works [191, 192] have addressed security topics in wireless sensor networks with energy harvesting capabilities. In [191], Taddeo et al. proposed an optimization mechanism that allows a EHWSN to change the communication security settings over time, based on the energy state of the network. Different types of packets, each having different priority level and security requirements, are handled, and a quality of service mechanism is introduced to favor high-priority packets when the harvesting energy intake is scarce. Pelissier et al. proposed in [192] a scheme that applies to stream ciphers, which allows energy harvesting systems to precompute and store keystream bytes, and to use them when the system energy availability is low. However, stream ciphers, being symmetric encryption algorithms, consume impressively less time and energy with respect to asymmetric cryptography schemes: indeed, the time and energy required to

perform a single public-key operation can be the same as encrypting tens of megabits using symmetric encryption [193].

In this chapter we show that smart caching and energy intake prediction can be combined to make computationally involved asymmetric cryptography schemes feasible in real wireless sensor networks with energy harvesting. In particular, in our work we focus on data access control and CP-ABE schemes. The problem of data access control in WSNs, which is of paramount importance in health care and assisted living applications, has received notable attention by the research community, but, to the best of our knowledge, no solution for networks with harvesting capabilities has been proposed so far. Recent works targeting data access control in traditional WSNs are based on Attribute Based Encryption (ABE), a cryptographic primitive introduced by Sahai and Waters in [183] and later extended by [184, 185], which proposed Key-Policy ABE (KP-ABE) and Ciphertext-Policy ABE (CP-ABE), respectively. The technical feasibility of KP-ABE techniques in wireless sensor networks have recently been demonstrated [187, 188]. In [187], Yu et al. presented a centralized fine-grained data access control scheme, based on KP-ABE, for distributed storage in wireless sensor networks, which has been specifically adapted to WSNs performance and security requirement. However, their solution only addresses single authority scenarios, in which compromising the single authority jeopardizes the security of the whole system. The framework proposed by Ruj et al. in [188] partially solved this limit, but their solution can only support strict “AND” policies and it requires a pre-determined set of authorities.

CP-ABE schemes, instead, support multi-authority [186] and provide a framework for dynamic access control which well fits the application requirements of traditional WSN applications. However, since they suffer from a significant higher overhead than KP-ABE approaches, their viability over both traditional and energy harvesting wireless sensor networks is still to be proven. Making CP-ABE schemes applicable in real-life is the objective of this work.

## 5.2 CP-ABE OVERVIEW

Our work capitalizes on a decentralized CP-ABE scheme recently proposed by Lewko and Waters, referred to in what follows as LW. In the next subsections we give an overview of such scheme and of its functionalities. The interested reader is referred to [186] for formal proofs of the security of the scheme.

### 5.2.1 PRELIMINARIES

The runtime operations of CP-ABE comprise two functionalities: *encryption*, performed by the sensor nodes in charge of gathering and delivering the sensed information, and *decryption*, performed by the data recipient which we non restrictively assume to be a back-end infrastructure device or an end user’s terminal (i.e., not a sensor node). CP-ABE operation is asymmetric. Similarly to ordinary asymmetric encryption (e.g., RSA), a sensor node does not need to store any secret key. Rather, in the general context of multiple authorities, the information needed by the system are:

- An *access control policy*, namely a boolean predicate over a set of attributes, which specifies the set of users that are allowed to decrypt the data.
- A set of *attributes*, which are ordinary strings of text arbitrarily formatted.
- A set of *public keys*, one per each attribute, potentially released by different authorities. An encrypted data for a given attribute may be decrypted only by a user possessing a secret key associated to the attribute name and to the authority releasing the attribute.

## 5.2.2 SETUP AND DECENTRALIZED ATTRIBUTE ISSUING

In CP-ABE schemes, involved parties agree on the following public parameters:

- Two multiplicative cyclic groups,  $G$  and  $G_T$ , of same prime order  $N$ , chosen such that the discrete logarithm problem is hard to solve on both  $G$  and  $G_T$ ;
- a generator  $g$  for the group  $G$ ;
- a global hash function  $H : \{0, 1\}^* \rightarrow G$  that maps arbitrary strings into elements of the group  $G$ ;
- a bilinear map  $e : G \times G \rightarrow G_T$ , satisfying the following properties: bilinearity, non degeneracy and computability [185].

CP-ABE supports multi-authority system, in which any party can be an independent Attribute Authority (AA) by creating and publishing a verification key coupled with a list of attributes it will manage. For each issued attribute  $i$ , the AA chooses two random exponents  $\alpha_i, y_i, \in \mathbb{Z}_N$ , and publishes  $PK_i = \{e(g, g)^{\alpha_i}, g^{y_i}\}$  as its public key. We recall that attributes are *permissions* to access encrypted data, and as such are issued not to encrypting sensor nodes, but to users. To identify different users, a global identity  $GID_u$  (a text string, e.g., the user's social security number) is associated to each user  $u$ .

## 5.2.3 MESSAGE ENCRYPTION

Messages are encrypted along with an access control policy over a set of attributes. Access structures are described through Linear Secret Sharing Scheme (LSSS) matrices [194]. To encrypt a message  $D$ , the first step consists of modeling the applicable access control policy in terms of an  $a \times l$  LSSS matrix  $LS$ , where  $a$  is the number of attributes involved in the policy and  $l$  is a parameter depending on the considered policy<sup>2</sup>.

We define  $\rho(x)$  as a function mapping rows  $x$  of  $LS$  to the corresponding attribute. We also recall that, by construction, the encrypting node knows the public key of each attribute  $\rho(x)$ .

The encryption algorithm chooses a random secret  $s \in \mathbb{Z}_N$  and a random vector  $v \in \mathbb{Z}_N^l = \langle s, v_2, v_3, \dots, v_l \rangle$ , having the secret  $s$  as its first entry and random values as the subsequent entries. It calculates  $\lambda_x = LS_x \cdot v$ , where  $LS_x$  is a row of  $LS$ . Similarly, it chooses a random vector  $w \in \mathbb{Z}_N^l = \langle 0, w_2, w_3, \dots, w_l \rangle$  with 0 as the first entry and it defines  $\omega_x = LS_x \cdot w$ . For each row  $LS_x$  of  $LS$ , it chooses a random  $r_x \in \mathbb{Z}_N$ . It finally encrypts the message  $D$  computing the following parameters:

$$\begin{aligned}
 C_0 &= De(g, g)^s \\
 C_{1,x} &= e(g, g)^{\lambda_x} e(g, g)^{\alpha_{\rho(x)} r_x} \forall x \\
 C_{2,x} &= g^{r_x} \forall x \\
 C_{3,x} &= g^{y_{\rho(x)} r_x} g^{\omega_x} \forall x
 \end{aligned} \tag{5.1}$$

## 5.2.4 MESSAGE DECRYPTION

To decrypt a message a user  $u$  needs to possess a secret keys  $K_{x, GID_u}$  for each attribute  $x$  belonging to a set of attributes which satisfy the access control policy embedded in the ciphertext. This is verified by checking whether there exists a subset  $X$  of attributes owned

<sup>2</sup>The reader can refer to Appendix G in [186] for a practical procedure to convert an arbitrary boolean policy into an LSSS matrix.

by the user, such that a linear combination of the relevant rows in the LSSS matrix  $LS$  yields the vector  $(1, 0, \dots, 0)$ . If this condition is verified, the user may decrypt the message  $D$ . For each  $x \in X$ , the user  $u$  computes:

$$\frac{C_{1,x}e(H(GID_u), C_{3,x})}{e(K_{\rho(x),GID_u}, C_{2,x})} = e(g, g)^{\lambda_x} e(H(GID_u), g)^{\omega_x} \quad (5.2)$$

Then user  $u$  chooses the constants  $c_x \in \mathbb{Z}_{\mathbb{N}}$ , such that  $\sum_{x \in X} c_x LS_x = (1, 0, \dots, 0)$  and computes:

$$\prod_{x \in X} (e(g, g)^{\lambda_x} e(H(GID), g)^{\omega_x})^{c_x} = e(g, g)^s \quad (5.3)$$

Note that  $\lambda_x = LS_x \cdot v$  and  $\omega_x = LS_x \cdot w$ , where  $v \cdot (1, 0, \dots, 0) = s$  and  $w \cdot (1, 0, \dots, 0) = 0$ .

Finally the user can obtain the original message  $D$  as:

$$D = C_0 / e(g, g)^s. \quad (5.4)$$

### 5.3 AGREE

In this section, we present our scheme, AGREE. In Section 5.3.1 we discuss the specific optimizations we devised to reduce the large overhead of CP-ABE in WSNs. In Section 5.3.2 we present a technique that enable our system to react to critical situations and changes of context. A mechanism that allows nodes to leverage energy harvesting opportunities to pre-compute policies is presented in Section 5.3.3. Finally, we introduce in Section 5.3.4 a caching strategy to pre-compute the most likely set of policies, as quantified by a Markov model of the sensor node's application state evolution.

#### 5.3.1 WSN SPECIFIC OPTIMIZATIONS

The main source of overhead introduced by CP-ABE schemes is due to message encryption, as several scalar multiplications must be performed to compute the parameters  $C_0, C_{1,x}, C_{2,x}$  and  $C_{3,x}$  described in Section 5.2.3, Equation (5.1). The first specific optimization we propose to adapt CP-ABE to resource-constrained devices is to have nodes ascribing the access policy to a *session key*,  $SSK$ , instead that to the data itself, as in traditional CP-ABE schemes. More in details, a session key  $SSK$  is generated and encrypted using CP-ABE. Each sensed data  $D$  is encrypted by means of a symmetric-key algorithm, such as AES [195], using  $SSK$  as secret key. Upon request for sensor data, the mote responds with both the encrypted session key  $SSK$  and the ciphertext of the sensed data  $D$ . If the user is an intended receiver, he will be able to decrypt the session key and to derive the data encryption key. Such optimization does not affect the security of the CP-ABE scheme, because, as explained in Section 5.2.4, to decrypt the session key the user should be an intended receiver, i.e., she/he would need to possess a secret key  $K_{x,GID_u}$  for each attribute  $x$  belonging to a set of attributes that satisfy the access control policy embedded in  $SSK$ . The rationale behind such optimization is that encrypting or decrypting data with a symmetric encryption algorithm, such as AES, is much more efficient than directly using ABE, which is several orders of magnitudes more resource demanding than symmetric encryption. Moreover, by using this approach, sensor nodes can pre-compute and store the parameters  $C_0, C_{1,x}, C_{2,x}$  and  $C_{3,x}$  when they have high energy and use them when the access policy changes or when a session key is refreshed.

As for further optimizations, the choice of the type of elliptic curve is important because it directly affects the performance of operations such as scalar multiplication and pairing. A generic pairing function is defined as  $e : \mathbb{G}_1 \times \mathbb{G}_2 \rightarrow \mathbb{G}_T$ , where  $\mathbb{G}_1$  and  $\mathbb{G}_2$  are two

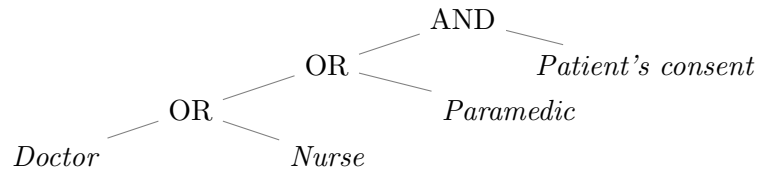


Figure 5.1: Description of the policy  $p_2$  as a tree representing the corresponding boolean function.

distinguished subgroups of order  $p$  in which the Elliptic Curve Decisional Diffie-Hellman problem (ECDDH) is hard to solve [196]. CP-ABE requires a prime order group with a symmetric pairing  $e : \mathbb{G}_1 \times \mathbb{G}_1 \rightarrow \mathbb{G}_T$ , which only exists on supersingular elliptic curves. In order to reduce ciphertext size, we choose a supersingular curve over a binary field, having the form  $y^2 + y = x^3 + x$  with an embedding degree of 4. This kind of curve is well suited for WSNs environments and it can be implemented very efficiently in terms of memory and processing requirements, when compared with implementations on ordinary curves [197].

### 5.3.2 ACCESS POLICIES UPDATES

In many WSNs scenarios, the access provided to the data is highly dependent to the current context. For this reason, it is very important to consider the occurrence of critical events in the system and to react to them by providing fast mechanisms to change the access policies when needed. Critical events must be timely handled and a dynamic access control system is essential to this end. Any access provided to roles in response to an emergency is temporary and is rescinded after a specific amount of time, which depends on the specific emergency happened. For example, in a health care application scenario, a critical event may be the patient suffering from a heart attack while being at home. In such context, sensitive data that are normally accessible only to her/his doctor should also be made available to the emergency paramedical team as quickly as possible. To handle such situations, the basic idea is to have a hierarchy of access policies. Each level of the hierarchy corresponds to a level of criticality. Let  $L$  be the number of levels that the system can support. If the system is using the access policy level  $n$ , it will ignore all the access policies of level  $n + 1, \dots, L$ . For example, consider this set of access policies associated with an ECG sensor of a patient:

1.  $p_1 = \text{Doctor AND Patient's consent}$
2.  $p_2 = (\text{Doctor OR Nurse OR Paramedic}) \text{ AND } (\text{Patient's consent})$
3.  $p_3 = \text{Doctor OR Nurse OR Paramedic}$

Figure 5.1 shows the description of the policy  $p_2$  as a tree representing the corresponding boolean function. Initially, the sensor node adopts the policy  $p_1$ . Policies  $p_2$  and  $p_3$  are not used, as their hierarchical level is higher than the current criticality level of the system, but the sensor node may pre-compute them for future use, if it has enough energy and cache memory available. Whenever a critical event occurs, according to the context in which the patient is located and to the importance of the event, the sensor node will adopt a policy of higher level, thus ensuring the timely adjustment of data access. Changing the access policy of the data implies updating the session key  $SSK$  by running the encryption algorithm described in Section 5.2.3. More in detail, if a new policy  $p'$  is adopted, the following operations should be performed by the node:

1. generate a new session key  $SSK_{p'}$ ;
2. convert the access policy  $p'$  into an LSSS matrix;
3. apply CP-ABE to encrypt  $SSK_{p'}$  with the access policy  $p'$ , by computing the new parameters  $C_0, C_{1,x}, C_{2,x}$  and  $C_{3,x}$ ;

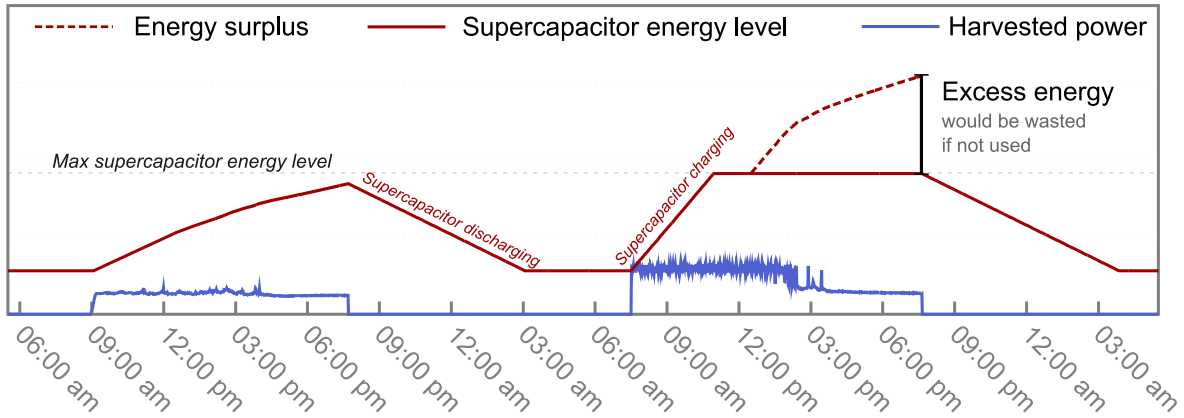


Figure 5.2: Traces of the light energy harvested indoor over two days. There is an energy surplus between 12:00 PM and 7:30 PM on the second day: since the supercapacitor is full, the energy harvested by the node during such period of time should be used immediately or it would be wasted.

4. locally store the parameters of the new policy  $p'$ :  $(SSK_{p'}, C_0, C_{1,x}, C_{2,x}, C_{3,x})$ ;
5. send the new encrypted session key to the users.

Such operations, however, are quite slow and expensive in terms of energy consumption and pose a significant burden to resource and energy constrained WSNs. In the next Section 5.3.3, we propose a mechanism to mitigate such energy consumption by leveraging characteristics of EHWSNs.

### 5.3.3 PRE-COMPUTATION OF POLICIES

In energy harvesting enabled WSNs, available energy varies over time in a non monotonic yet partially predictable [4] fashion and there might even be situations in which we have an excess of energy available, which is wasted unless used in the short term. In fact, since the storage device has a finite size, some energy may be lost if the energy buffer is full while the node is harvesting energy. Figure 5.2 shows an example of such situation. As described in Section 5.4.2, we interfaced Telos B motes with photovoltaic cell, we deployed them indoors, and collected data about the energy that the nodes were able to harvest from artificial light, i.e., by ceiling and table lamps, and from solar light entering the room from the windows. Figure 5.2 shows the energy harvested during two different days with this setup and the energy surplus that occurred during this time frame. On the first day, due to low light energy coming from the windows and from artificial illumination, the node does not harvest enough energy to fully recharge its capacitor. The surplus energy is thus zero. During the second day, on the contrary, the node supercapacitor is recharged up to its maximum capacity at around 12:00 PM. After then, the energy harvested should be used immediately by the node or it is going to be wasted. Short after 7:30 PM, the harvesting power decreases and the supercapacitor starts discharging.

To avoid wasting energy, policies pre-computations are performed when there is an energy surplus, i.e., when the storage device is fully charged and the harvesting power is higher than the power consumption of the node. By exploiting such energy surplus, the number of CP-ABE operations that must be performed by the nodes when the harvested power is low can be minimized, thus allowing to save energy and to exploit recharge opportunities more effectively. The drawback of this approach, however, is the fact that pre-computed policies must be stored in the typically limited RAM memory of the nodes.

Table 5.1: Table of notation.

Symbol	Explanation
$S$	set of system states
$P_i$	set of policies associated to the state $S_i$
$R$	amount of cache memory available in each state
$l(p_i^k)$	size of the $k^{th}$ policy of the state $S_i$
$M$	Markov chain modeling system states and transitions probabilities
$T$	matrix of transition probabilities
$O_x$	set of policies stored in the cache
$S_{O_x}$	set of system states which are incomplete when using the set of stored policies $O_x$
$M_{O_x}$	absorbing Markov chain obtained from $M$ based on $O_x$
$T_{O_x}$	matrix of the transition probability of $M_{O_x}$
$AB_{O_x}$	characteristic vector of the absorbing states of $M_{O_x}$
$NH$	number of timeslots before the next harvesting event will occur
$Pr_{miss}(NH)$	probability that a cache miss will occur within the $N$ timeslots before the next harvesting event

### 5.3.4 CACHING STRATEGY

Since the memory available on a sensor node is clearly unable to store all the possible sets of access control policies, we propose in this section a caching strategy to pre-compute and store the set of policies that are the most likely to be useful at runtime. The system is characterized by a finite set of application states,  $S = \{S_1, \dots, S_{|S|}\}$ . To each state of the system,  $S_i$ , a set of policies,  $P_i = \{p_i^1, p_i^2, \dots, p_i^{n_i}\}$  is associated, which define the policies that the system needs in such state. A stored policies is a tuple of five elements:  $(SSK^{p_i^k}, C_0, C_{1,x}, C_{2,x}, C_{3,x})$ . We denote the size of each policy  $p_i^k \in P_i$  as  $l(p_i^k)$ .

When the system is in the state  $S_i$  and a given amount of excess harvested energy is available, such energy surplus is used to pre-compute and cache policies that may be useful to the system in the future. The number of policies that may be stored in the cache depends on the available cache size,  $R$ , and on the size of the pre-computed policies,  $l(p_i^k)$ . For simplicity, we assume that in each state  $S_i$  there is enough cache memory,  $R$ , to store all the policies needed in the current state<sup>3</sup>, i.e.,

$$R \geq \sum_{p_i^k \in P_i} l(p_i^k), \quad \forall S_i \in S.$$

However, in general the cache memory would not be large enough to store the full set of access control policies associated to all possible application states, thus leading to potential cache misses when the state of the system changes, i.e., when there is a transition from state  $S_i$  to state  $S_j$ .

In fact, a cache miss occurs if a policy  $p_j^k$  is not available in the cache when needed and must be computed on-the-fly. Computing a given policy has an energy cost that depends on its size (Table 5.2).

The goal of our optimization is to minimize the number of cache misses, by wisely selecting in each state the policies that should be pre-computed. Our strategy is based on the knowledge of the application dynamics, which can be obtained at design time. The optimization is performed by the sink and then disseminated to the nodes in the network. To reduce memory

<sup>3</sup>This is indeed the case in realistic scenarios given that only a few policies are expected per application state, each combining few different attributes.

and communication overhead, caching strategies are stored in a compressed form, by using a bitmap representation of the policies that should be precomputed in each application state. The caching strategy is updated by the sink and retransmitted to the node whenever a major change in either the application or in the energy source dynamics occurs.

We formalize this problem using a discrete-time Markov chain,  $M$ , with  $|S|$  states. The associated transition matrix is  $T$ . We recall that the set  $S$  models the application states, as defined during the design phase, while  $T$  indicates the probability  $t_{ij}$  to transit to a state  $S_j$ , given that the system is currently in the state  $S_i$ . To minimize the number of cache misses, we employ the following approach:

- We explore all the possible combinations of policies stored in the cache. Each of such combinations is a set  $O_x$ . We define a state  $S_i$  as *incomplete* if there is at least a policy,  $p_i^k$ , which is needed in state  $S_i$  but is not included in the set  $O_x$  of stored policies. Given the set of policies  $O_x$ , we define by  $S_{O_x} = \{S_i, \dots, S_j\}$  the set of incomplete states:

$$S_{O_x} = \{S_i \text{ s.t. } \exists p_i^k \in P_i \text{ and } p_i^k \notin O_x\}$$

- For each set of policies  $O_x$ , we define a new absorbing Markov chain,  $M_{O_x}$ , as the Markov chain obtained from  $M$  by setting to zero the output transition probability of each incomplete state, i.e., by making each incomplete state in  $S_{O_x}$  an absorbing state. We name the new transition probability matrix obtained in this way as  $T_{O_x}$ . The characteristic vector  $A_{O_x}$  is also defined. It associates a value equal to 1 to each absorbing state and a value of 0 to each non-absorbing state, i.e.,  $AB_{O_x}(i) = 1$  if  $S_i \in S_{O_x}$ ,  $AB_{O_x}(i) = 0$  otherwise.
- Time is discretized into timeslots of equal length. We denote with  $NH$  the number of timeslots before the next harvesting event will occur. We then compute the state probability as  $pr(NH) = T_{O_x}^{NH} \times [0, 0, \dots, 1, 0, 0, \dots]$ . The second factor in the matrix multiplication is a unitary vector of size  $S$  that indicates that the system starts in a given state  $S_k$ . The probability that a cache miss will occur within the  $NH$  timeslots before the next harvesting event can thus be computed as:

$$Pr_{miss}(NH) = pr(NH) \times AB_{O_x}$$

Such formalization allows to minimize the cache miss probability by selecting the best set  $O_x$  of policies that must be stored in the memory. If two or more sets of policies,  $O_1, O_2, \dots, O_k$ , have the same, minimum cache miss probability, we take into account the fact that, whenever a cache miss occurs, computing the missing policy has an energetic cost proportional to the size of the policy. Thus, in such case, we select the set  $O_i$  which minimizes both the cache miss probability and the energetic cost of computing the missing policies whenever a cache miss occurs.

It is worth noting that the number of possible Markov chains  $M_{O_x}$  is significantly smaller than the number of possible policies combinations, since different policies set may generate the same absorbing chain. For this reason, it is feasible to explore the possible combinations of policies stored in the cache and defining the associated chain. Additionally, some optimizations may be employed when computing each  $O_x$  sets. For instance, it is reasonable to consider only sets of policies that are maximal, i.e., such that no policy may be added to the set without exceeding the memory constraint  $R$ . Moreover, if the system starts in the state  $S_i$ , the  $O_x$  sets which do not contain all the policies in  $P_i$  (i.e., those needed in state  $S_i$ ) can be pruned from the exploration.



Table 5.2: Energy consumption for policy computation (mJ), for both Telos B and Mica2 platforms. The energy cost of an encryption operation depends on the number of attributes of the access policy and on the number of bytes sent to transmit the encrypted key.

Attributes	Policy Length [bytes]	Tx [bytes]	Scalar Multi.	Energy (Telos B)	Energy (Mica2)
2	242	$242 +  key $	7	80.7	451.6
3	349	$349 +  key $	10	115.3	645.1
$\vdots$	$\vdots$	$\vdots$	$\vdots$	$\vdots$	$\vdots$
10	1154	$1154 +  key $	31	357.6	1999.9
11	1277	$1277 +  key $	34	392.2	2193.4

## 5.4 PERFORMANCE EVALUATION

### 5.4.1 EXPERIMENTAL RESULTS: ENERGY COST OF CP-ABE ENCRYPTION

In our implementation, we have specifically focused on two families of nodes: the Telos B [23] and Mica2 [198] motes. Telos B features an 8MHz MSP430 micro-controller, a 16b RISC processor, 10 kB of RAM, 48 kB of program memory (ROM), 1024 kB of external flash, and the Chipcon CC2420 IEEE 802.15.4 compliant transceiver. The Mica2 motes are equipped with the 4MHz Atmel ATmega128L 8b micro-controller, 4 kB of RAM, 128 kB of ROM, 512 kB of external flash and the Chipcon CC1000 low-power wireless transceiver. We implemented a nesC library supporting CP-ABE in TinyOS 2.x for both Telos B and Mica2 motes. Our library is based on Relic<sup>4</sup>, an open source cryptographic meta-toolkit with emphasis on efficiency and flexibility. As recommended by NIST [199], we adopt a security level of 80-bit using a binary field  $\mathbb{F}_{2^{271}}$ . To encrypt data we use AES encryption, performed in hardware on the Telos B mote, which provides AES in Counter mode with CBC-MAC (CCM) within the CC2420 chip. Such combined mode supports integrity, authentication and confidentiality. For Mica2 motes, we use a software implementation of AES<sup>5</sup> in CBC mode.

Pairing and scalar multiplication are the most expensive operations among the ones performed, so we focus on them in our evaluation. We compute the overhead of CP-ABE as follows. While encrypting the data, one pairing operation is performed to calculate  $e(g, g)$ . For each attribute  $a$ , three scalar multiplications must be performed to compute  $C_{1,x}$ ,  $C_{2,x}$  and  $C_{3,x}$ . Since decryption operations are not performed by sensor nodes, but only by the final users who receive the encrypted data, we do not account for them in our evaluation. Finally, the communication overhead of transmitting an encrypted key is  $|SSK| + a^2 + \log|G_T| + a(\log|G_T| + 2\log|G|)$  bytes, where  $|SSK|$  is the size of the secret session key used to encrypt the data with a symmetric encryption algorithm. At most  $a^2$  bytes are needed for the matrix  $LS$ , and  $a(|G_T| + 2|G|) + |G_T|$  bytes to transfer  $C_0$ ,  $C_{1,x}$ ,  $C_{2,x}$  and  $C_{3,x}$ . Table 5.2 shows the energy cost of an encryption operation, depending on the number of attributes of the access policy and the amount of information to be sent to transmit the encrypted key, for both Telos B and Mica2 platforms. Performing one pairing operation and one scalar multiplication takes 1.29s and 1.73s for the Telos B mote and 1.9s and 2.24s for the Mica2 mote. Supposing an access policy is composed of 5 attributes, 16 scalar multiplication operations have to be performed. Assuming, for Telos B motes, an operating current of 1.8mA and an operating voltage of 3V, those operations cost 184.6mJ. Mica2 motes work with the same voltage, but their operating current is 8mA, so for the same operations the energy cost is 1032mJ. For a key size of 128 bit, the size of the information to be sent is  $569 + 16$  byte.

<sup>4</sup><http://code.google.com/p/relic-toolkit>

<sup>5</sup><http://byte-oriented-aes.googlecode.com>

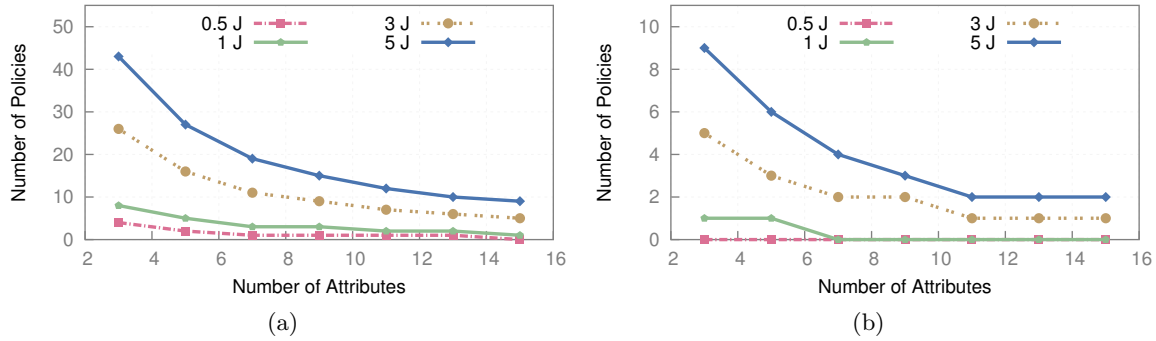


Figure 5.3: Number of policies which can be pre-computed per day, as a function of the number of attributes and the average energy surplus per day for (a) Telos B and (b) Mica2 motes.

Figure 5.3 shows the number of policies that can be pre-computed per day by using excess harvested energy, depending on their number of attributes and on the average energy surplus experienced per day, for both Telos B and Mica2 motes.

#### 5.4.2 ENERGY MODEL AND REAL-LIFE ENERGY HARVESTING TRACES

In our experiments, we consider a Telos B mote powered by a hybrid harvesting systems consisting of a photovoltaic (PV) cell, a supercapacitor and a non rechargeable battery, which provides a backup energy source. PV cells are common sources of energy harvesting and, being unobtrusive, have been considered before in wearable systems. For example, in [200] Leonov et al. demonstrated an electroencephalography system and an electrocardiography system in a shirt, powered by photovoltaic cells and a thermoelectric generator.

The supercapacitor we used for energy storage is a  $25F$  Panasonic Gold capacitor [180], which can nominally hold around  $90J$  of charge and has a round-trip (charging and discharging) efficiency of  $90+\%$  [174]. The leakage experienced by the supercapacitor is modeled as in [26], i.e., by using a piecewise linear approximation of the empirical leakage pattern experienced by the supercapacitor we have experimentally validated.

We focus on a remote vital signs monitoring scenario, in which the heart rate and the blood oxygenation level of a patient are monitored through a wearable pulse oximeter, such as [201]. Pulse and oxygenation values are measured at 60 second intervals and such measurements requires up to 8 seconds [202], thus leading to a duty cycle of  $\approx 13\%$ . Measured data are delivered immediately after reading and a low-power, state-of-the-art communication protocol, such as [203, 25], is used for data delivery. The rest of the time the MCU is in idle (sleep) mode, thus leading to an average power consumption of  $2.02$  mW. In such setting a node can run for almost three hours using only the energy stored in its supercapacitor (assuming it is full).

For our first set of experiments, a dataset of real-life indoor light traces has been used. The dataset was obtained through a testbed of ten Telos B motes equipped with a  $0.5W$  PV cell, deployed indoor for a week in the student office of the CS Department building of Sapienza University of Rome. Nodes were able to harvest energy from artificial light generated by ceiling and table lamps and from solar light entering the room from the windows. A dedicated TinyOS application was developed to periodically track the amount of energy harvested by the cell.

The second type of energy traces we used is a database of indoor radiant light measurements collected in several office buildings in New York City within the EnHANTs (Energy Harvesting

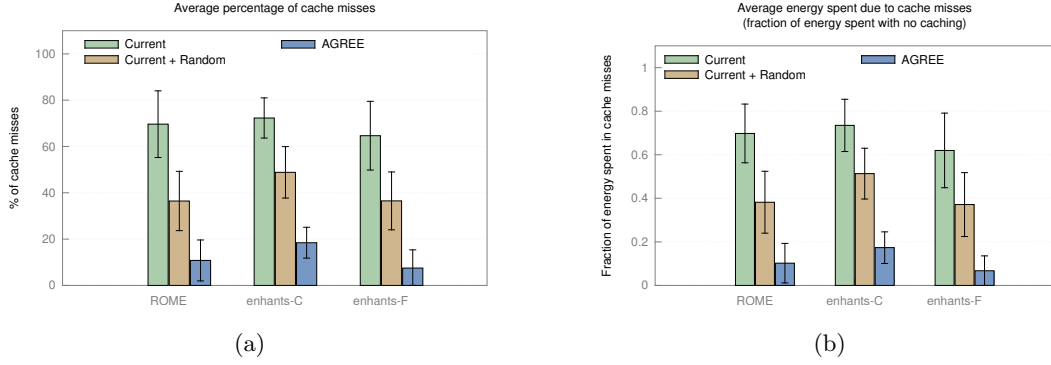


Figure 5.4: Performance of caching strategies *Current*, *Current + Random* and AGREE in term of (a) average percentage of cache misses and (b) average energy spent to compute policies on-the-fly due to cache misses, as a fraction of the energy spent when no caching is performed.

Active Networked Tags) project of Columbia University [204]. In particular, we used data from Setup C (departmental conference room) and Setup F (student office), obtaining from the radiant energy measurements the corresponding power harvestable by a photovoltaic cell of size of  $7 \times 5 \text{ cm}^2$  with efficiency of 15%.

### 5.4.3 AGREE SIMULATION RESULTS

In this section we describe the results of a simulation-based performance evaluation of AGREE, conducted by using a custom-built simulator developed in C and Python.

Our setup is as follows: We consider a system with a number of application states,  $|S|$ , ranging from 3 to 9. The transition probability between each couple of states, denoted by  $t_{ij}$ , is randomly generated as to represents different application scenarios. The corresponding Markov's chain  $M$  is defined based on the set of states  $S$  and the transition matrix  $T$ . To each state of the chain, a random number of policies (between 1 and 6) is associated. The size of such policies varies from 242 to 1277 bytes, depending on the number of their attributes (Table 5.2). In our experiments, we model a scenario where 7kB of the Telos B mote RAM are allocated to storing cache policies, while the rest of the memory is reserved for the application.

Results, displayed in Figure 5.5, show that AGREE is able to last for a long time, as it is able to operate mostly based on energy harvesting, resorting to battery energy only rarely.

To validate our proposed caching strategy, we compared three different versions of the protocol: AGREE, which is the complete solution described in Section 5.3.4, and *Current* and *Current + Random*, two variants of AGREE that do not leverage information about the harvesting process and the dynamics of the application.

Specifically, *Current* and *Current + Random* are defined as follows:

- *Current*: in each system state  $S_i$ , nodes pre-compute and cache only the policies  $P_i$  needed in the current state;
- *Current + Random*: in each system state  $S_i$ , nodes pre-compute and cache the policies  $P_i$  needed in the current state, plus as many other policies as possible, randomly chosen among those needed in neighbors states, until the RAM memory of the node is full.

To perform a comparative performance evaluation of the three approaches, we randomly

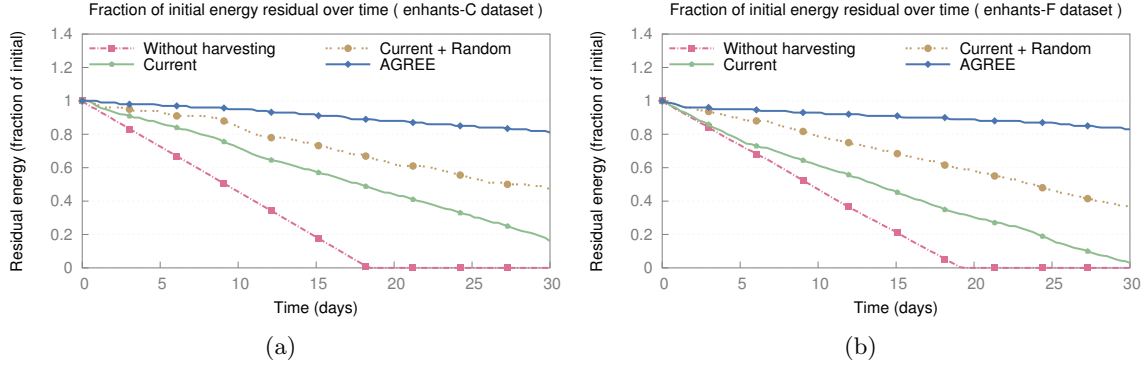


Figure 5.5: Fraction of initial energy residual over time for a system without energy capabilities and performing no caching and for caching strategies *Current*, *Current + Random* and AGREE computed over one month using: (a) enhants-C and (b) enhants-F indoor light traces datasets.

choose a state  $S_i$  as the initial state of the system and follow the evolution of the chain for a week.

We evaluate the performance of the different strategies with respect to the following metrics:

1. average percentage of cache misses (Figure 5.4(a));
2. energy spent by the nodes due to cache misses (Figure 5.4(b)).

Figure 5.4 shows the results of such performance evaluation for the three different light energy datasets we consider. Each data point is obtained by averaging the results over 10 runs. Both the average value and the standard deviation are reported. The fact that our approach is able to successfully pre-compute the most likely set of policies is confirmed by Fig. 5.4(a), which shows that AGREE leads to the smallest number of cache misses with respect to the other strategies. Specifically, the first comparison strategy, *Current*, obtains a number of cache misses that, depending on the considered energy harvesting dataset, is between 3.9 and 8.6 times higher than that of AGREE, while the strategy *Current + Random* obtains a number of cache misses that is between 2.6 and 4.8 times higher than that of AGREE.

Fig. 5.4(b) shows the total energy spent by nodes due to cache misses over a week of simulation, as a fraction of the total energy spent over the same time period when no caching is performed. Results in Fig. 5.4(b) confirm that taking into account the dynamics of both the harvesting source and the system works well, as the total energy spent by AGREE due to cache misses is, on average, approximately one seventh of the first comparison strategy, *Current*, and one fourth of *Current + Random*.

Figure 5.5 confirms that such energy saving has a significant impact on the overall lifetime of the system. To study the long-term behavior of our application, we used the same setup as before, but followed the evolution of the system for a longer period (a month instead of a week) using enhants-C and enhants-F indoor light traces datasets to simulate the harvesting process. Fig.5.5(a) and Fig.5.5(b) show the average residual energy over time, as a fraction of the initial battery energy of the nodes, for the caching strategies *Current*, *Current + Random* and AGREE, and for a system without energy capabilities and performing no caching at all.

The fraction of initial energy remaining over time is a significant metric because, although nodes may recharge through energy harvesting, a mote with no residual battery will suffer from fluctuations of the environmental source. In fact, energy stored in the supercapacitor

would allow the node to run in normal operation (i.e., monitoring data but not refreshing policies) for less than three hours. Such energy reservoir would not be enough to continue the data collection during a whole night, thus leading to periods of inactivity that significantly degrade the end user perceived performance.

The fact that AGREE allows to spend significant less battery energy with respect to other caching strategies is confirmed by Fig.5.5(a), showing simulation results for the enhants-C dataset. As can be seen from the figure, after one month of operation the average residual battery energy of nodes running AGREE is still 82% of their initial energy, while nodes running *Current* and *Current + Random* retain only 16% and 47% of their battery energy, respectively. Results are similar for the second harvesting dataset we considered, enhants-F: The average residual battery after one month is 85% of the initial energy when nodes run AGREE, while only 3% (37%) of the nodes initial energy is available when nodes run *Current* and *Current + Random*, respectively. Finally, for both datasets, a system without energy harvesting capabilities and performing no caching at all depletes its battery in less than 20 days.

## 5.5 CONCLUSIONS

In this chapter, we presented AGREE, a context-aware decentralized data access control for EHWSNs. Our scheme is based on CP-ABE, supports multi-authority and allows to dynamically change access policies based on context dependent user settings. AGREE is developed for WSN scenarios. We have proposed several optimizations for dealing with resource and energy constrained embedded systems. We have implemented the basic schema on Telos B and Mica2 nodes and experimentally evaluated our proposed solution. A simulation-based performance evaluation of AGREE confirmed that our caching mechanism is able to efficiently operate based on the excess harvested energy and that it significantly outperforms other caching strategies which do not leverage information about the harvesting process and the dynamics of the application. Our evaluation shown that, in spite of literature trends, complex cryptographic primitives are feasible in realistic EHWSNs scenarios.



## CONCLUDING REMARKS

---

Despite significant research efforts, energy continues to remain a severe bottleneck for applications in which battery-powered systems are expected to operate for long periods of time. For this reason, there is a growing interest in the design of harvesting systems that are able to draw energy from the environment, supplementing or even replacing batteries. The ultimate goal of these emerging energy harvesting technologies is to obtain self-powered devices that are suitable for long-term operations, being their theoretical lifetime only limited by the duration of the hardware components they are made of.

The design challenges posed both at the hardware and at the software levels by the development of this new class of energy-autonomous devices are many. One of the biggest difficulties is to effectively deal with the variable behavior of environmental sources, where the amount and the rate of the energy available vary over time. In addition, as the energy available is usually limited, is of paramount importance to minimize the power wasted across scavenging, conversion and storage circuits. At the software level, harvesting-aware algorithms and protocols are needed, which effectively exploit recharge opportunities by adapting the workload scheduling of the nodes to the source dynamics.

This PhD thesis has focused on some of the key challenges raised by these novel energy provisioning techniques, addressing critical points such as devising mechanisms for energy prediction and management, improving the efficiency of the energy scavenging process, developing protocols for harvesting-aware resource allocation, and providing solutions that enable robust and reliable security support.

In Chapter 2 we presented **Pro-Energy** [4], a novel energy prediction model that leverages past energy observations to provide accurate estimations of future energy availability in multi-source energy harvesting WSNs. To assess the performance of our proposed solution, we used real-life solar and wind traces that we collected by interfacing TelosB nodes with solar cells and wind micro-turbines, as well as publicly available traces of solar and wind obtained from weather monitoring stations in the US. A comparative performance evaluation between Pro-Energy and others energy predictors previously proposed in the literature, such as EWMA and WCMA, has shown that our solution significantly outperforms existing algorithms for both short and medium term prediction horizons, improving the energy prediction accuracy up to 60%.

A practical application of energy prediction techniques in a challenging scenario is discussed in Chapter 3. In such work, we presents a power management technique for improving the efficiency of harvesting energy from air-flows generated by trains passing in an underground tunnel. The key feature of the proposed solution is the adaptive AC-DC converter, a hybrid voltage rectifier that exploits both passive and active topologies combined with power prediction algorithms [6]. Such a combined approach significantly outperforms other rectification

topologies, resulting in an increase of efficiency between 10% and 30% with respect to the only-passive and the only-active rectifiers. To evaluate the effectiveness of the presented approach, a data collection campaign has been conducted in a tunnel of the new Underground *Metro B1* line in Rome. Six Telos B motes equipped with wind micro-turbines were used to instruments 220m of tunnel, collecting air-flow data for 33 days. We found that, by using the adaptive AC-DC converter, nodes deployed in the tunnel can harvest up to 22% more energy than that harvested by using the active-only or the passive-only topology. Moreover, we proposed a *smart* power-management strategy that exploits predictable energy harvesting patterns in the underground tunnel scenario to reduce the overhead of the system (in terms of average number of sampling performed per day by a node) of up to 93%.

By providing virtually unlimited energy to nodes, energy harvesting techniques change the way WSNs operate and disprove the general underlying assumption that the energy reservoir of the network is finite and monotonically decreasing over time. In Chapters 4 and 5 we investigated how this impacts on two important problems that had so far been addressed for traditional battery-powered WSNs only.

Chapter 4 is dedicated to the problem of sensor-mission assignment in energy harvesting wireless sensor networks. We addressed such a problem by providing both an analytical model and a distributed heuristic, called **EN-MASSE**, specifically tailored to energy harvesting WSNs [7, 5]. A comparative performance evaluation between our proposed scheme and other solutions previously proposed in the literature has shown that EN-MASSE significantly outperforms existing energy-harvesting-unaware assignment schemes. In addition, using our analytical model as a benchmark, we have also shown that the profit earned by our proposed scheme is close to the optimum. Finally, we have implemented EN-MASSE in TinyOS and experimentally validated its performance, showing the effectiveness of our proposed approach on a real hardware testbed of Telos B motes.

In Chapter 5 we have shown that smart caching and energy intake prediction can be combined to make computationally involved asymmetric cryptography schemes feasible in real wireless sensor networks with energy harvesting. More specifically, we focused on the support of extremely powerful, but complex, fine-grained data-centric access control mechanisms based on multi-authority Ciphertext Policy Attribute Based Encryption (CP-ABE). By integrating access control policies into the (encrypted) data, such mechanisms do not require any server-based access control infrastructure and are thus highly desirable in many wireless sensor network scenarios. However, as we have concretely shown by a proof-of-concept implementation carried out on TelosB and MicaZ motes, the computational complexity and the energy toll of state-of-the-art multi-authority CP-ABE schemes are still critical. To mitigate the relatively large energy consumption of the CP-ABE cryptographic operations, we proposed **AGREE** (Access control for GREEN wireless sensor networks), a framework which exploits energy harvesting opportunities to pre-compute and cache suitably chosen CP-ABE-encrypted keys, so as to minimize the need to perform CP-ABE encryptions when no energy from harvesting is available [1]. We assessed the performance of AGREE by means of simulation and actual implementation, and by validating its operation with real-world energy-harvesting traces collected indoor by Telos B motes equipped with photovoltaic cells, as well as publicly available traces of radiant light energy. Our results have shown that complex security mechanisms may become significantly less demanding when implemented so as to take advantage of energy harvesting opportunities.

To summarize, energy harvesting capabilities embedded in modern sensor nodes are deeply changing some of the key principles based on which wireless sensor networks are designed and operated. In this thesis we have addressed some of the most challenging problems of this emerging research area, providing insight into the design of harvesting-aware solutions.



## BIBLIOGRAPHY

---

- [1] G. Bianchi, A. T. Caposelle, C. Petrioli, and D. Spenza, “AGREE: exploiting energy harvesting to support data-centric access control in WSNs,” *Elsevier Ad Hoc Networks*, vol. 11, pp. 2625 – 2636, 2013.
- [2] S. Basagni, M. Y. Naderi, C. Petrioli, and D. Spenza, “Wireless sensor networks with energy harvesting,” in *Mobile Ad Hoc Networking: The Cutting Edge Directions*, ser. IEEE Series on Digital and Mobile Communication. Hoboken, NJ: John Wiley and Sons, Inc., 2013, ch. 20.
- [3] A. Cammarano, D. Spenza, and C. Petrioli, “Energy-harvesting WSNs for structural health monitoring of underground train tunnels,” in *The 32nd IEEE International Conference on Computer Communications, IEEE INFOCOM 2013, INFOCOM WKSHPs*, Torino, Italy, 14-19 April 2013, pp. 75–76, **Best Student Poster**.
- [4] A. Cammarano, C. Petrioli, and D. Spenza, “Pro-Energy: a novel energy prediction model for solar and wind energy harvesting WSNs,” in *Proceedings of the 9th IEEE International Conference on Mobile Ad hoc and Sensor Systems*, ser. IEEE MASS 2012, Las Vegas, Nevada, October 8-11 2012, pp. 75–83.
- [5] T. La Porta, C. Petrioli, and D. Spenza, “Sensor-mission assignment in wireless sensor networks with energy harvesting,” in *Proceedings of the 8th Annual IEEE Communications Society Conference on Sensor, Mesh and Ad Hoc Communications and Networks*, ser. IEEE SECON 2011, Salt Lake City, UT, June 27-30, 2011, pp. 413–421.
- [6] D. Porcarelli, D. Spenza, D. Brunelli, A. Cammarano, C. Petrioli, and L. Benini, “Adaptive rectifier driven by power intake predictors for energy harvesting sensor networks,” *IEEE Journal of Emerging and Selected Topics in Power Electronics*, 2014, To appear.
- [7] T. La Porta, C. Petrioli, C. Phillips, and D. Spenza, “Sensor-mission assignment in rechargeable wireless sensor networks,” *ACM Transactions on Sensor Networks*, 2014, To appear.
- [8] L. Atzori, A. Iera, and G. Morabito, “The internet of things: A survey,” *Comput. Netw.*, vol. 54, no. 15, pp. 2787–2805, Oct. 2010.
- [9] Ericsson Corporate Public and Media Relations, “CEO to shareholders: 50 billion connections 2020,” Press Release, April 13 2010, <http://www.ericsson.com/thecompany/press/releases/2010/04/1403231>.

- 
- [10] U.S. National Intelligence Council, “Disruptive Civil Technologies - six technologies with potential impacts on us interests out to 2025, Conference Report 2008-07,” [http://www.dni.gov/nic/NIC\\_home.html](http://www.dni.gov/nic/NIC_home.html), April 2008.
- [11] C. Alcaraz, P. Najera, J. Lopez, and R. Roman, “Wireless sensor networks and the internet of things: Do we need a complete integration?” in *1st International Workshop on the Security of the Internet of Things (SecIoT'10)*, Tokyo (Japan), December 2010.
- [12] D. Christin, A. Reinhardt, P. Mogre, and R. Steinmetz, “Wireless sensor networks and the internet of things: Selected challenges,” in *Proceedings of the 8th GI/ITG KuVS Fachgespräch Drahtlose Sensornetze; Hamburg, Germany*, T. U. H.-H. Institut für Telematik, Ed., August 2009, pp. 31–34.
- [13] Yvonne Klöpping, “Active Implantable Medical Devices: Winning the Power Struggle,” *European Medical Device Technology*, vol. 3, no. 2, March/April 2012.
- [14] G. Anastasi, M. Conti, M. Di Francesco, and A. Passarella, “Energy conservation in wireless sensor networks: A survey,” *Ad Hoc Netw.*, vol. 7, no. 3, pp. 537–568, May 2009.
- [15] I. Buchmann, *Batteries in a portable world: A handbook on rechargeable batteries for non-engineers*, 2nd ed. Cadex Electronics, Inc., May 2001.
- [16] T. B. Reddy and D. Linden, Eds., *Linden’s Handbook of Batteries*, 4th ed. New York, NY: McGraw Hill, October 2010.
- [17] S. Sudevalayam and P. Kulkarni, “Energy harvesting sensor nodes: survey and implications,” *IEEE Communications Surveys and Tutorials*, vol. 13, no. 3, pp. 443–461, Third quarter 2011.
- [18] H. Rowaihy, M. P. Johnson, D. Pizzocaro, A. Bar-Noy, L. M. Kaplan, T. F. L. Porta, and A. D. Preece, “Detection and localization sensor assignment with exact and fuzzy locations,” in *Proceedings of DCOSS 2009*, Marina del Rey, CA, 2009, pp. 28–43.
- [19] H. Rowaihy, M. P. Johnson, A. Bar-Noy, T. Brown, and T. F. L. Porta, “Assigning sensors to competing missions,” in *Proceedings of IEEE GLOBECOM 2008*, November 30–December 4 2008, pp. 1–6.
- [20] A. Bar-Noy, T. Brown, M. P. Johnson, T. F. L. Porta, O. Liu, and H. Rowaihy, “Assigning sensors to missions with demands,” in *Algorithmic Aspects of Wireless Sensor Networks*, ser. Lecture Notes in Computer Science, M. Kutylowski, J. Cichon, and P. Kubiak, Eds. Springer, June 2008, vol. 4837, pp. 114–125.
- [21] M. P. Johnson, H. Rowaihy, D. Pizzocaro, A. Bar-Noy, S. Chalmers, T. La Porta, and A. Preece, “Sensor-mission assignment in constrained environments,” *IEEE Transactions on Parallel and Distributed Systems*, vol. 21, no. 11, pp. 1692–1705, November 2010.
- [22] I. F. Akyildiz and M. C. Vuran, *Wireless Sensor Networks*, ser. Advanced Texts in Communications and Networking. Hoboken, NJ: John Wiley & Sons, August 2010.
- [23] Crossbow Technology, “TelosB mote platform datasheet,” 2004, document Part Number: 6020-0094-01 Rev B.
- [24] Crossbow Technology, Inc., “Datasheet MICAz,” 2004.

- [25] U. M. Colesanti, S. Santini, and A. Vitaletti, "DISSense: An Adaptive Ultralow-power Communication Protocol for Wireless Sensor Networks," in *Proceedings of IEEE DCOSS 2011*, Barcelona, Spain, June 27-29, 2011, pp. 1–10.
- [26] T. Zhu, Z. Zhong, Y. Gu, T. He, and Z.-L. Zhang, "Leakage-aware energy synchronization for wireless sensor networks," in *Proceedings of the 7th international conference on Mobile systems, applications, and services*, ser. MobiSys '09, New York, NY, USA, 2009, pp. 319–332.
- [27] D. Brunelli, "Miniaturized solar scavengers for ultra-low power wireless sensor nodes," in *Proceedings of WEWSN 2008*, Santorini Island, Greece, June 2008.
- [28] F. Simjee and P. H. Chou, "Everlast: Long-life, supercapacitor-operated wireless sensor node," in *Proceedings of ISLPED 2006*, Tagernsee, Germany, October 4–6 2006, pp. 197–202.
- [29] P. Dutta, J. Hui, J. Jeong, S. Kim, C. Sharp, J. Taneja, G. Tolle, K. Whitehouse, and D. Culler, "Trio: Enabling sustainable and scalable outdoor wireless sensor network deployments," in *Proceedings of ACM/IEEE IPSN 2006*, Nashville, TN, April 19–21 2006, pp. 407–415.
- [30] X. Jiang, J. Polastre, and D. Culler, "Perpetual environmentally powered sensor networks," *Proceedings of ACM/IEEE IPSN 2005*, pp. 463–468, April 25–27 2005.
- [31] C. Park and P. Chou, "Ambimax: Autonomous energy harvesting platform for multi-supply wireless sensor nodes," in *Proceedings of IEEE SECON 2006*, vol. 1, Reston, Virginia, USA, September 25-28, 2006, pp. 168–177.
- [32] P. Corke, P. Valencia, P. Sikka, T. Wark, and L. Overs, "Long-duration solar-powered wireless sensor networks," in *Proceedings of the 4th workshop on Embedded networked sensors*, ser. EmNets 2007, 2007, pp. 33–37.
- [33] C. Park and P. H. Chou, "Power utility maximization for multiple-supply systems by a load-matching switch," *Proceedings of ISLPED 2004*, pp. 168–173, August 9–11 2004.
- [34] V. Raghunathan, A. Kansal, J. Hsu, J. Friedman, and M. Srivastava, "Design considerations for solar energy harvesting wireless embedded systems," in *Proceedings of the 4th International Symposium on Information Processing in Sensor Networks (IPSN 2005)*, Apr 15 2005, pp. 457–462.
- [35] G. V. Merrett, A. S. Weddell, A. P. Lewis, N. R. Harris, B. M. Al-Hashimi, and N. M. White, "An empirical energy model for supercapacitor powered wireless sensor nodes," in *Proceedings of IEEE ICCCN 2008*, St. Thomas, US Virgin Islands, August 3–7 2008, pp. 1–6.
- [36] A. Kansal, J. Hsu, S. Zahedi, and M. B. Srivastava, "Power management in energy harvesting sensor networks," *ACM Transactions in Embedded Computing Systems*, vol. 6, no. 4, p. Article 32, September 2007.
- [37] C. Renner, J. Jessen, and V. Turau, "Lifetime prediction for supercapacitor-powered wireless sensor nodes," in *Proceedings of FGSN 2009*, Hamburg, Germany, August 13–14 2009, pp. 55–58.
- [38] C. F. Chiasserini and R. R. Rao, "Pulsed battery discharge in communication devices," in *Proceedings of ACM/IEEE MobiCom 1999*, Seattle, WA, August 15–20 1999, pp. 88–95.

- [39] R. Rao, S. Vrudhula, and D. N. Rakhmatov, "Battery modeling for energy aware system design," *Computer Magazine*, vol. 36, no. 12, pp. 77–87, December 2003.
- [40] M. Doyle, T. F. Fuller, and J. Newman, "Modeling of galvanostatic charge and discharge of the lithium/polymer/insertion cell," *Journal of the Electrochemical Society*, vol. 140, no. 6, pp. 1526–1533, 1993.
- [41] T. F. Fuller, M. Doyle, and J. Newman, "Simulation and optimization of the dual lithium ion insertion cell," *Journal of the Electrochemical Society*, vol. 141, no. 1, pp. 1–10, 1994.
- [42] M. Pedram, "Design considerations for battery-powered electronics," in *Proceedings of Design Automation Conference*, New Orleans, LA, June 21–25 1999, pp. 861–866.
- [43] K. C. Syracuse and W. D. K. Clark, "A statistical approach to domain performance modeling for oxyhalide primary lithium batteries," in *Proceedings of the 12th Annual Battery Conference on Applications and Advances*, Long Beach, CA, January 14–17 1997, pp. 163–170.
- [44] C. F. Chiasserini and R. R. Rao, "Energy efficient battery management," *IEEE Journal on Selected Areas in Communications*, vol. 19, no. 7, pp. 1235–1245, July 2001.
- [45] H. J. Bergveld, W. S. Kruijt, and P. H. L. Notten, "Electronic-network modeling of rechargeable NiCd cells and its application to the design of battery management systems," *Journal of Power Sources*, vol. 77, no. 2, pp. 143–158, March 1999.
- [46] S. Gold, "A PSPICE macromodel for lithium-ion batteries," in *Proceedings of the 12th Annual Battery Conference on Applications and Advances*, Long Beach, CA, USA, January 14–17 1997, pp. 215–222.
- [47] L. Benini, G. Castelli, A. Macii, E. Macii, M. Poncino, and R. Scarsi, "A discrete-time battery model for high-level power estimation," in *Proceedings of DATE 2000*, Paris, France, March 27–30 2000, pp. 35–41.
- [48] D. N. Rakhmatov and S. B. K. Vrudhula, "An analytical high-level battery model for use in energy management of portable electronic systems," in *Proceedings of IEEE/ACM ICCAD 2001*, San Jose, CA, November 4–8 2001, pp. 488–493.
- [49] P. D. Mitcheson, E. M. Yeatman, G. K. Rao, A. S. Holmes, and T. C. Green, "Energy harvesting from human and machine motion for wireless electronic devices," *Proceedings of the IEEE*, vol. 96, no. 9, pp. 1457–1486, September 2008.
- [50] E. O. Torres, "An electrostatic CMOS/BiCMOS li ion vibration-based harvester-charger IC," Ph.D. dissertation, Georgia Institute of Technology, May 2010.
- [51] E. O. Torres and G. A. Rincón-Mora, "Long-lasting, self-sustaining, and energy-harvesting system-in-package (SiP) wireless micro-sensor solution," in *Proceedings of INCEED 2005*, Charlotte, NC, July 24–30 2005.
- [52] F. Yildiz, "Potential ambient energy-harvesting sources and techniques," *The Journal of Technology Studies*, vol. 35, no. 1, pp. 40–48, 2009.
- [53] S. Roundy, P. K. Wright, and J. Rabaey, "A study of low level vibrations as a power source for wireless sensor nodes," *Computer Communications*, vol. 26, no. 11, pp. 1131–1144, July 2003.

- [54] V. R. Challa, M. G. Prasad, and F. T. Fisher, "Towards an autonomous self-tuning vibration energy harvesting device for wireless sensor network applications," *Journal of Smart Materials and Structures*, vol. 20, no. 2, pp. 1–11, February 2011.
- [55] Y. Chen, D. Vasic, F. Costa, W. Wu, and C. K. Lee, "Self-powered piezoelectric energy harvesting device using velocity control synchronized switching technique," in *Proceedings of IEEE IECON 2010*, Phoenix, AZ, November 7–10 2010, pp. 1785–1790.
- [56] J. G. Rocha, L. M. Goncalves, P. F. Rocha, M. P. Silva, and S. Lanceros-Mendez, "Energy harvesting from piezoelectric materials fully integrated in footwear," *IEEE Transactions on Industrial Electronics*, vol. 57, no. 3, pp. 813–819, March 2010.
- [57] Y. Suzuki and S. Kawasaki, "An autonomous wireless sensor powered by vibration-driven energy harvesting in a microwave wireless power transmission system," in *Proceedings of EUCAP 2011*, Roma, Italy, April 11–15 2011, pp. 3897–3900.
- [58] M. Zhu and E. Worthington, "Design and testing of piezoelectric energy harvesting devices for generation of higher electric power for wireless sensor networks," in *Proceedings of the IEEE Sensors*, Christchurch, New Zealand, October 25–28 2009, pp. 699–702.
- [59] R. Moghe, Y. Yang, F. Lambert, and D. Divan, "A scoping study of electric and magnetic field energy harvesting for wireless sensor networks in power system applications," in *Proceedings of IEEE ECCE 2009*, San Jose, CA, September 20–24 2009, pp. 3550–3557.
- [60] S. J. Roundy, "Energy scavenging for wireless sensor nodes with a focus on vibration to electricity conversion," Ph.D. dissertation, University of California at Berkeley, Berkeley, CA, May 2003.
- [61] M. K. Stojcev, M. R. Kosanovic, and L. R. Golubovic, "Power management and energy harvesting techniques for wireless sensor nodes," in *Proceedings of TELSIKS 2009*, Niš, Serbia, October 7–9 2009, pp. 65–72.
- [62] C. He, A. Arora, M. E. Kiziroglou, D. C. Yates, D. O'Hare, and E. M. Yeatman, "MEMS energy harvesting powered wireless biometric sensor," in *Proceedings of BSN 2009*, Berkeley, CA, June 3–5 2009, pp. 207–212.
- [63] M. E. Kiziroglou, C. He, and E. M. Yeatman, "Flexible substrate electrostatic energy harvester," *IEEE Electronics Letters*, vol. 46, no. 2, pp. 166–167, January 2010.
- [64] S. Chalasani and J. Conrad, "A survey of energy harvesting sources for embedded systems," in *Proceedings of IEEE Southeastcon*, april 2008, pp. 442–447.
- [65] J. C. Park, D. H. Bang, and J. Y. Park, "Micro-fabricated electromagnetic power generator to scavenge low ambient vibration," *IEEE Transactions on Magnetics*, vol. 46, no. 6, pp. 1937–1942, June 2010.
- [66] O. Zorlu, E. T. Topal, and H. Küandlah, "A vibration-based electromagnetic energy harvester using mechanical frequency up-conversion method," *IEEE Sensors Journal*, vol. 11, no. 2, pp. 481–488, February 2011.
- [67] S. Ayazian, E. Soenen, and A. Hassibi, "A photovoltaic-driven and energy-autonomous CMOS implantable sensor," in *Proceedings of IEEE VLSIC 2011*, June 2011, pp. 148–149.

- [68] M. Barnes, C. Conway, J. Mathews, and D. K. Arvind, "ENS: An energy harvesting wireless sensor network platform," in *Proceedings of ICSNC 2010*, August 2010, pp. 83–87.
- [69] C. Chen and P. H. Chou, "DuraCap: A supercapacitor-based, power-bootstrapping, maximum power point tracking energy-harvesting system," in *Proceedings of ISLPED 2010*, August 2010, pp. 313–318.
- [70] P. Sitka, P. Corke, L. Overs, P. Valencia, and T. Wark, "Fleck - A platform for real-world outdoor sensor networks," in *Proceedings of ISSNIP 2007*, December 2007, pp. 709–714.
- [71] V. Kyriatzis, N. S. Samaras, P. Stavroulakis, H. Takruri-Rizk, and S. Tzortzios, "Enviromote: A new solar-harvesting platform prototype for wireless sensor networks," in *Proceedings of IEEE PIMRC 2007*, September 2007, pp. 1–5.
- [72] M. Minami, T. Morito, H. Morikawa, and T. Aoyama, "Solar biscuit: A battery-less wireless sensor network system for environmental monitoring applications," in *The 2nd International Workshop on Networked Sensing Systems*, 2005.
- [73] L. Selavo, A. Wood, Q. Cao, T. Sookoor, H. Liu, A. Srinivasan, Y. Wu, W. Kang, J. Stankovic, D. Young, and J. Porter, "Luster: wireless sensor network for environmental research," in *Proceedings of the 5th international conference on Embedded networked sensor systems*, ser. SenSys '07. New York, NY, USA: ACM, 2007, pp. 103–116.
- [74] N. S. Hudak and G. G. Amatucci, "Small-scale energy harvesting through thermoelectric, vibration, and radio frequency power conversion," *Journal of Applied Physics*, vol. 103, no. 10, pp. 1–24, May 2008.
- [75] J. G. Webster, *The measurement, instrumentation, and sensors handbook*, ser. The electrical engineering handbook series. CRC Press, December 1998.
- [76] R. Abbaspour, "A practical approach to powering wireless sensor nodes by harvesting energy from heat flow in room temperature," in *Proceedings of IEEE ICUMT 2010*, October 2010, pp. 178–181.
- [77] X. Lu and S. H. Yang, "Thermal energy harvesting for WSNs," in *Proceedings of IEEE SMC 2010*, October 2010, pp. 3045–3052.
- [78] L. Gu and J. Stankovic, "Radio-triggered wake-up capability for sensor networks," *Real-Time Systems Journal, special issue of best papers from RTAS*, vol. 29, no. 2-3, pp. 157–182, March 2005.
- [79] L. Chen, S. Cool, H. Ba, W. Heinzelman, I. Demirkol, U. Muncuk, K. Chowdhury, and S. Basagni, "Range extension of passive wake-up radio systems through energy harvesting," in *Proceedings of ICC 2013*, Budapest, Hungary, June 2013.
- [80] R. Heer, J. Wissenwasser, M. Milnera, L. Farmer, C. Höpfner, and M. Vellekoop, "Wireless powered electronic sensors for biological applications," in *Proceedings of IEEE EMBC 2010*, September 4 2010, pp. 700–703.
- [81] S. Mandal, L. Turicchia, and R. Sarpeshkar, "A low-power, battery-free tag for body sensor networks," *IEEE Pervasive Computing*, vol. 9, no. 1, pp. 71–77, March 2010.

- [82] H. Reinisch, S. Gruber, H. Unterassinger, M. Wiessflecker, G. Hofer, W. Pribyl, and G. Holweg, "An electro-magnetic energy harvesting system with 190 nW idle mode power consumption for a BAW based wireless sensor node," *IEEE Journal of Solid-State Circuits*, vol. 46, no. 7, pp. 1728–1741, July 2011.
- [83] S. P. Matova, R. Elfrink, R. J. M. Vullers, and R. van Schaijk, "Harvesting energy from airflow with a micromachined piezoelectric harvester inside a Helmholtz resonator," *Journal of Micromechanics and Microengineering*, vol. 21, no. 10, pp. 1–6, 2011.
- [84] F. Fei, J. D. Mai, and W. J. Li, "A wind-flutter energy converter for powering wireless sensors," *Sensors and Actuators A: Physical*, vol. 173, no. 1, pp. 163–171, January 2012.
- [85] E. Sardini and M. Serpelloni, "Self-powered wireless sensor for air temperature and velocity measurements with energy harvesting capability," *IEEE Transactions on Instrumentation and Measurement*, vol. 60, no. 5, pp. 1838–1844, May 2011.
- [86] Y. K. Tan and S. K. Panda, "Energy harvesting from hybrid indoor ambient light and thermal energy sources for enhanced performance of wireless sensor nodes," *IEEE Transactions on Industrial Electronics*, vol. 58, no. 9, pp. 4424–4435, September 2011.
- [87] C. Y. Sue and N. C. Tsai, "Human powered MEMS-based energy harvest devices," *Applied Energy*, vol. 93, pp. 390–403, 2012.
- [88] C. Xu, C. Pan, Y. Liu, and Z. L. Wang, "Hybrid cells for simultaneously harvesting multi-type energies for self-powered micro/nanosystems," *Nano Energy*, vol. 1, no. 2, pp. 259–272, 2012.
- [89] F. Davis and S. P. J. Higson, "Biofuel cells-recent advances and applications," *Biosensors and Bioelectronics*, vol. 22, no. 7, pp. 1224–1235, 2007.
- [90] C. B. Williams, C. Shearwood, M. A. Harradine, P. H. Mellor, T. S. Birch, and R. B. Yates, "Development of an electromagnetic micro-generator," *Proceedings of the IEEE Circuits, Devices and Systems*, vol. 148, no. 6, pp. 337–342, December 2001.
- [91] B. J. Hansen, Y. Liu, R. Yang, and Z. L. Wang, "Hybrid nanogenerator for concurrently harvesting biomechanical and biochemical energy," *ACS Nano*, vol. 4, no. 7, pp. 3647–3652, 2010.
- [92] S. Sherrit, "The physical acoustics of energy harvesting," in *Proceedings of IEEE IUS 2008*, November 2008, pp. 1046–1055.
- [93] F. Liu, A. Phipps, S. Horowitz, K. Ngo, L. Cattafesta, T. Nishida, and M. Sheplak, "Acoustic energy harvesting using an electromechanical Helmholtz resonator," *Journal of the Acoustical Society of America*, vol. 123, no. 4, pp. 1983–1990, 2008.
- [94] T. T. Le, "Efficient power conversion interface circuits for energy harvesting applications," Ph.D. dissertation, Oregon State University, April 2008.
- [95] A. Denisov and E. Yeatman, "Stepwise microactuators powered by ultrasonic transfer," in *Proceedings of the Eurosensors XXV*, Athens, Greece, September 2011.
- [96] Y. Zhu, S. O. R. Moheimani, and M. R. Yuce, "A 2-DOF MEMS ultrasonic energy harvester," *IEEE Sensors Journal*, vol. 11, no. 1, pp. 155–161, January 2011.

- [97] M. A. Green, K. Emery, Y. Hishikawa, and W. Warta, "Solar cell efficiency tables (version 37)," *Progress in Photovoltaics: Research and Applications*, vol. 19, no. 1, pp. 84–92, 2011.
- [98] M. Belleville, H. Fanet, P. Fiorini, P. Nicole, M. J. M. Pelgrom, C. Piguet, R. Hahn, C. V. Hoof, R. Vullers, M. Tartagni, and E. Cantatore, "Energy autonomous sensor systems: Towards a ubiquitous sensor technology," *Microelectronics Journal*, vol. 41, no. 11, pp. 740–745, 2010.
- [99] R. J. M. Vullers, R. van Schaijk, I. Doms, C. V. Hoof, and R. Mertens, "Micropower energy harvesting," *Solid-State Electronics*, vol. 53, no. 7, pp. 684–693, April 2009.
- [100] L. Huang, V. Pop, R. de Francisco, R. Vullers, G. Dolmans, H. de Groot, and K. Imaura, "Ultra low power wireless and energy harvesting technologies - an ideal combination," in *Proceedings of IEEE ICCS 2010*, November 17–19 2010, pp. 295–300.
- [101] P. Mane, J. Xie, K. K. Leang, and K. Mossi, "Cyclic energy harvesting from pyroelectric materials," *IEEE Transactions on Ultrasonics, Ferroelectrics and Frequency Control*, vol. 58, no. 1, pp. 10–17, January 2011.
- [102] D. Vanderpool, J. H. Yoon, and L. Pilon, "Simulations of a prototypical device using pyroelectric materials for harvesting waste heat," *International Journal of Heat and Mass Transfer*, vol. 51, no. 21, pp. 5052–5062, 2008.
- [103] J. A. Paradiso and T. Starner, "Energy scavenging for mobile and wireless electronics," *IEEE Pervasive Computing*, vol. 4, no. 1, pp. 18–27, January-March 2005.
- [104] S. P. Beeby, R. N. Torah, M. J. Tudor, P. Glynn-Jones, T. O'Donnell, C. R. Saha, and S. Roy, "A micro electromagnetic generator for vibration energy harvesting," *Journal of Micromechanics and Microengineering*, vol. 17, no. 7, pp. 1257–1265, 2007.
- [105] Powercast, <http://www.powercast.com.>, 2011.
- [106] S. Roundy, E. S. Leland, J. Baker, E. Carleton, E. Reilly, E. Lai, B. Otis, J. M. Rabaey, P. K. Wright, and V. Sundararajan, "Improving power output for vibration-based energy scavengers," *IEEE Pervasive Computing*, vol. 4, no. 1, pp. 28–36, January–March 2005.
- [107] M. Bolić, D. Simplot-Ryl, and I. Stojmenović, *Rfid Systems: Research Trends and Challenges*. John Wiley & Sons, 2010.
- [108] D. R. Cox, "Prediction by exponentially weighted moving averages and related methods," *Journal of the Royal Statistical Society. Series B (Methodological)*, vol. 23, no. 2, pp. 414–422, 1961.
- [109] J. R. Piorno, C. Bergonzini, D. Atienza, and T. S. Rosing, "Prediction and management in energy harvested wireless sensor nodes," in *Proceedings of Wireless VITAE 2009*, May 17–20 2009, pp. 6–10.
- [110] C. Moser, L. Thiele, D. Brunelli, and L. Benini, "Adaptive power management in energy harvesting systems," in *Proceedings of IEEE DATE 2007*, Nice, France, April 16–20, 2007, pp. 773–778.
- [111] C. Bergonzini, D. Brunelli, and L. Benini, "Algorithms for harvested energy prediction in batteryless wireless sensor networks," in *Proceedings of IWASI 2009*, June 25–26 2009, pp. 144–149.



- [112] D. K. Noh and K. Kang, "Balanced energy allocation scheme for a solar-powered sensor system and its effects on network-wide performance," *Journal of Computer and System Sciences*, vol. 77, no. 5, pp. 917–932, September 2011.
- [113] J. Lu, S. Liu, Q. Wu, and Q. Qiu, "Accurate modeling and prediction of energy availability in energy harvesting real-time embedded systems," in *Proceedings on the 1st Green Computing Conference*, ser. IEEE IGCC 2010, Chicago, IL, USA, August 15–18, 2010, pp. 469–476.
- [114] N. Sharma, J. Gummesson, D. Irwin, and P. Shenoy, "Cloudy computing: Leveraging weather forecasts in energy harvesting sensor systems," in *Proceedings of SECON 2010*, Boston, MA, June 21–25 2010, pp. 1–9.
- [115] A. Kansal, D. Potter, and M. B. Srivastava, "Performance aware tasking for environmentally powered sensor networks," *SIGMETRICS Perform. Eval. Rev.*, vol. 32, pp. 223–234, June 2004.
- [116] C. M. Vigorito, D. Ganesan, and A. G. Barto, "Adaptive control of duty cycling in energy-harvesting wireless sensor networks," in *Proceedings of IEEE SECON 2007*, June 2007, pp. 21–30.
- [117] C. Moser, J. J. Chen, and L. Thiele, "Dynamic power management in environmentally powered systems," in *Proceedings of ASP-DAC 2010*, January 2010, pp. 81–88.
- [118] D. Audet, L. C. De Oliveira, N. MacMillan, D. Marinakis, and K. Wu, "Scheduling recurring tasks in energy harvesting sensors," in *Proceedings of IEEE INFOCOM 2011 Workshop on Green Communication and Networking*, April 2011, pp. 277–282.
- [119] C. Rusu, R. Melhem, and D. Mossé, "Multi-version scheduling in rechargeable energy-aware real-time systems," *Journal of Embedded Computing*, vol. 1, no. 2, pp. 271–283, April 2005.
- [120] H. EL Ghor, M. Chetto, and R. H. Chehade, "A real-time scheduling framework for embedded systems with environmental energy harvesting," *Computers and Electrical Engineering Journal*, vol. 37, no. 4, pp. 498–510, July 2011.
- [121] J. B. Steck and T. S. Rosing, "Adapting task utility in externally triggered energy harvesting wireless sensing systems," in *Proceedings of INSS 2009*, June 2009, pp. 1–8.
- [122] S. Liu, Q. Qiu, and Q. Wu, "Energy aware dynamic voltage and frequency selection for real-time systems with energy harvesting," in *Proceedings of DATE 2008*, March 2008, pp. 236–241.
- [123] S. Liu, Q. Wu, and Q. Qiu, "An adaptive scheduling and voltage/frequency selection algorithm for real-time energy harvesting systems," in *Proceedings of ACM/IEEE DAC 2009*, July 2009, pp. 782–787.
- [124] S. Liu, J. Lu, Q. Wu, and Q. Qiu, "Harvesting-aware power management for real-time systems with renewable energy," *IEEE Transactions on Very Large Scale Integration (VLSI) Systems*, 2012, to appear.
- [125] A. Ravinagarajan, D. Dondi, and T. S. Rosing, "DVFS based task scheduling in a harvesting WSN for structural health monitoring," in *Proceedings of DATE 2010*, Leuven, Belgium, March 8–12 2010, pp. 1518–1523.

- [126] Z. A. Eu, H. P. Tan, and W. K. G. Seah, "Opportunistic routing in wireless sensor networks powered by ambient energy harvesting," *Computer Networks*, vol. 54, no. 17, pp. 2943–2966, December 2010.
- [127] C. Moser, D. Brunelli, L. Thiele, and L. Benini, *Lazy Scheduling for Energy Harvesting Sensor Nodes*, ser. IFIP International Federation for Information Processing. Springer, October 2006, vol. 225, pp. 125–134.
- [128] C. Moser, J. J. Chen, and L. Thiele, "Power management in energy harvesting embedded systems with discrete service levels," in *Proceedings of ACM/IEEE ISLPED 2009*, 2009, pp. 413–418.
- [129] C. Moser, D. Brunelli, L. Thiele, and L. Benini, "Real-time scheduling for energy harvesting sensor nodes," *Real-Time Syst.*, vol. 37, no. 3, pp. 233–260, Dec. 2007.
- [130] M. Magno, S. Marinkovic, D. Brunelli, E. Popovici, B. O'Flynn, and L. Benini, "Smart power unit with ultra low power radio trigger capabilities for wireless sensor networks," in *Proceedings of IEEE DATE 2012*, Dresden, Germany, March 12-16, 2012, pp. 75–80.
- [131] "NREL: Measurement and Instrumentation Data Center," 2011, <http://www.nrel.gov/midc/>.
- [132] M. Ali, B. Al-Hashimi, J. Recas, and D. Atienza, "Evaluation and design exploration of solar harvested-energy prediction algorithm," in *Proceedings of IEEE DATE 2010*, Dresden, Germany, March 8-12, 2010, pp. 142–147.
- [133] G.K. Ottman, H.F. Hofmann, A.C. Bhatt, and G.A. Lesieutre, "Adaptive piezoelectric energy harvesting circuit for wireless remote power supply," *IEEE Transactions on Power Electronics*, vol. 17, no. 5, pp. 669 – 676, Sep 2002.
- [134] H. Lhermet, C. Condemine, M. Plissonnier, R. Salot, P. Audebert, and M. Rosset, "Efficient power management circuit: from thermal energy harvesting to above-ic microbattery energy storage," *IEEE Journal of Solid-State Circuits*, vol. 43, no. 1, pp. 246–255, Jan 2008.
- [135] F.I. Simjee and P.H. Chou, "Efficient charging of supercapacitors for extended lifetime of wireless sensor nodes," *IEEE Transactions on Power Electronics*, vol. 23, no. 3, pp. 1526 –1536, May 2008.
- [136] D. Dondi, A. Bertacchini, D. Brunelli, L. Larcher and L. Benini, "Modeling and optimization of a solar energy harvester system for self-powered wireless sensor networks," *IEEE Transactions on Industrial Electronics*, vol. 55, no. 7, pp. 2759 –2766, Jul 2008.
- [137] J.W. Kimball, B.T. Kuhn and R.S. Balog, "A system design approach for unattended solar energy harvesting supply," *IEEE Transactions on Power Electronics*, vol. 24, no. 4, pp. 952 –962, Apr 2009.
- [138] D. Carli, D. Brunelli, D. Bertozzi and L. Benini, "A high-efficiency wind-flow energy harvester using micro turbine," in *Power Electronics Electrical Drives Automation and Motion (SPEEDAM), 2010 International Symposium*, Jun 14-16 2010, pp. 778–783.
- [139] Y. K. Tan and S. Panda, "Optimized wind energy harvesting system using resistance emulator and active rectifier for wireless sensor node," *IEEE Transactions on Power Electronics*, vol. 26, no. 1, pp. 38–50, Jan 2011.

- [140] M. A. Weimer, T. S. Paing, and R. A. Zane, "Remote area wind energy harvesting for low-power autonomous sensors," in *Proceedings 37th IEEE Power Electronics*, Jun 18-22 2006, pp. 1–5.
- [141] T. S. Paing, and R. A. Zane, "Resistor emulation approach to low-power energy harvesting," in *Proceedings 37th IEEE Power Electronics Specialists Conference (PESC 2006)*, Jun 18-22 2006, pp. 1–7.
- [142] L. Karthikeyan, B. Amrutur, "Signal-powered low-drop-diode equivalent circuit for full-wave bridge rectifier," *IEEE Transactions on Power Electronics*, vol. 27, no. 10, pp. 4192 – 4201, Oct 2012.
- [143] Y. H. Lam, W. H. Ki, C. Y. Tsui, "Integrated low-loss cmos active rectifier for wirelessly powered devices," *IEEE Transactions on Circuits and Systems II: Express Briefs*, vol. 53, no. 12, pp. 1378 –1382, Dec 2006.
- [144] E. Dallago, D. Miatton, G. Venchi, V. Bottarel, G. Frattini, G. Ricotti, M. Schipani, "Active autonomous ac-dc converter for piezoelectric energy scavenging systems," in *IEEE Custom Integrated Circuits Conference, 2008 (CICC 2008)*, Sept 2008, pp. 555 – 558.
- [145] S. Cheng, Y. Jin, Y. Rao, D.P. Arnold, "An active voltage doubling AC/DC converter for low-voltage energy harvesting applications," *IEEE Transactions on Power Electronics*, vol. 26, no. 8, pp. 2258 –2265, Aug 2011.
- [146] S. Cheng, R. Sathe, R.D. Natarajan, D.P. Arnold, "A voltage-multiplying self-powered AC/DC converter with 0.35-V minimum input voltage for energy harvesting applications," *IEEE Transactions on Power Electronics*, vol. 26, no. 9, pp. 2542 –2549, Sept 2011.
- [147] M. Ceriotti, M. Corra, L. D’Orazio, R. Doriguzzi, D. Facchin, S. Guna, G. Jesi, R. Cigno, L. Mottola, A. Murphy, M. Pescalli, G. Picco, D. Pregolato, and C. Torghele, "Is there light at the ends of the tunnel? wireless sensor networks for adaptive lighting in road tunnels," in *Proceedings of the 10th International Conference on Information Processing in Sensor Networks*, ser. IPSN 2011, april 2011, pp. 187 –198.
- [148] F. Stajano, N. Hoult, I. Wassell, P. Bennett, C. Middleton, and K. Soga, "Smart bridges, smart tunnels: Transforming wireless sensor networks from research prototypes into robust engineering infrastructure," *Ad Hoc Networks*, vol. 8, no. 8, pp. 872 – 888, 2010.
- [149] L. Mottola, G. P. Picco, M. Ceriotti, c. Gunã, and A. L. Murphy, "Not all wireless sensor networks are created equal: A comparative study on tunnels," *ACM Trans. Sen. Netw.*, vol. 7, no. 2, pp. 15:1–15:33, Sep. 2010.
- [150] S. Cheekiralla, "Wireless sensor network-based tunnel monitoring," Stockholm, Sweden, June 20-21 2005, poster presentation.
- [151] R. Liu, I. Wassell, and K. Soga, "Relay node placement for wireless sensor networks deployed in tunnels," in *Proceedings of IEEE 6th International Conference on Wireless and Mobile Computing, Networking and Communications (WiMob)*, oct. 2010, pp. 144 –150.
- [152] D. Wu, L. Bao, and R. Li, "A holistic approach to wireless sensor network routing in underground tunnel environments," *Comput. Commun.*, vol. 33, no. 13, pp. 1566–1573, Aug. 2010.

- [153] D.Porcarelli, D.Brunelli, M.Magno, L.Benini, “A multi-harvester architecture with hybrid storage devices and smart capabilities for low power systems,” in *International Symposium on Power Electronics, Electrical Drives, Automation and Motion (SPEEDAM) 2012*, Jun 20-22 2012, pp. 946–951.
- [154] TinyOS, “The TinyOS operating system for embedded wireless devices,” <http://www.tinyos.net/>.
- [155] N. Ye, *The handbook of data mining*. Lawrence Erlbaum, 2003.
- [156] N. Bartolini, T. Calamoneri, T. F. L. Porta, C. Petrioli, and S. Silvestri, “Sensor activation and radius adaptation (SARA) in heterogeneous sensor networks,” *ACM Transactions on Sensor Networks*, vol. 8, 2012.
- [157] H. Rowaihy, S. Eswaran, M. Johnson, D. Verma, A. Bar-noy, and T. Brown, “A survey of sensor selection schemes in wireless sensor networks,” in *Defense and Security Symposium on Unattended Ground, Sea, and Air Sensor Technologies and Applications*, ser. DSS 2007, Orlando, FL, USA, 2007.
- [158] S. K. P., Y. D. Chen, C. Chiang, and B. J. Liu, “A distributed active sensor selection scheme for wireless sensor networks,” in *Proceedings of ISCC 2006*, June 26–29 2006, pp. 923–928.
- [159] M. Gomez, A. Preece, M. P. Johnson, G. Mel, W. Vasconcelos, C. Gibson, A. Bar-Noy, K. Borowiecki, T. Porta, D. Pizzocaro, H. Rowaihy, G. Pearson, and T. Pham, “An ontology-centric approach to sensor-mission assignment,” in *Proceedings of the 16th international conference on Knowledge Engineering: Practice and Patterns*, ser. EKAW 2008. Berlin, Heidelberg: Springer-Verlag, 2008, pp. 347–363.
- [160] A. Preece, D. Pizzocaro, K. Borowiecki, G. de Mel, M. Gomez, W. Vasconcelos, A. Bar-Noy, M. Johnson, T. La Porta, H. Rowaihy, G. Pearson, and T. Pham, “Reasoning and resource allocation for sensor-mission assignment in a coalition context,” in *Military Communications Conference*, ser. IEEE MILCOM 2008, nov. 2008, pp. 1–7.
- [161] T. Le, T. J. Norman, and W. W. Vasconcelos, “Agent-based sensor-mission assignment for tasks sharing assets,” in *Proceedings of ATSN 2009*, May 2009, pp. 33–40.
- [162] H. Rowaihy, M. P. Johnson, O. Liu, A. Bar-Noy, T. Brown, and T. La Porta, “Sensor-mission assignment in wireless sensor networks,” *ACM Transactions on Sensor Networks*, vol. 6, pp. 36:1–36:33, July 2010.
- [163] D. Pizzocaro, M. P. Johnson, H. Rowaihy, S. Chalmers, A. Preece, A. Bar-Noy, and T. La Porta, “A knapsack approach to sensor-mission assignment with uncertain demands,” in *Proceedings of SPIE 2008*, vol. 7112, October 2008, pp. 711 205(1–12).
- [164] T. P. Le, T. J. Norman, and W. Vasconcelos, “Adaptive negotiation in managing wireless sensor networks,” in *Proceedings of the 13th international conference on Principles and Practice of Multi-Agent Systems*, ser. PRIMA 2010. Berlin, Heidelberg: Springer-Verlag, 2010, pp. 121–136.
- [165] H. Rowaihy, “Location privacy and energy preservation in sensor allocation systems,” *International Journal of Distributed Sensor Networks*, vol. 2012, p. 10, 2012, article ID 197592.

- [166] M. Erol-Kantarci and H. Mouftah, "Mission-aware placement of rf-based power transmitters in wireless sensor networks," in *IEEE Symposium on Computers and Communications*, ser. ISCC 2012, Cappadocia, Turkey, July 2012, pp. 12–17.
- [167] F. Bian, D. Kempe, and R. Govindan, "Utility based sensor selection," in *Proceedings of ACM/IEEE IPSN 2006*, 2006, pp. 11–18.
- [168] Z. Chen, G. Barrenetxea, and M. Vetterli, "Share Risk and Energy: Sampling and Communication Strategies for Multi-Camera Wireless Monitoring Networks," in *Proceedings of IEEE INFOCOM 2012*, Orlando, Florida, USA, March 25–30 2012.
- [169] IXYS Corporation, "XOB17 IXOLAR High Efficiency Solar Bits technical information," June 2009.
- [170] "U.S. Climate Reference Network (USCRN)," 2011, <http://www.ncdc.noaa.gov/crn/>.
- [171] C. Park, J. Liu, and P. H. Chou, "Eco: An ultra-compact low-power wireless sensor node for real-time motion monitoring," in *Proceedings of ACM/IEEE IPSN 2005*, Los Angeles, CA, 2005, pp. April 25–27.
- [172] C. Park and P. H. Chou, "A wearable wireless sensor platform for interactive art performance," in *Proceedings of PERCOM 2006*, March 2006, pp. 52–59.
- [173] M. Technologies, "Datasheet HC power series ultracapacitors," August 2009. [Online]. Available: [http://www.maxwell.com/products/ultracapacitors/docs/datasheet\\_hc\\_series\\_1013793.pdf](http://www.maxwell.com/products/ultracapacitors/docs/datasheet_hc_series_1013793.pdf)
- [174] P. P. Barker, "Ultracapacitors for use in power quality and distributed resource applications," in *Proceedings of IEEE Power Engineering Society Summer Meeting*, July 2002, pp. 316–320.
- [175] Maxwell Technologies, "Design considerations for ultracapacitors," April 2009. [Online]. Available: [http://www.maxwell.com/products/ultracapacitors/docs/200904\\_whitepaper\\_designinguide.pdf](http://www.maxwell.com/products/ultracapacitors/docs/200904_whitepaper_designinguide.pdf)
- [176] L. Gasparini, R. Manduchi, and M. Gottardi, "An ultralow-power wireless camera node: Development and performance analysis," *IEEE Transactions on Instrumentation and Measurement*, vol. 60, no. 12, pp. 3824–3832, December 2011.
- [177] R. Bixby and E. Rothberg, "Progress in computational mixed integer programming – A look back from the other side of the tipping point," *Annals of Operations Research*, vol. 149, pp. 37–41, 2007.
- [178] 4D Systems, " $\mu$ Cam Serial JPEG Camera Module Data Sheet," 2011, <http://www.4dsystems.com.au/downloads/micro-CAM/Docs/uCAM-DS-rev7.pdf>.
- [179] LinkSprite, "JPEG Color Camera with Serial UART Interface," 2009, <http://www.linksprite.com/product/showproduct.php?lang=en&id=50>.
- [180] Panasonic Corporation, "Electric Double Layer Capacitors (Gold Capacitor)/ HW Series," January 2008.
- [181] D. Moss, J. Hui, P. Levis, and J. I. Choi, "TEP 126: CC2420 Radio Stack," <http://www.tinyos.net/tinyos-2.x/doc/html/tep126.html>.

- [182] J. Ko, C. Lu, M. Srivastava, J. Stankovic, A. Terzis, and M. Welsh, "Wireless sensor networks for healthcare," *Proceedings of the IEEE*, vol. 98, no. 11, pp. 1947–1960, 2010.
- [183] A. Sahai and B. Waters, "Fuzzy identity based encryption," in *Proceedings of IACR EUROCRYPT 2005*, Aarhus, Denmark, May 22-26, 2005, pp. 457–473.
- [184] V. Goyal, O. Pandey, A. Sahai, and B. Waters, "Attribute-based encryption for fine-grained access control of encrypted data," in *Proceedings of ACM CCS 2006*, Alexandria, Virginia, USA, October 30 - November 3, 2006, pp. 89–98.
- [185] J. Bethencourt, A. Sahai, and B. Waters, "Ciphertext-policy attribute-based encryption," in *Proceedings of IEEE SP 2007*, Oakland, California, USA, May 20-23, 2007, pp. 321–334.
- [186] A. Lewko and B. Waters, "Decentralizing attribute-based encryption," in *Proceedings of ACR EUROCRYPT 2011*, Tallinn, Estonia, May 15-19, 2011, pp. 568–588.
- [187] S. Yu, K. Ren, and W. Lou, "Fdac: Toward fine-grained distributed data access control in wireless sensor networks," *IEEE Transactions on Parallel and Distributed Systems*, vol. 22 (4), pp. 673–686, April 2011.
- [188] S. Ruj, A. Nayak, and I. Stojmenovic, "Distributed fine-grained access control in wireless sensor networks," in *Proceedings of IEEE IPDPS 2011*, Anchorage, Alaska, USA, May 16-20, 2011, pp. 352–362.
- [189] Y. Ren, V. Oleshchuk, F. Li, and X. Ge, "Security in mobile wireless sensor networks – a survey," *Journal of Communications*, vol. 6 (2), pp. 128–142, 2011.
- [190] Y. Zhou, Y. Fang, and Y. Zhang, "Securing wireless sensor networks: a survey," *IEEE Communications Surveys & Tutorials*, vol. 10 (3), pp. 6–28, 2008.
- [191] A. V. Taddeo, M. Mura, and A. Ferrante, "Qos and security in energy-harvesting wireless sensor networks," in *Proceedings of ICETE SECRYPT 2010*, Athens, Greece, July 26-28, 2010, pp. 1–10.
- [192] S. Pelissier, T. Prabhakar, H. Jamadagni, R. Venkatesha Prasad, and I. Niemegeers, "Providing security in energy harvesting sensor networks," in *Proceedings of IEEE CCNC 2011*, Las Vegas, Nevada, USA, January 9-12, 2011, pp. 452–456.
- [193] J. Goodman, A. P. Chandrakasan, and A. P. Ch, "An energy-efficient reconfigurable public-key cryptography processor," *IEEE Journal of Solid-State Circuits*, vol. 36, pp. 1808–1820, 2001.
- [194] A. Beimel, "Secure schemes for secret sharing and key distribution," Ph.D. dissertation, Israel Institute of Technology, Technion, Haifa, Israel, June 1996.
- [195] N. FIPS, "197: Announcing the Advanced Encryption Standard (AES)," *Information Technology Laboratory, National Institute of Standards and Technology*, vol. 5 (4), November 2001.
- [196] D. Page, N. P. Smart, and F. Vercauteren, "A comparison of mnt curves and supersingular curves," *Applicable Algebra in Engineering, Communication and Computing*, vol. 17 (5), pp. 379–392, October 2006.

- 
- [197] P. S. L. M. Barreto, S. D. Galbraith, C. O'Eigeartaigh, and M. Scott, "Efficient pairing computation on supersingular abelian varieties," *Designs, Codes and Cryptography*, vol. 42 (3), pp. 239–271, February 2007.
- [198] Crossbow Technology, "MICA2 mote platform datasheet," 2003, document Part Number: 6020-0042-04.
- [199] E. Barker, W. Barker, W. Burr, W. Polk, and M. Smid, "Recommendation for key management - part 1: General (revised)," NIST Special Publication, Tech. Rep. 800-57, 2007.
- [200] V. Leonov, T. Torfs, R. Vullers, and C. Van Hoof, "Hybrid thermoelectric-photovoltaic generators in wireless electroencephalography diadem and electrocardiography shirt," *Journal of Electronic Materials*, vol. 39 (9), pp. 1674–1680, 2010.
- [201] M. Tavakoli, L. Turicchia, and R. Sarpeshkar, "An ultra-low-power pulse oximeter implemented with an energy-efficient transimpedance amplifier," *IEEE Transactions on Biomedical Circuits and Systems*, vol. 4 (1), pp. 27–38, feb. 2010.
- [202] O. Chipara, C. Lu, T. C. Bailey, and G.-C. Roman, "Reliable clinical monitoring using wireless sensor networks: experiences in a step-down hospital unit," in *Proceedings of ACM SenSys '10*, Zurich, Switzerland, 2010, pp. 155–168.
- [203] P. Dutta, S. Dawson-Haggerty, Y. Chen, C.-J. M. Liang, and A. Terzis, "Design and evaluation of a versatile and efficient receiver-initiated link layer for low-power wireless," in *Proceedings of ACM SenSys '10*, Zurich, Switzerland, November 3-5, 2010, pp. 1–14.
- [204] M. Gorlatova, A. Wallwater, and G. Zussman, "Networking low-power energy harvesting devices: Measurements and algorithms," in *Proceedings of IEEE INFOCOM 2011*, Shanghai, China, april 2011, pp. 1602–1610.